Universitat Autònoma de Barcelona

3D Systems for Immune cells culture and their applications in Immunotherapy

Eduardo Pérez del Río

Universitat Autònoma
de Barcelona

3D Systems for immune cell culture and their applications in Immunotherapy

Eduardo Pérez del Río

Doctor of Philosophy in Biochemistry, Molecular Biology and Biomedicine by the Autonomous University of Barcelona

Director: Dr. Imma Ratera

Co-Director: Dr. Judith Guasch

Tutor: Dr. Carles Arús

February 2020

This Thesis is presented for the partial fulfillment of the degree of Doctor of Philosophy by:

Eduardo Pérez del Río

Accepted by:

Imma Ratera

Judith Guasch

Carles Arús

Dr. IMMA RATERA and Dr. JUDITH GUASCH, Scientific Researchers of the Spanish Research Council at the Materials Science Institute of Barcelona (ICMAB-CSIC):

CERTIFIES

That **Eduardo Pérez del Río**, chemical engineering and Master in Biomedical Research, has performed, under her supervision, the research entitled "3D Systems for Immune cells culture and their applications in Immunotherapy". This work has been performed under the framework of the Biochemistry, Molecular Biology and Biomedicine PhD program of the Autonomous University of Barcelona.

And in witness of this, below this is signed,

Director	Co-director
Dr. Imma Ratera	Dr. Judith Guasch

February, 2020

Acknowledgements/Agradecimientos

> Don't lose yourself in your quest for perfection. Imperfection is what makes scientific experimentation possible. Imperfection is beautiful.
>
> - Tecnia -

Mudarme a Barcelona a perseguir mi meta de hacer un doctorado en investigación biomédica ha sido una de las mejores decisiones que he tomado, aunque no fue la más fácil. Supuso muchos cambios para mí, alejarme de mis amigos y familiares, y el miedo propio de empezar desde cero en un destino nuevo en el que no conoces a nadie. Sin embargo, lo que me encontré al llegar aquí, todo lo que he aprendido, las personas que he conocido y lo que he podido construir y madurar en los últimos años me ha hecho agradecer una y mil veces el tomar esta decisión.

Me gustaría empezar agradeciendo a la Dra. Imma Ratera y Dra. Judith Guasch el darme la oportunidad de trabajar con ellas comenzando este nuevo proyecto con el cual he aprendido, disfrutado y trabajado tanto. Se dice que una de las partes más importantes de hacer un doctorado, junto a que te guste el proyecto en el que vas a trabajar, es estar a gusto con tus directores, y estoy completamente de acuerdo. Son ell@s los que te dirigen y orientan, sobre todo cuando estas empezando, y su pasión por lo que hacen es contagiosa. Sentirse escuchado, entendido, respetado y respaldado facilita y enriquece tu forma de trabajar, y así es como me he sentido yo trabajando con ellas, por lo cual estoy muy agradecido. En especial quiero agradecer a Judith los esfuerzos que ha hecho para sacar tantas cosas adelante pese a su embarazo y todo lo que ello conlleva. De verdad muchas gracias por tu trabajo y tu atención.

También me gustaría agradecer a nuestros colaboradores, el Dr. Joaquin Arribas, Dr. Miguel Angel Mateos Timoneda, y Dra. Elisabeth Engel, por su papel en el desarrollo de esta tesis. Gracias a vosotros hemos podido desarrollar un paso más allá nuestra investigación, probando nuestros materiales para nuevas aplicaciones y técnicas, como es el caso de la impresión 3D del grupo de la Dra. Elisabeth Engel y el Dr. Miguel Mateos; y llevando a cabo experimentos que no estaban a nuestro alcance, como la cuantificación de la citotoxicidad de las células con el anticuerpo biespecífico desarrollado por el grupo del Dr. Joaquin Arribas. En referencia a esto también quiero agradecer a la Dr. Irene Rius y al, próximamente doctor, Sergi Rey su paciencias y atención a la hora de diseñar y realizar los experimentos.

During my stay in A.N.Nesmeyanov Institute of Organoelement of Russian Academy of Sciences (INEOS RAS), the role of Dra. Olga Sinitsyna, Dra. Nadejda Davydova, and Dr. Vladimir Sergeev was essential. Thanks to them I felt integrated in the group and I learned a lot of things about AFM and organic chemistry. Besides, they were very kind showing me different parts of Russia and involving me in their culture.

Como no podía ser de otra forma, también quiero agradecer al grupo NANOMOL, y a todos los compañeros y amigos que he hecho en este tiempo. Tanto con las personas con las que he trabajado directamente bajo la dirección de Imma como Marc, Xavi, Gabriela, Fabiao y Julia, como con el resto del grupo, se respira un ambiente muy cómodo de compañerismo, que facilita a estar motivado en el día a día. También he contado con los ánimos y el apoyo de todos mis compañeros de despacho, Inés, Toni, Simo, Guillem, Marc, Paula, Ramón, Dolo, Nathaly y Sara. Con ellos es imposible aburrirse. Siempre han tenido desde consejos a la hora de escribir la tesis hasta algo para picar, ánimos en los momentos más duros, alguna broma para relajar el ambiente, o la paciencia de aguantar las mías. Lo importante es que abunda la confianza y el buen rollo, y espero que eso nunca cambie para los futuros despachos que se formen (al menos siempre seremos el despacho de la comida). Quiero agradecer en especial a Marc, Mario, Toni, Albert, David y Ángel por todos los momentos inolvidables que he pasado con ellos, por descubrirme el mundo del rol, una de mis nuevas pasiones, y también por apoyarme y escucharme cuando lo he necesitado. Sin vosotros esta tesis no hubiese sido la misma.

No me puedo olvidar del sector Cerdanyola, mi compi de piso Quique, Bego, Cristiano, Cris, Juanan… y sus ganas de levantarse a las 6 de la mañana un sábado para ir a por setas; y a Raúl y los miembros del coro, que te garantizaban en la medida de lo posible una hora de desconexión a la semana.

Finalmente quiero agradecer a las personas que llevan conmigo toda mi vida y a las que tanto quiero. A mis padres por apoyarme en mis decisiones profesionales e intentar ayudarme en la medida de lo posible. A Marcos, Leo, y Yaiza, por esforzarse a estar ahí a pesar de la distancia. A Viki, sin la cual literalmente no estaría aquí, ya que fue la que me enseño el anuncio en el que se buscaba mi perfil y me motivó a dar el paso. A Bea por sus visitas y nuestras frecuentes partidas. Y en general a todos mis amigos de Palencia, a Dafne, Oscar, Dani, Kike, Cris(s), Lore y Beba, a los cuales espero seguir viendo, aunque casi todos hayamos tenido que emigrar para buscar trabajo.

Abstract

Recent achievements in the field of immunotherapy, such as the development of engineered T cells used in adoptive cell therapy, are introducing more efficient strategies to combat cancer. Nevertheless, these T cells are challenging to manufacture, manipulate, and control. Specifically, there are limitations in producing the large amounts of T cells needed for these therapies in a short period of time and in an economically viable manner. In this thesis, we have studied different 3D systems with the objective of achieving higher proliferation rates and tune the resulting phenotypes, resembling the natural environment of the secondary lymphoid organs.

Matrigel and a 3D polystyrene scaffold were studied as two of the most suitable commercially available options, showing an increase in cell proliferation compared to standard suspension systems. This research proved not only the beneficial effect of the addition of a 3D physical support, but also the importance of the chemical input to stimulate cell expansion. However, these systems were not designed for secondary lymphoid organ mimicking and thus, they significantly differ in terms of ECM composition. Consequently, a new platform was developed for this application to improve the obtained results.

Hydrogels composed of poly(ethylene) glycol (PEG) covalently combined with low molecular weight heparin (PEG-Hep hydrogels) were synthesized and completely characterized for this purpose. PEG confers the 3D structure to the hydrogel, and can be manipulated to change its mechanical properties. Heparin, which is a negatively charged molecule, is used as an anchor for positively charged proteins that can affect cell behavior. This system was used for immune cell expansion under different conditions, specifically, unloaded hydrogels were employed as well as hydrogels loaded with cytokines related to immune cell proliferation like CCL21 and CCL19. All the conditions resulted in an increase of CD4+ T cell proliferation but the highest proliferation indexes were achieved with hydrogels loaded with CCL21 together with the addition of CCL19 in suspension, which are the conditions that best mimic the extracellular matrix of lymph nodes. Besides, the resulting phenotypes of CD4+ T cells cultured in PEG-Hep hydrogels showed an increase of the T_{EM} percentage in comparison with cells expanded in suspension.

The same systems were used for peripheral blood mononuclear cells (PBMCs). 3D polystyrene improved the proliferation parameters in comparison with suspension systems. However, the killing capacity of the resulting cells did not change in comparison with cells cultured in suspension due to the lack of chemical input in this system. The beneficial results obtained with PEG-Hep hydrogels for the culture of CD4+ T cells could not be reproduced for this population. Nevertheless, PEG-Hep hydrogels did show an effect in the resulting phenotypes achieved, increasing the CD45RO+/CD62L- percentage (T_{EM} population for T cells).

Finally, PEG-Hep hydrogels were studied as bioink for 3D printing, optimizing the protocol of hydrogel formation for this application which required a scaling up process. The resulting printed scaffolds were applied to immune cell culture. It was observed increases in the proliferation parameters of CD4+ T cells and changes in their resulting phenotypes in comparison with non-printed hydrogels. In this case an increase in the T_{CM} phenotype was observed, which is related to good clinical outcomes. For PBMCs no proliferation enhancement was observed and the resulting phenotypes were comparable with the ones obtained without printing. However, a further optimization of the use of PEG-Hep hydrogels as bioink for 3D printing is still necessary.

Abbreviations

2D	Two-dimensional
3D	Three-dimensional
ACT	Adoptive cellular therapy
ALL	Acute Lymphoblastic Leukemia
APCs	Antigen-presenting cells
AR	aspect radio
AuNPs	Gold nanoparticles
CAR	Chimeric antigen receptor
CCL21	C-C chemokine ligand 21
CCL19	C-C chemokine ligand 19
CD	Cluster of differentiation
CEA	Carcinoembryonic antigen
CFSE	Carboxyfluorescein succinimidyl ester
CIKs	Cytokine-induced killer cells
CLL	Chronic lymphocytic leukemia
CTL	Cytotoxic T lymphocytes
DC	Dendritic cell
ECM	Extracellular matrix
ELISA	Enzyme-linked immunosorbent assay
FDCs	Follicular dendritic cells
FITC	Fluorescein isothiocyanate
FRCs	Fibroblastic reticular cells
G'	Storage modulus
G''	Loss modulus

GAGs	Glycosaminoglycans
Ge	Equilibrium shear modulus of a gel
GFP	Green fluorescence protein
Hep	Low molecular weight heparin
Hep-Mal	Maleimide-functionalized low molecular weight heparin
HER-2	human epidermal growth factor-2
HEVs	High endothelial venules
HLA	Human leukocyte antigen
ICAM-1	Intercellular adhesion molecule-1
IL-2	Interleukin-2
IS	Immunological synapse
LAKs	Lymphokine-activated killer cells
LFA-1	Lymphocyte function-associated antigen 1
LNs	Lymph nodes
mAb	monoclonal antibody
MHC	Major histocompatibility complex
NK	Natural Killers
PBMCs	Peripheral blood mononuclear cells
PBS	Phosphate buffered saline
PE	Phycoerythrin
PEG	Poly(ethylene glycol)
PGA	Poly(glycolic acid)
PLA	Poly(lactic acid)
RPMI	Roswell Park Memorial Institute medium
SAOS	Small-amplitude oscillatory shear
SEM	Scanning electron microscopy

SLOs	Secondary lymphoid organs
TCB	T cell bispecific antibody
T_{CM}	T central memory cells
TCR	T cell receptor
T_{EM}	T effector memory cells
TILs	Tumor-infiltrating lymphocytes
T_N	T naïve cells
WP	Well plate

Contents

CHAPTER 1
Introduction and Objectives

1.1 Immunotherapy. Historical background

Immunotherapy is a medical strategy that offers a different approach to chemotherapy, radiation, and surgery in the treatment of cancer, which is based on employing and reinforcing the immune system of patients. This system protects the organisms against disease, distinguishing between self and non-self body cells. However, cancer appears from the organism own cells, and it creates a tumor microenvironment with immune evasion and immunosuppression signals capable of avoiding the immune response. The main objective of immunotherapy is to develop different strategies able to surpass cancer immunosuppression methods, detect, and eliminate malignant cells without damaging healthy tissues.[1]

The knowledge about the natural defenses present in the body to combat cancer exists long before the modern period. Throughout history, from ancient Egypt up to the Europe in the early 18th century, there are some accounts of tumors "miraculously disappearing", sometimes spontaneously or after a febrile or an infectious episode. However, the scientific basis for the attempts to modulate the immune system to treat cancer can be found in the second half of the 18th century, when two German physicians, Busch and Fehleisen, independently noticed the regression of tumors in cancer patients after accidental infections by erysipelas in 1868 and 1882 respectively.[2] In 1891, an American surgeon, William Coley, of the Bone Tumor Service at the Memorial Hospital in New York, today known as the Memorial Sloan Kettering Cancer Center, observed a long-term regression of a sarcoma after an erysipelas infection. Following this results, he developed a treatment consisting of injecting heat-inactivated bacteria ("Coley's toxins") into patients with inoperable cancers.[3] Although he reported a significant number of regressions and cures in more than 1,000 patients, most with sarcomas, his treatment gradually disappeared from use because of the development of radiation therapy and chemotherapy, and his failure to follow good scientific protocols and consistently obtain reproducible results. Even viral infections were believed to have a cancer suppressive effect, when in 1896 George Dock at the University of Michigan observed the remission of an acute leukemia in a 42-year-old woman after an infection with influenza.[4] After some years with little progress on the topic, Coley's principles were clinically supported by Morales et al.[5] in 1976, when the effectiveness of the bacterium Bacillus Calmette-Guérin (BCG) was established in the treatment of superficial bladder cancer. This study was based on a previous one from 1959 of Old et al.[6] showing the anti-tumor effects of BCG in a mouse model.

The beginning of the immunotherapy's modern era was in the fifties with the discovery of interferon by Isaacs and Lindenmann (1957),[7,8] and the founding of the Cancer Research Institute of New York dedicated to the development of immune-based treatments for cancer, by William Coley's daughter, Helen Coley Nauts.[9] In 1959 Ruth and John Graham published the first ever cancer vaccine study with 114 gynecologic cancer patients treated with adjuvanted tumor lysate, observing a 22% incidence of

remission or stable disease.[10] However, this study did not achieve a lot of attention. The critical role of the cellular immune response in adaptive immunity was fully characterized by Jacques Miller's seminal publication in 1967 titled 'Cellular basis of the immunological defects in thymectomized mice'.[11] It was followed by other crucial discoveries that would set the stage for a faster evolution of cancer immunotherapy, like the discovery and characterization of dendritic cells (DCs) by Ralph Steinman in 1973,[12] Zinkernagel and Doherty's description of the major histocompatibility complex (MHC) restriction in 1974,[13] and Eva Klein's documentation of natural killer (NK) cell activity in 1975.[14,15] Besides, in this period some immune-based cancer treatments began to be performed. This is the case of bone marrow transplantation for the treatment of hematologic malignancies, which was pioneered in the mid-seventies at the University of Minnesota. However, as in William Coley's time, the immunologic component of these regimens was not understood. Together with these first treatments a simultaneous revolution in molecular biology allowed Talpaz and colleagues at the MD Anderson Cancer Center to molecularly clone the interferon gene for its further industrial-scale production and application for treating chronic myeloid leukemia patients.[16]

Recently, the field of immunotherapy has been marked by some events that forced acceptance of immuno-oncology onto ambivalent clinical practitioners. One of this events was the FDA approval of the inhibitor ipilimumab for the treatment of stage IV melanoma patients.[17] Similarly, the FDA approved sipuleucel-T, an autologous active cellular immunotherapy which showed evidence of efficacy in reducing the risk of death among men with stage IV metastatic castration-resistant prostate cancer.[18] Finally, it was also of great importance the success showed in early clinical studies by the chimeric antigen receptor (CAR) strategy, first experimentally described in 1993.[19] This receptor linked the CD19 antigen, which is found on many types of B-cell cancers, single-chain immunoglobulin variable region (scFv) to CD3-ζ and other stimulatory signaling domains like CD28.[20,21] Following this strategy, Carl H. June et al.[22] reported in 2011 a phase I clinical trial using CD19 targeted CAR T cells for the treatment of three patients with advanced chronic lymphocytic leukemia (CLL). A CD19-specific immune response in all patients was achieved with a complete remission in two of them, accompanied by the persistence of a portion of these cells as memory CAR+ T cells, retaining the anti-CD19 effector functionality.[22] Due to the success obtained, this treatment was applied to treat 14 patients with relapsed and refractory CLL, observing an overall response rate of 8 of 14 patients, with 4 complete remissions and 4 partial remissions.[23]

These facts provided to the immunotherapy field the support to keep progressing and broaden the application of CAR T cell therapy to additional diseases, such as acute lymphoblastic leukemia (ALL) in 2013[24] and refractory multiple myeloma in 2015.[25] Moreover, by the end of 2016, different checkpoint inhibitor drugs were approved by the FDA to treat melanoma, renal cell carcinoma, lung cancer, lymphoma, and cancers of the bladder. The mechanism of action of these drugs consists of blocking the proteins

responsible for inactivating the immune response, allowing the immune cells to detect and kill cancer cells.[26] In 2018, James P. Allison and Tasuku Honjo were awarded with the Nobel Prize in Medicine for their contribution to the discovery of cancer therapy by the inhibition of negative immune regulation.

The success shown by the novel anticancer immunotherapies proving their capacity to elicit clinically meaningful and durable responses in different tumor types, has targeted them as ones of the most promising strategies to fight cancer. However, the response rates are still modest in many cases, especially in solid tumors, and, more efforts are required for a better understanding of the mechanisms that underlie this approach to improve the clinical outcomes.[27]

1.2 Immune system

The secondary lymphoid organs (SLOs) are in charge of generating and coordinating the immune responses in mammals, and they are positioned at strategic locations throughout the body. SLOs include lymph nodes (LNs), spleen, Peyer's patches, and mucosal tissues such as the nasal-associated lymphoid tissue. In these organs there is a high concentration and transit of immune cells, which move throughout the body in a fluid named lymph, and is where T and B cells scan for the presence of their cognate antigen. SLO development depends on the precisely regulated expression of cooperating lymphoid chemokines and cytokines. When there is no antigen recognition, immune cells only receive homeostatic survival signals allowing them to continue their journey through the LNs. However, if T or B cells do recognize an antigen, the SLOs provide an optimal environment for cellular activation, proliferation, and selection for high affinity antibodies.[28,29]

1.2.1 Immune cells

The cells of the immune system can be classified in three types: lymphocytes (T cells, B cells and NK cells), neutrophils, and monocytes/macrophages. Peripheral blood mononuclear cells (PBMCs) are formed approximately by an 80% of T and B cells, 10% NK cells, and 10% myeloid cells, mostly monocytes (figure 1.1). These blood cells play an important role in the immune response that preserves the host's homeostasis, fight infection, and cope with intruders.[30]

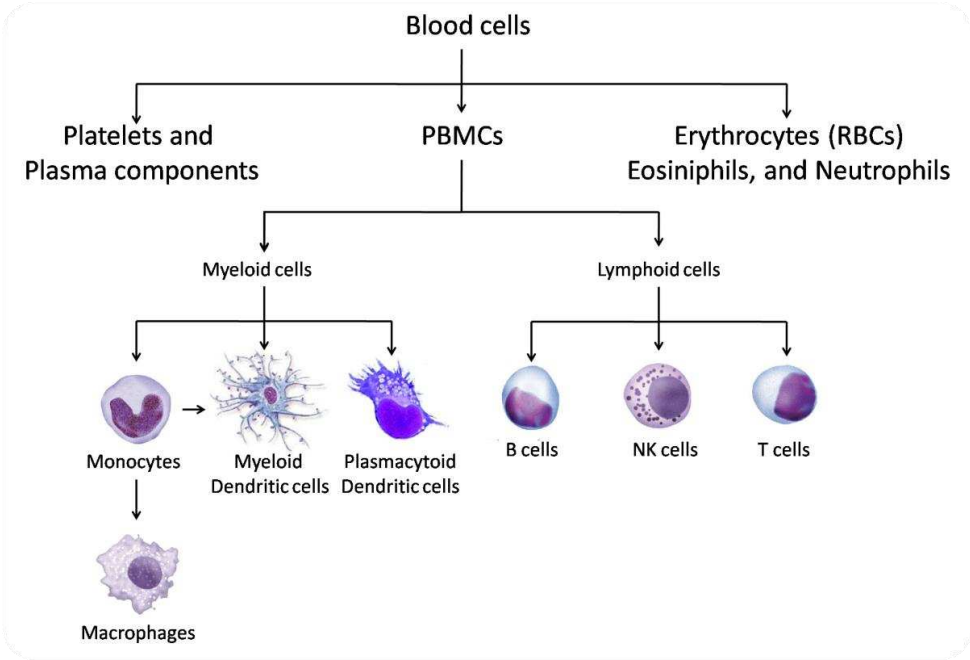

Figure 1.1 Diagram of the cells present in blood focusing in the composition of PBMCs. Cell images courtesy of Wikimedia.org (in February 2020).

Cellular immunotherapy mainly focuses on modifying the activity of T cells to drive an anti-tumor response. The differentiation state and subset specification of T cells can influence their metabolism, cytotoxicity, and longevity. T cell differentiation states include naïve T cells (T_N), central memory T cells (T_{CM}), effector memory T cells (T_{EM}), and finally terminally differentiated T_{EMRA} (figure 1.2).[31] T_{CM} has been reported to be the preferable phenotype for therapy success.[32,33]

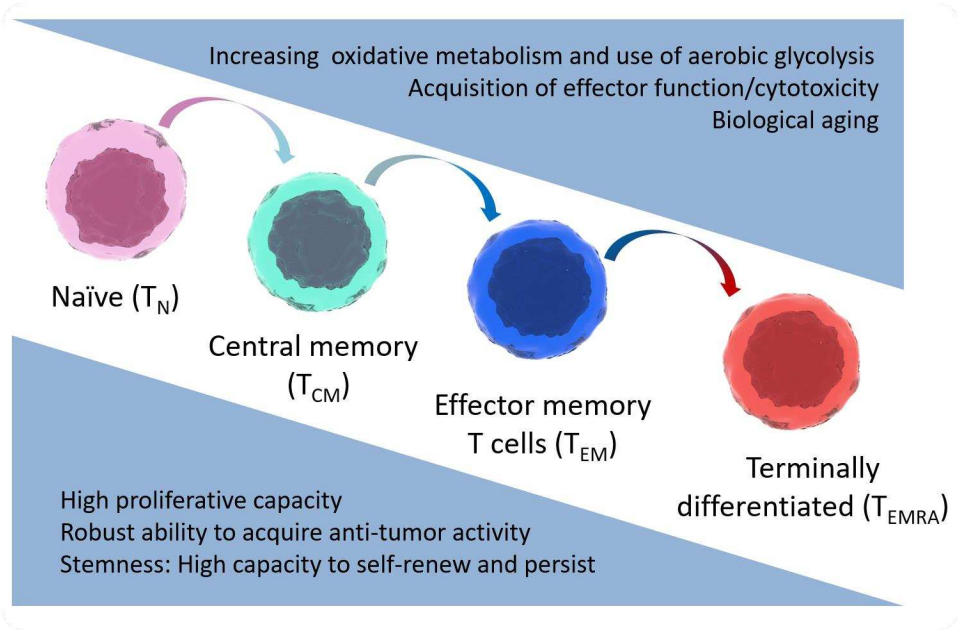

Figure 1.2 Linear differentiation of T cells from T_N to T_{CM}, T_{EM}, and finally T_{EMRA}. The diagram shows the alterations in metabolic characteristics that accompany T cell differentiation.

1.2.2 Natural structure and function of secondary lymph nodes

LNs are the organ where it is produce the activation of the immune responses in case of antigen recognition. They are kidney-shaped structures ranging from the size of a few millimeters to about 1–2 cm, which can get inflamed or enlarged in various conditions like infections and malignancies. Humans have around 450 LNs placed at vascular junctions along the lymphatic "highways", where lymphatic vessels converge. They contain large numbers of lymphocytes, macrophages, and antigen-presenting cells (APCs).[34]

A capsule derived from the lymphatic vessels surrounds the inner structure of the LNs, which is distributed in different sub-compartments with distinct cellular micro-domains, as represented in figure 1.3. These compartments are almost exclusively colonized by either T or B cells to facilitate cell-to-cell contact and recognition as well as to provide a favorable environment for signaling and induction mechanisms. This distribution is critically dependent on cytokines, adhesion molecules, and extra cellular matrix (ECM) proteins produced by non-hematopoietic stromal cells.[35,36]

Factors that enter the LNs through the afferent lymph can be either transported deep into the LN cortex or move via the subcapsular sinus and leave through efferent lymphatic vessels. Cells and antigen also enter the LNs via an arteriole at the medullary sinus, which branches into a capillary bed with post-capillary venules, called high endothelial venules (HEVs). HEVs are placed in the T zone, and are the main points of

entry for naïve T and B cells in response to 'homing' chemokines like CCL19 and CCL21. Finally, in the superficial cortex are found B cell follicles, where B cells interact with follicular dendritic cells (FDCs), which present unprocessed immune complexes to B cells during germinal center reactions. Besides, they secrete the B cell chemoattractant CXCL13 that is essential to maintain the structural integrity of the B cell follicle under homeostatic conditions.[28,29,34]

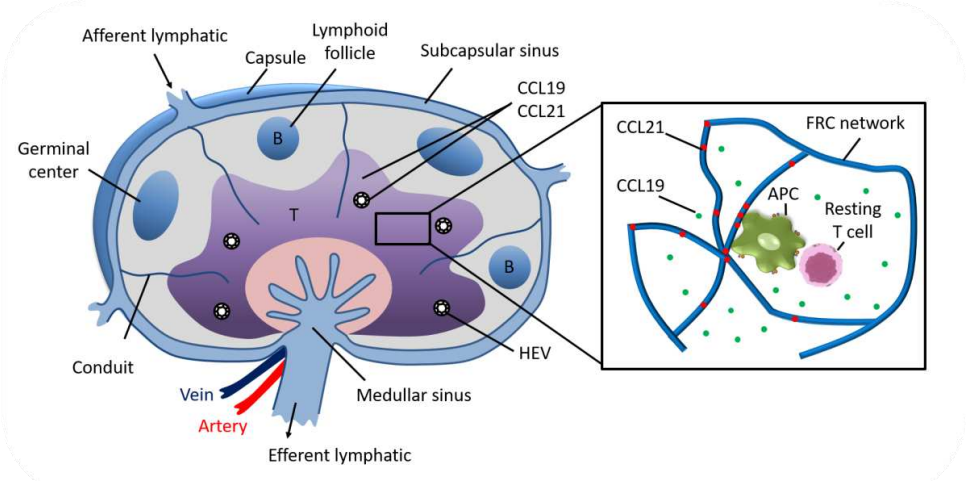

Figure 1.3 Representation of the general structure of a lymph node, where T represents the T zone populated for T cells, and B represents the B zone populated by B cells.

The stroma or structural part of the LNs is in its majority formed by fibroblastic reticular cells (FRCs). Besides the supporting function, FRCs are involved in the immune response by guiding lymphocyte migration both physically, by providing anatomical arrangements that influence the traffic patterns of lymphocytes, and chemically, by secreting the chemokines CCL19 and CCL21 that attract T cells, B cells, and DCs, i.e. CCR7-expressing cells. FRCs form a set of interconnected channels termed FRC conduit system, by wrapping reticular fibers mainly made of type III and IV collagen, elastin, and laminin, for the efficient and rapid transfer of soluble molecules, such as antigens, chemokines and immune complexes, from the subcapsular sinus to the deeper cortex, the HEVs, and the follicular compartment.[37,38] Simplifying, this complex structure results in a sponge-like framework composed mostly of collagen fibers covered by reticular cells which provide an optimal environment as defense against the invasion of pathogens at any site in the body.

1.3 Current Immunotherapies

1.3.1 Adoptive cellular therapy

Adoptive cellular therapy (ACT) is an approach that consists of using autologous T cells, which have been modified or selected, and expanded *in vitro*, for a further reinfusion into the patient to mediate tumor destruction (figure 1.4).[39] To apply these treatments a preparative lymphodepletion, which is the temporary ablation of the immune system of the patient, needs to be performed by chemotherapy alone or combined with total body irradiation. Thus, in order to cause a durable antitumor therapeutic immunity leading to tumor eradication can be obtained, as has been seen in metastatic melanoma, lymphoma, lymphoid leukemias and other refractory tumors.[40–43]

Initial ACTs in cancer involved expanding infiltrating tumor-specific T lymphocytes (TILs) *ex vivo*, relaying on the tumor specificity of these cells, however, recent advances have demonstrated that employing engineered T cells may be an even better strategy to target cancer. Nowadays, the main ACT strategies under study are lymphokine-activated killer (LAK) cells, TILs, cytokine-induced killer (CIK) cells, T cell receptor (TCR) gene-modified T cells, and chimeric antigen receptor (CAR) T cells.[44]

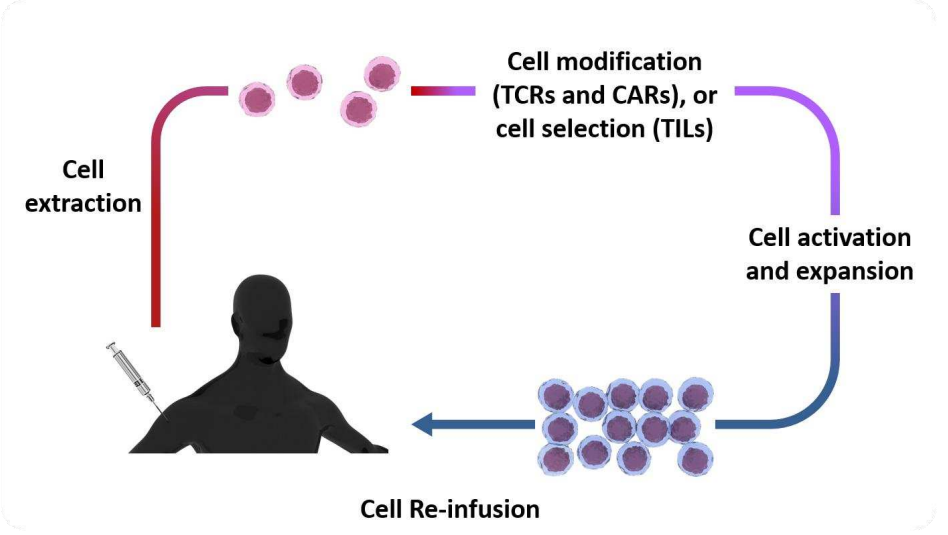

Figure 1.4 Simplified diagram of the process of adoptive cellular therapy in cancer.

LAK cells are white blood cells stimulated to kill tumor cells and have been mostly applied to treat a minority of tumors like renal carcinoma and melanoma.[45] LAK cells that are stimulated and activated with interleukin 2 (IL-2) result in effector cells with non-specific cytotoxicity derived from PBMCs. They have a broad anticancer spectrum and non-MHC restrictive cytotoxic effect. They show the advantage of destroying tumor cells both sensitive and non-sensitive NK cells, but they have a limited amplification and produce serious side effects like liquid retention.[44]

CIK cells are heterogeneous *ex vivo* expanded lymphocytes with a mixed T NK cell phenotype. They are another non-specific and non-MHC-restrictive cytotoxic effector cell type also derived from PBMCs whose main cell population is CD3+CD56+ effector cells.[44] They are generated by the incubation of PBMCs with cytokines such as interferon gamma, IL-2, and anti-CD3 monoclonal antibody.[46] Between the advantages of this strategy, there is the rapid cell proliferation, high efficiency and broad spectrum in killing tumor cells, little toxicity against normal human, hematopoietic precursor cells, and strong resistance to apoptosis induced by tumor cells.[44,47] The main problem of this technique is the lack of fine precision, causing unspecific cytotoxicity. To overcome such limitation, different combined techniques are being studied.[48]

TILs are generally mixtures of CD8+ and CD4+ T cells, infiltrated in the tumor bed that specifically recognize tumor-associated antigens and have the capacity to traffic to the tumor site after reinfusion. Although TILs growth has been described for a variety of solid cancers like renal, ovarian, breast, and colon,[49] this strategy has mainly been applied to melanoma, where over two-thirds of T cells grown show autologous tumor recognition after being cultured with IL-2.[50] However, this strategy still has some limitations, like the limited number of tumors where reproductive TILs are detected, their inefficacy in provide responses for long periods of time, the absence of a standardized protocols for TIL expansion *in vitro*, and the possibility of immunosuppression of reinfused TILs due to the tumor microenvironment.[44,50]

TCR-T cell therapy was developed in order to overcome the fact that TILs could almost exclusively be applied to treat patients with malignant melanoma, because of the difficulty of isolating and expanding pre-existing tumor-reacting T cells. In the TCR-T cell strategy, the lymphocytes of patients are genetically engineered with genes derived from a tumor-reactive T cell clone to express its TCR (α and β chains), which recognizes the human leukocyte antigen (HLA, term for human MHC), thus conferring the antigen-specificity of the transferred TCR to the cells (figure 1.5).[1,51] The first successful results were obtained by using T cells genetically modified with a TCR targeting MART-1 for the treatment of patients with melanoma.[52] Additionally, numerous preclinical and clinical studies have demonstrated various levels of feasibility, safety, and efficacy using TCR engineered T cells to treat cancer and viral infections.[53] However, it is becoming more evident that it implies a high probability of causing severe adverse events, destroying healthy tissues that express the same target antigen. Other challenges are the improvement of gene transfer efficiencies, the identification of target antigens highly selective for tumor cells rather than normal cells, and the use of allogeneic (cells are collected from a matching donor) instead of autologous cells (cells are collected from the patient's own body).[1,51]

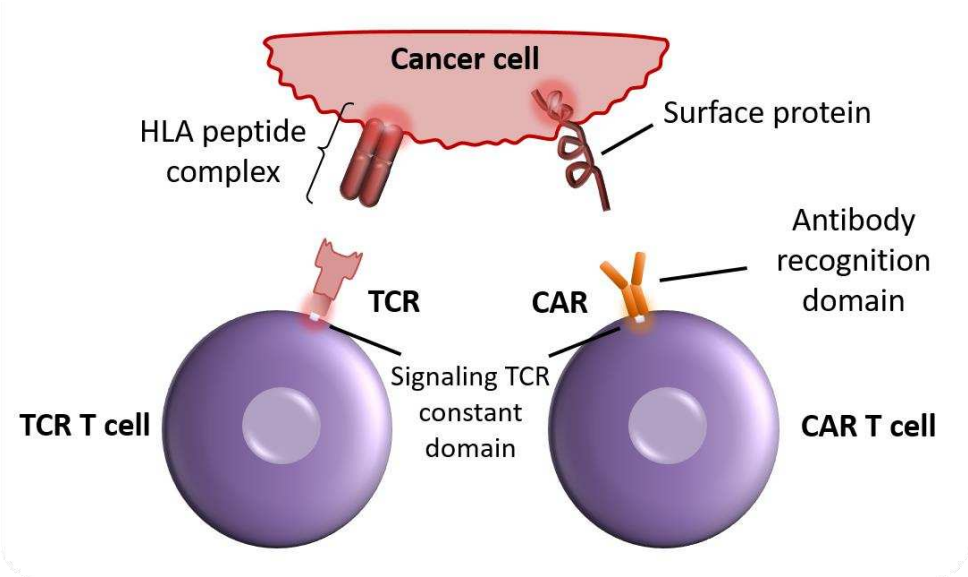

Figure 1.5 Representation of the antigen-specificity of the transferred TCR-T cells and CAR-T cells.

CAR-T cells have tumor-reactivity because their transduction with an artificial receptor, the CAR, which consists of an antibody variable domain fused to a TCR constant domain (figure 1.5). Following this strategy, T cells obtain the antigen-recognition properties of antibodies. Thus, the need of a functional antigen processing machinery by tumor or dendritic cells such as the MHC class molecules is omitted.[54] Additionally, CARs are capable of recognizing both protein and non-protein surface antigens including glycolipids and carbohydrates, which could be molecules of importance due to their specificity for tumor cells.[55] Nowadays CAR-T cells represent a potential tool to treat persistent cancers. The most effective treatment reported is the use of CAR engineered T cells targeting CD19 and CD20 to treat CLL, B-cell lymphoma and ALL.[22,24,56–58] This strategy was also studied for the treatment of solid cancers, however, the success achieved to date is limited, especially due to the difficulty of identifying suitable target antigens.[49] Despite the observed potential of this strategy, the mechanism of action is less well known than the one of TCR-T cells due to e.g. features that vary among different target antigens and CAR constructs. It is therefore important to find a balance between antigen (antigen surface level, epitope location, and antigen mobility) and CAR structure (CAR surface level, affinity, and signaling domains).[59]

In summary, there are different advantages and disadvantages for each cell type, but all of them have a common step consisting of expanding the respective cell populations *ex vivo*. This step is currently one of the limiting factors for the broad use of ACT in clinics. Thus, it is very important to improve the performance of the state of the art immune cell expansion systems to obtain the large needed clinical doses in a short period of time and in an economic way.[60,61]

1.3.2 Therapeutic cancer vaccine

The term “cancer vaccine” can refer either to a prophylactic vaccine, given to prevent cancer, or to a therapeutic vaccine, given to eradicate an existing tumor, stopping it from growing or spreading. Normally, a cancer vaccine contains a desired tumor antigen and an adjuvant, which is able to generate an immune response, emitting signals that stimulate the maturation of DCs. Then, DCs present the tumor antigens from the vaccine on MHC surface molecules and subsequently stimulate an anti-cancer T cell response.[62] First-in-human clinical trials of cancer vaccines have shown the feasibility, safety, and immunotherapeutic activity of this strategy.[63,64] However, the accumulation of genetic alterations specific for each tumor calls for a personalized selection of vaccine targets, which might be possible thanks to technological advances in genomics and data science, which might allow a rapid mapping of the mutations within a genome.[65]

1.3.3 Immunotherapy with antibodies

Antibody-based immunotherapeutics are specific therapeutic agents based on the affinity of antibodies to target antigens at (even) nanomolar levels (Fv region) as well as their ability to engage components of the host immune system (Fc region).[66] The most commonly used are monoclonal antibodies (mAb), which are antibodies produced against a single epitope. Clinical trials of mAbs are ongoing for several types of cancers such as breast, colon, and lymphomas.[67] The cancer immunotherapeutic efficacy of mAb is based on three main mechanisms: the antibody-dependent cellular cytotoxicity caused by mAbs that bind to specific tumor associated antigens, complement-dependent cytotoxicity by complement activation, and the inhibition of the factors and receptors that activate the signal pathways used by cancer cells in division and angiogenesis by antibody binding. The first mAb approved by the FDA for cancer immunotherapy was named Rituximab in 1997, targeting the CD20 antigen in the treatment of B-cell non-Hodgkin’s lymphomas. The following years more mAbs with different targets were approved, such as Trastuzumab in 1998, a humanized mAb which inhibits human epidermal growth factor-2 (HER-2)-activated signaling pathways in (breast) cancer cells; Ipilimumab in 2011 for the treatment of metastatic melanoma, targeting cytotoxic T lymphocyte antigen-4 (CTLA-4) which plays a role in delivering inhibitory signals to cells; or Avelumab in 2017 for non-small cell lung, ovarian, and stomach cancers, and renal cell carcinoma binding to PD-L1.[66] Thanks to the advances in antibody technology, the number of approved and developing mAbs for cancer therapy is increasing. However, this treatment is also facing several challenges such as the alleviation of various side effects such as fever, trembling, fatigue, headache and muscle pain, nausea/vomiting, difficulty in breathing, rash, and bleeding.[68]

1.3.4 Current challenges of Immunotherapy

Recent success of novel anticancer immunotherapies has led to a new era of cancer treatment, eliciting clinically meaningful and durable responses in multiple tumor types. Unfortunately, the response rates to immunotherapy are still modest, and, clearly, more efforts are required to improve outcomes with these treatments.[27] Although each strategy confront different limitations, there are some common challenges faced by immunotherapies which need to be improved in order to increase the efficacy of these therapies.

It is of vital importance to obtain a deep understanding of the mechanisms that regulate the immune response and the anti-tumor activity of the used immunotherapies in order to shed light on the different degrees of clinical responses. This information will also contribute to design combinatorial immunotherapeutic strategies to target tumor cells and their microenvironment, and counteract the multiple immune escape mechanisms utilized by tumor cells. To reduce the side effects, it is necessary to develop treatments with an enhanced degree of specificity and identify new antigens highly selective for tumor cells.

An additional challenge is the use of ACT in a clinical scale. For that, further automation and control of the cell therapy manufacturing processes is necessary in order to reduce patient risk, achieve better product robustness, and lower costs. As mentioned before, most cell therapies require a step of cell expansion. The improvement of this process could lead to the production of relevant quantities of therapeutic cells to reach the necessary clinical doses. With the objective to overcome these limitations, mimicking the natural tissue of the immune cells could help design better culture systems for a deeper understanding of the mechanisms that rule immune responses, and with the potential to provide higher proliferation rates and affect the resulting phenotypes.

1.4 Current clinical expansion strategies

Different activation and expansion systems of T cells have been mostly used in clinical trials and also in two products that are already in the market named Kymriah (Novartis, USA) and Yeskarta (Genentech, USA), based on autologous T cells genetically modified with an anti-CD19 CAR. With the objective of improving current expansion technologies and designing new ones, it is vital to have a deep understanding of the T cell activation process.

1.4.1 T cell activation

T cells have the task of identifying small numbers of specific foreign antigens, usually peptides, from a very noisy environmental background of endogenous self-peptides. To fulfill this mission, they need the APCs to process and present such antigens bound to a MHC. T cells can then detect this complex through the TCRs, which are located at their surface. These receptors are generated somatically through site-specific DNA recombination, resulting in a large repertoire capable of recognizing most of the encountered antigens. The interaction of both, TCR and the foreign peptide presented by MHC molecules, becomes a primary signal for T cell activation and dictates the initial activation of T cells. Nevertheless, this signal is not enough to fully activate naïve T cells, which require co-stimulation. Although there are multiple molecular contacts between a T cell and an APC that provide co-stimulatory signals, the most relevant one is the interaction of CD28 on the T cell with CD80 or CD86 on the APC.[69,70] A diagram of this natural T cell activation process is represented in figure 1.6.A.

A strategy followed to mimic *in vitro* this interaction is the use of advanced biomaterials that replicate specific properties of the APC surface by functionalizing them with ligands that specifically bind to known receptors on the immune cell surface. These materials have the potential to form an artificial immunological synapse (IS) with cells.[71] Nowadays, *in vitro* T lymphocyte stimulation is a technique extensively used to facilitate T cell expansion mainly for research, but also in the clinics.

A common strategy in the past was the use of a soluble anti-CD3 mAb, which recognized the CD3 unit present in the TCR and activated T cells by signal transduction through this complex, together with the addition of high-doses of the cytokine IL-2, and allogeneic PBMCs as feeder cells, which released growth factors to further enhance the proliferation of T cells. The combination of these three components was first described to expand TILs to treat melanoma patients,[72] but it was also used in different ACT-based studies, such as engineered TCRs to treat patients with metastatic synovial cell sarcoma and melanoma,[73] or anti-CD19 CAR T cells to treat CLL, mantle cell lymphoma (MCL), and ALL.[74–76]

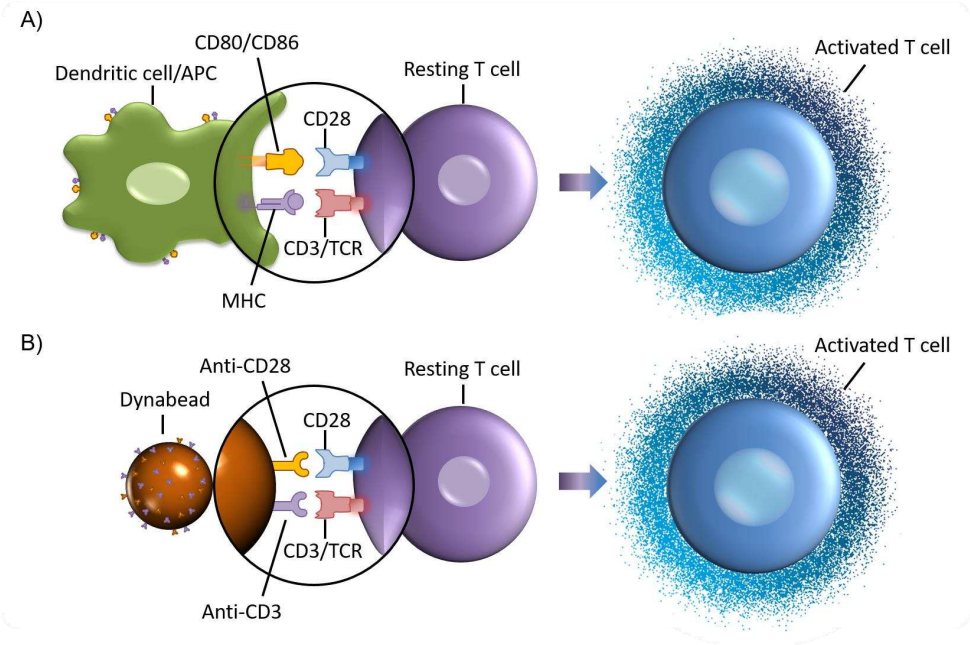

Figure 1.6 Schematic representation of the IS. A) Natural T cell activation process due to its interaction with an APC (dendritic cell). B) *In vitro* activation of a T cell through the use of Dynabeads®.

Although the capacity of clinical grade anti-CD3 mAb and IL-2 for T cell expansion was demonstrated, some studies reported that the repetitive use of soluble antibody could cause activation induced cell death, being the lack of costimulatory signals one of the causes.[77] For this reason a new strategy to replicate the T cell activation procedure was developed, which included the use of an antibody specific for CD28 (anti-CD28) to provide a co-stimulatory signal together with the one specific for the TCR-CD3 complex (anti-CD3). Besides, the antibodies were bound to a solid surface (e.g. accessory cells, beads, and planar surfaces),[78] observing a significant impact of the anchoring on the expansion efficacy, especially with the antiCD3 due to its capacity of mechanotransduction, thus resulting in different registered products. The most used one is Dynabeads® (Invitrogen, USA), which consists of superparamagnetic beads coated with a thin polymer shell that is decorated with the antibodies to encase the magnetic material with a homogeneous size of 4.5 µm of diameter. Its production allows a high batch-to-batch reproducibility ensuring the quality of the results unlike feeder cells. A representation of the activation mechanism of Dynabeads® can be seen in figure 1.6.B. After the activation and expansion of the T cell population, the magnetic beads can be easily removed by using a magnet.

1.4.2 Use of 2D surfaces

Planar bidimensional (2D) surfaces have been shown to be valuable systems due to their capacity to mimic the *in vivo* environment in a well-controlled and simplified manner.

They were used in the study of the IS between a T cell and an APC, the identification of the TCR and LFA-1 signaling in the regulation of the T cell-APC interaction, and on the elucidation of mechanical forces in T cell activation.[79]

The IS was deeply studied with 2D strategies proving that is organized into two concentric clusters of proteins. The center was named central supramolecular aggregative clusters (SMAC) and is enriched with TCR/CD3 complexes and the co-receptors CD4 and CD8 that stabilize the interaction between the MHC class I and II, respectively. The outer ring, the peripheral SMAC, is enriched with adhesion molecules such as lymphocyte function-associated antigen 1 (LFA-1), that enhances actomyosin forces, and intercellular adhesion molecule-1 (ICAM-1), which secures the T cell-APC interaction. Analysis of very early T cell activation following the interaction of antigen-specific T cells and a planar bilayer containing specific antigen peptide-MHC, revealed that the TCR begins clustering immediately after T cell recognition, prior to mature IS formation, establishing initial clusters that recruit downstream signaling molecules and mediate the activation signal.[80]

An interesting method used to deepen the understanding of immune cell interactions at nanoscale levels are bioactive quasi-hexagonal arrays consisting of biofunctionalized gold nanoparticles (AuNPs) with a controlled interparticle spacing.[81] This strategy showed that the initial T and NK cellular response to stimulation decreased with increasing the spacing between AuNPs, proving the causative role of nanoscale spatial structure in immune cell activation.[81] It was also used to demonstrate that T cell activation was significantly higher on Au nanoarrays than on anti-CD3 coated plastic slides, highlighting the importance of the chosen material.[82] Additionally, the role of integrin-mediated adhesion was also assessed, demonstrating that the RGD peptide enhances T cell activation.[83] Another strategy employed surfaces coated with CCL21 and ICAM-1 together with IL-6 media enrichment as an *ex vivo* synthetic immune niche with the objective of effectively stimulating the proliferation of antigen-activated CD4+ T cells. It was found that plate surface functionalization dramatically increased T cell proliferation and changed the culture topology from cell clusters in suspension to a firm, substrate-attached monolayer of cells.[84]

Although a lot of valuable information was obtained with 2D studies, the natural T cell-APC interaction occurs in a three dimensional (3D) space. To compare 2D with 3D configurations, an experiment was performed using a TCR ligand anchored to lithographically patterned NP clusters surrounded by mobile adhesion molecules on a supported lipid bilayer (SLB). The TCR ligand could be co-planar with the SLB (2D), or elevated by 10 nm on solid nanopedestals (3D). This resulted in different T cell responses and it was possible to identify important contributions of lateral and axial components of ligand positioning, suggesting the importance of the 3D mimicking in order to truly replicate immune interactions *in vitro.*[85]

1.5 Toward 3D culture

Although classical 2D and suspension systems can provide very valuable information, cells cultured in 3D models might exhibit features that are closer to the complex conditions present in the original environment of cells, and thus are more realistic systems for translating the findings to *in vivo* applications. Thus, the development of suitable 3D environments for cell culturing is highly desired, which not only can benefit cell culture techniques, but also tissue engineering, a discipline that aims at regenerating tissues and creating study models through cell-material interactions.[86,87]

A large variety of different 3D approaches have been studied to recreate the extracellular original conditions of many different cell lines *in vitro*, such as the formation of spheroids, the use of de-cellularized tissues, cell printing, and the culture of cells in 3D matrices using a high selection of different types of materials, which are summarized in Table 1.1. They include natural and synthetic polymers, ceramics, metals, etc., all with their inherent advantages and disadvantages (around 380 cell lines, and 100 types of matrices and scaffolds of both organic and inorganic nature).[87]

3D Hydrogels are a particularly interesting strategy, which offers more realistic results than hard planar substrates such as standard polystyrene dishes, thus potentially revealing fundamental phenomena associated to cell behavior and providing tools for the expansion and directed differentiation in ways that are not possible with conventional culture substrates.[88] Hydrogels can be generated by using various materials, from natural polymers such as collagen, gelatin, elastin, silk fibroin, chitosan, fibrin, fibrinogen, etc.; to synthetic polymers, such as poly(glycolic acid) (PGA), poly(lactic acid) (PLA), or, poly(ethylene glycol) (PEG). Composites of both natural and synthetic substances are also being used. A scheme of a generic hydrogel used for cell culture can be seen in the figure below.

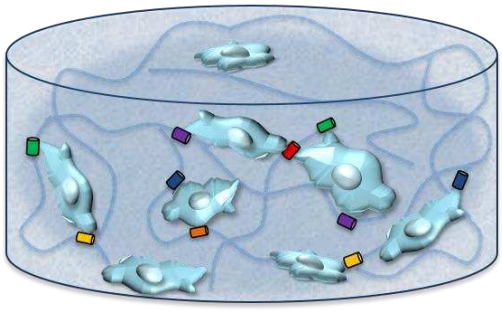

Figure 1.7 Schematic image of a generic hydrogel used for cell culture.

Table 1.1 Common scaffolds and matrices for 3D culturing cells.

Matrix/scaffold	Examples	Properties	Major applications
Natural structures	- Decellularized tissues - Structural collagen - Basement membranes such as laminin - Fibrin, alginate, chitosan, hyaluronic acid, silk fibroin, cellulose acetate, fibrinogen, gelatin, elastin, etc.	- Maximum resemblance to the *in vivo* conditions - Batch to batch variation - Favorable for cellular attachment, proliferation, and differentiation - Poor mechanical properties with variable physical properties - Immunogenic problems	- Induce specific cell and tissue responses, such as cell differentiation, by mimicking the native ECM
Synthetic polymers	- Hyaluronic acid (HA) - Poly(ethylene glycol) (PEG) - Self-assembling protein hydrogels - Poly(lactic-co-glycolic acid) (PLGA) - Polycaprolactone (PCL) - Polyurethane	- Possess predictable and reproducible chemical and physical properties - They can be combined with biomolecules such as growth factors and antibiotics	- Used as carriers for growth factors, drug delivery, gene transfection, etc. - Cell therapy
Hybrids	- PCL-chitosan - PLLA-Hydroxyapatite - Hydroxyapatite-bioglass-ceramic - Hydroxyapatite-collagen	- Possess predictable and reproducible physical properties (e.g. flexible mechanical properties) - Enhanced biodegradability	- Stimulate healing injuries and impart stability until the cells integrate with the native tissue - *In vitro* 3D models to study organ disease

Metals	- Magnesium and its alloys - Titanium and its alloys	- Lack of biological activity	- Osseointegration and *in vivo* bone formation when coated - Used as implanting materials for dental and orthopedic defects
Ceramics and bioactive glass	- Titanium - Hydroxyapatite - Bioactive silicate glass - Calcium phosphate glass	- Excellent cell support - Cells infiltrate and proliferate effectively in the porous structures	- High bone ingrowth and mineralization

1.5.1 Natural hydrogels

Polymers with a natural origin are often used in tissue engineering, as they are either components of the natural ECM or have similar properties. The most prominent one is collagen.

Collagen is the primary organic constituent of native tissues, and around a 90% of their 29 identified types in the human body are fibrillar. The most common one is type I collagen, as it is the major structural component of many tissues.[89] This type of collagen is commonly used in 3D culture systems due to its intrinsic properties, which allow cell adhesion without modification, present a native viscoelastic environment to resident cells, cytocompatibility, ease in processing, low-cost, and flexibility for alive cell manipulation. Besides, the structural properties of the resulting hydrogel such as pore size, ligand density, and stiffness can be varied by changing the concentration of collagen or introducing chemical cross-linking compounds.[90,91] These hydrogels have been thoroughly used as a model of cellular microenvironments for studies on topics ranging from mesenchymal stem cell differentiation[92] to carcinoma cell reprogramming.[93] However, this material has also important limitations, some of them shared with the majority of other natural materials, like its limited long-term stability, batch-to-batch variability, and low stiffness (stiffness higher than 1 kPa require extensive chemical crosslinking, which alters the degradability of collagen).[88] Despite these drawbacks, collagen is still an excellent choice for *in vitro* studies of cell behavior such as migration in a tissue-like environment[94,95] like the LNs, since it is their major structural component.

1.5.2 Synthetic hydrogels

Synthetic polymers are attractive due to the possibility to control their chemical, structural, and physical properties, when the proper fabrication methods are used. PEG is probably the most used synthetic material, which we also employed, as shown in the next chapters. PEG is a non-toxic, hydrophilic, and inert polymer, which can have a high water content when cross-linked into networks. Besides, it does not generally elicit an immune response, is resistant to non-specific protein adsorption, and exhibits rapid clearance from the body. Additionally, PEG may be used to encapsulate molecules in order to confer them non-toxicity or solubility. PEG hydrogels are chemically well-defined and can be modified by multiple chemical strategies to study different biological processes,[96–98] such as stem cell differentiation and migration of encapsulated T cells and DCs.[99,100]

1.6 Current 3D models of lymph node microenvironments

As mentioned before, technologies such as Dynabeads® allow to *in vitro* activate T cells. However, mimicking the 3D environment of a LN, the organ where this process takes place, suppose a challenge due to variables such as the high level of complexity resulting from the variety of cell types, the highly organized stromal and lymphoid structure, the rapid cellular motility of lymphocytes and DCs, and the staggering cell density. Nowadays, engineering a LN is more complex than engineering larger organs like the heart or kidneys.[28] Yet, the creation of an artificial *ex vivo* site for culturing immune cells could be a powerful strategy to manipulate their behavior prior to adoptive immunotherapy.[100]

A few approaches have been used to recreate the SLO environment with goals such as the achievement of better models to study the role of different immune cells in the human body, mimic the tumor microenvironment, and provide tissue engineering platforms for new ACT, resulting in improvements in tissue engineering and immunotherapies.

1.6.1 3D scaffolds

Different 3D scaffolds have been investigated to mimic primary and secondary lymphatic organs and/or their function. For example, a **sponge-like collagenous** hydrogel was used to transplant a thymus-derived stromal cell line and DCs into mice renal subcapsular spaces, proving the generation of lymphoid tissue-like organoids with distinct compartmentalized B and T cell clusters and a similar CD4+/CD8+ ratio than the natural SLOs.[101] These artificial structures were also proved to be transplantable to normal as well as immunodeficient mice lacking functional lymphocytes, where they supported the induction of antigen-specific secondary immune responses, which were maintained over time after, resulting in the development of memory B cells and long-lived plasma cells.[102]

A **polyurethane matrix embedded in type I collagen and Matrigel** in a ratio of 9:1 collagen/Matrigel was used as a tissue-engineered model of the stromal cell network of SLOs to study the effects of 3D culture and interstitial flow on regulating FRC morphology and CCL21 expression. Collagen matrices were also studied for these purposes, but their low stiffness prevented proper cell culturing unlike the systems with polyurethane, which provided sufficient tensile strength. These results suggest that although a 3D environment is important for FRC culture, to acquire *in vivo*-like properties, the matrix needs to be stiff enough to allow cell extension and withstand the contractile forces of FRCs. These cells were also showed to be responsive to the interstitial flow, reacting with an increased organization, CCL21 expression, and *in vitro* proliferation at high flows.[103]

To mimic natural lymphocyte migration along collagen fibers, a synthetic collagen-mimetic peptide that binds to lymphocytes via the α2β1 collagen receptor, was integrated into **polymerized alginate** scaffolds used as implants for cell delivery.[104] T cell migration through the matrix was observed under time-lapse microscopy, achieving similar velocities than those in lymphoid organs, averaging 8.9 μm/min.[105] These scaffolds were tried in a mouse breast cancer resection model and a multifocal ovarian cancer model, showing that the implants effectively support tumor-targeting T cells throughout resection beds and reduce tumor relapse compared to conventional delivery modalities.[104] With the same objective, **heparin-conjugated PEG hydrogels infused with collagen** showed mechanical stability and the potential to anchor supporting cytokines/chemokines. They supported intra-scaffold migration of murine primary T cells and DCs, and when the cytokine CCL21 was bound to the structure, the motility of the T cells could be quantitatively compared to the *in vivo* migration observed in native SLOs.[106] **Thermoreversible PEG-*g*-chitosan** gels, which have a transition from solution to gel at around 32°C, were used for steady T cell release. These gels were loaded with therapeutic T cells to be locally delivered to glioblastoma cells for brain tumor immunotherapy. In this case, T cell invasion through the gel and subsequent cytotoxicity to glioblastoma were assessed *in vitro*, using Matrigel as a control. T cells encapsulated in the gel retained their antiglioblastoma activity, and shown to be more effective in killing glioblastoma than those in Matrigel. This improvement was attributed to the optimal pore size of the gel allowing a better invasion of T cells, and showing again the importance of the porosity of the material.[107]

Polyisocyanopeptide hydrogels were studied for *in vitro* expansion and *in vivo* local delivery of pre-activated T cells, finding higher rates of survival and expansion of T cells. The reversible thermo-sensitive gelation at temperatures above 16°C of these scaffolds favored a straightforward recovery of cells, and caused the instant gelation of the hydrogels when subcutaneously injected *in vivo*. Cells encapsulated in the gels egressed gradually and migrated into distant organs, showing that this material can be used to locally deliver cells within a supportive environment.[108] Another strategy to facilitate the expansion of T cells was the use of **3D-printed polycaprolactone** lattices with highly organized micron-scale architectures, similar to 3D polystyrene. This scaffold was functionalized via plasma polymerization to bind mAbs that trigger the expansion of therapeutic human T cell subsets.[109] **Alginate hydrogel tubes** were proposed as a novel cell culture technology to expand primary human T cells for adoptive immunotherapy. This system consisted in culturing T cells in microscale alginate hydrogel tubes with the objective of protecting cells from hydrodynamic stresses, ensuring an efficient mass transport, and controlling cell aggregation. It was observed that the alginate tubes produced controllable mono-dispersed cell masses and the negative effects caused by strong hydrodynamic conditions were reduced, allowing to scale up the culture volume without changes in the growth rate.[110]

Finally, in a different approach, **3D microfluidic tumor microenvironment models of PDMS** were used to study the immunosuppressive potential of monocytes towards hepatitis B virus-specific TCR T cells via PD-L1/PD-1 signaling. Interestingly, it was observed that, although the ability of the T cells to kill cancer cells was preserved regardless of the presence of monocytes in the 2D system, they produced a reduced cytotoxic activity in a 3D model, thus highlighting the differences between 2D and 3D systems.[111,112]

1.6.2 Bioreactors

Bioreactors are the most commonly used systems for the clinical use of ACT. Currently, there are different designs described, being the most utilized the static gas permeable culture bags, G-Rex bioreactors, WAVE bioreactors, and the CliniMACS Miltenyi Prodigy system, as shown in figure 1.8.[113]

Figure 1.8 A) G Rex flask, B) WAVE bioreactor, and C) Miltenyi Prodigy system. Images courtesy of A) WilsonWolf (USA), B) GE Healthcare Life Sciences (Japan), and C) CliniMACS Miltenyi Biotec (Germany).

Preliminary studies were performed with **G-Rex flasks**, which consist of standard cell culture flasks with a gas-permeable membrane at the base that supports large media volumes. These flasks were used for different applications such as the clinical manufacture of antigen-specific cytotoxic T lymphocytes (CTL) for ACT[114] or to achieve a simple method for a rapid expansion of TILs.[115] To fully optimize the efficiency of this system, the optimal cell seeding density, maximal cell output that could be achieved, volume of medium that would support maximal cell growth, and cell growth kinetics were studied. Thus, it was demonstrated that the optimized culture conditions were linearly scalable and adaptable as a closed system, simplifying the translation of cell-based therapeutics from the laboratories to the clinics.[116]

To achieve a reproducible and effective process with an accurate control of critical variables such as pH or media flow, new bioreactor systems have been described such as the WAVE bioreactor or the CliniMACS Miltenyi Prodigy system.

The **WAVE bioreactor** uses disposable, transparent, sterile culture bags that allow media perfusion, harvest, sampling, and gas exchange, resting over a tray that can be heated and agitated in different rocking angles and rates. The system can be programmed to add or remove culture media and allows high cell densities.[117] Moreover, R.P. Somerville et al.[118] developed a rapid expansion protocol for TILs and genetically modified peripheral blood lymphocytes under GMP conditions, producing relevant numbers of T cells for clinical trials. They compared the efficacy of the WAVE bioreactor protocol with the standard static gas permeable culture bags using pre-stimulated T cells with feeder cells, anti-CD3, and IL-2. No statistical differences were shown in the fold expansions achieved by the two systems, therefore proving that the WAVE bioreactor is a valid alternative to the static culture bags in terms of cell quantities. Nevertheless, differences in the generated cell phenotypes were observed, which could impact the frequency and durability of clinical responses.[118]

Following a similar protocol, TILs from melanoma patients were expanded in the WAVE bioreactor and in traditional static culture methods (T-flasks or gas-permeable bags). Cell viability, final cell number, phenotype, and effector function were measured. In this case, a rapid expansion of TILs was also achieved in the WAVE bioreactor, but no phenotypic, nor specificity differences between processes were detected.[117]

The WAVE bioreactor has also been used to expand other types of cells such as NK cells, CIK cells, and DCs, confirming to be safe and sterile. It showed a significant potential in CIK and NK cell cultivation. Specifically, the viability of both cell types was significantly higher in the WAVE bioreactor than in standard cultures. Moreover, the bioreactor could increase the quantities of CD8+ T cells and CD3+CD56+ T cells, simultaneously suppressing the growth of regulatory T cells in expanded CIK cell populations. Nevertheless, no significant differences were observed in DC cultivation in comparison with the standard methods. This result could be a signal that the WAVE bioreactor might not be a favorable method for the cultivation of adherent cells such as DCs.[119]

The most recent device developed is the **CliniMACS Prodigy system** (Miltenyi Biotec, Germany), which is the first computer controlled unit that automates each of the required processing steps in a completely closed system. It has been approved to be used in cell separation procedures and for the selection and culture of antigen-reactive T cells. Due to the short time that this system has been available, most of the investigations have been directed to optimize the protocols for each application and demonstrate the robustness and reproducibility of the system.[120–123] For example, it was used to separate primary human NK cells, which were further used outside the instrument to optimize an expansion protocol that contained NK cells modified to express CARs against CD123, a common marker for acute myeloid leukemia (AML). More interestingly, the efficiency of the Prodigy system has already been proven for the production of CAR-T cells,[124] enormously simplifying a process that required multiple open processing steps into a closed-system process.

The system was also used to prepare genetically engineered anti-CD20 specific CAR T cells in less than 2 weeks.[123] The robustness and reproducibility was strongly assessed by using different conditions, including various operators. Although this process had already been tested with healthy donors,[121,122] this was the first time that it was assessed using lymphoma or melanoma patient material. Interestingly, the results obtained from patients were comparable to those of healthy donors with respect to cell composition, phenotype, and function.[123]

The CliniMACS Prodigy was also tested for CD45RA depletion. The adoptive transfer of alloreactivity-depleted donor T cells is supposed to serve to accelerate immune reconstitution, surveillance, and eradication of residual leukemia cells. CD45RA-depleted donor lymphocyte infusion was studied to avoid lethal graft-versus-host disease (GVHD) produced by haplo-identical (family) donors in patients who needed a stem cell transplantation. The quality and robustness of the process and the generated product shows promise to be used in clinical set-ups.[125]

1.6.3 Combined systems

A disposable **miniaturized bioreactor** in combination with macroporous **agarose hydrogels**, which supported the spreading of primed DCs prior to its integration into the bioreactor, was used as a device to recreate the human LN environment *in vitro*. This system provided wide ranges of cell feeding rates, gas supply, and cell recycling, resulting in T cell clustering which suggests functionality.[126] This same strategy was also used with the objective of studying the interactions between mesenchymal stromal cells, known for their high immune modulatory capacity, and immune cells. Rat LN cells and allogeneic bone marrow-derived mesenchymal stromal cells were seeded within the agarose matrix of the bioreactor. A clear suppressive effect of the stromal cells on the pro-inflammatory cytokine release produced by the immune cells, which were stimulated with concanavalin A, was detected, together with a significant increase in stromal cell proliferation due to the presence of immune cells.[127]

1.7 Objectives

The main objective of this PhD thesis is to obtain a versatile 3D platform to be used as 3D culture system of immune cells for i) mimicking the ECM of SLO in order to faithfully reproduce the behavior of immune cells, ii) improving the proliferation rates currently achieved with suspension cultures, and iii) tuning the differentiation pathways taken by the cells affecting the resulting phenotypes.

With these goals, we aim at helping to overcome current limitations of ACT providing high immune cell expansion rates of relevant phenotypes and fabricating a model platform. Such platform could be used for different applications such as the study of the mechanisms that rule the immune responses, immune cell delivery (by implantation of the scaffold), and analyze the responses of the immune cells under different physicochemical properties of their environment (e.g. stiffness), which would be modified *in situ* through the application of different external stimuli (e.g. complexing agents, temperature, etc.).

To carry out these general objectives, we have focused on the following specific tasks, which are organized in five different experimental chapters:

- Study the current commercially available systems for CD4+ T cell activation, proliferation and differentiation (Chapter 2).
- Design, synthesis, and characterization of a 3D matrix aimed at mimicking the original ECM of the LNs in order to study CD4+ T cell proliferation and differentiation (Chapter 3).
- Culture of PBMCs in the 3D matrix presented in the previous chapters and pre-clinical assessment of the expanded cells against tumor cells using bifunctional antibodies (Chapter 4).
- Optimization of the proposed 3D matrix as bioink for 3D printing. The resulting scaffolds are applied for both CD4+ T cells and PBMCs culture (Chapter 5).

1.8 References

1. Farkona, S., Diamandis, E. P. & Blasutig, I. M. Cancer immunotherapy: the beginning of the end of cancer? *BMC Med.* **14**, 73 (2016).
2. Emens, L. A. *et al.* Cancer immunotherapy: Opportunities and challenges in the rapidly evolving clinical landscape. *Eur. J. Cancer* **81**, 116–129 (2017).
3. Coley, W. B. The treatment of malignant tumors by repeated inoculations of erysipelas. With a report of ten original cases. 1893. *Clin. Orthop. Relat. Res.* 3–11 (1991).
4. Larson, C. *et al.* Going viral: a review of replication-selective oncolytic adenoviruses. *Oncotarget* **6**, 19976–19989 (2015).
5. Morales, A., Eidinger, D. & Bruce, A. W. Intracavitary Bacillus Calmette-Guerin in the treatment of superficial bladder tumors. *J. Urol.* **116**, 180–183 (1976).
6. Old, L. J., Clarke, D. A. & Benacerraf, B. Effect of Bacillus Calmette-Guerin infection on transplanted tumours in the mouse. *Nature* **184,** 291–292 (1959).
7. Isaacs, A. & Lindenmann, J. Virus interference. I. The interferon. *Proc. R. Soc. London. Ser. B, Biol. Sci.* **147**, 258–267 (1957).
8. Isaacs, A., Lindenmann, J. & Valentine, R. C. Virus interference. II. Some properties of interferon. *Proc. R. Soc. London. Ser. B, Biol. Sci.* **147**, 268–273 (1957).
9. Decker, W. K. *et al.* Cancer Immunotherapy: Historical Perspective of a Clinical Revolution and Emerging Preclinical Animal Models. *Front. Immunol.* **8**, 829 (2017).
10. Graham, J. B. & Graham, R. M. The effect of vaccine on cancer patients. *Surg. Gynecol. Obstet.* **109**, 131–138 (1959).
11. Miller, J. F., Mitchell, G. F. & Weiss, N. S. Cellular basis of the immunological defects in thymectomized mice. *Nature* **214**, 992–997 (1967).
12. Steinman, R. M. & Cohn, Z. A. Identification of a novel cell type in peripheral lymphoid organs of mice. *J. Exp. Med.* **137**, (1973).
13. Zinkernagel, R. M. & Doherty, P. C. Restriction of in vitro T cell-mediated cytotoxicity in lymphocytic choriomeningitis within a syngeneic or semiallogeneic system. *Nature* **248**, 701–702 (1974).
14. Kiessling, R., Klein, E. & Wigzell, H. 'Natural' killer cells in the mouse. I. Cytotoxic cells with specificity for mouse Moloney leukemia cells. Specificity and distribution according to genotype. *Eur. J. Immunol.* **5**, 112–117 (1975).
15. Kiessling, R., Klein, E., Pross, H. & Wigzell, H. 'Natural' killer cells in the mouse. II. Cytotoxic cells with specificity for mouse Moloney leukemia cells. Characteristics of the killer cell. *Eur. J. Immunol.* **5**, 117–121 (1975).
16. Talpaz, M., McCredie, K. B., Mavligit, G. M. & Gutterman, J. U. Leukocyte interferon-induced myeloid cytoreduction in chronic myelogenous leukemia. *Blood* **62**, 689–692 (1983).

17. Hodi, F. S. *et al.* Improved survival with ipilimumab in patients with metastatic melanoma. *N. Engl. J. Med.* **363**, 711–723 (2010).

18. Kantoff, P. W. *et al.* Sipuleucel-T immunotherapy for castration-resistant prostate cancer. *N. Engl. J. Med.* **363**, 411–422 (2010).

19. Eshhar, Z., Waks, T., Gross, G. & Schindler, D. G. Specific activation and targeting of cytotoxic lymphocytes through chimeric single chains consisting of antibody-binding domains and the gamma or zeta subunits of the immunoglobulin and T-cell receptors. *Proc. Natl. Acad. Sci. U. S. A.* **90**, 720–724 (1993).

20. Jensen, M. C. *et al.* Antitransgene rejection responses contribute to attenuated persistence of adoptively transferred CD20/CD19-specific chimeric antigen receptor redirected T cells in humans. *Biol. Blood Marrow Transplant.* **16**, 1245–1256 (2010).

21. Buning, H., Uckert, W., Cichutek, K., Hawkins, R. E. & Abken, H. Do CARs need a driver's license? Adoptive cell therapy with chimeric antigen receptor-redirected T cells has caused serious adverse events. *Hum. Gene Ther.* **21**, 1039–1042 (2010).

22. Kalos, M. *et al.* T cells with chimeric antigen receptors have potent antitumor effects and can establish memory in patients with advanced leukemia. *Sci. Transl. Med.* **3** (2011).

23. Porter, D. L. *et al.* Chimeric antigen receptor T cells persist and induce sustained remissions in relapsed refractory chronic lymphocytic leukemia. *Sci. Transl. Med.* **7** (2015).

24. Grupp, S. A. *et al.* Chimeric antigen receptor-modified T cells for acute lymphoid leukemia. *N. Engl. J. Med.* **368**, 1509–1518 (2013).

25. Garfall, A. L. *et al.* Chimeric Antigen Receptor T Cells against CD19 for Multiple Myeloma. *N. Engl. J. Med.* **373**, 1040–1047 (2015).

26. Haanen, J. B. A. G. & Robert, C. Immune Checkpoint Inhibitors. *Prog. tumor Res.* **42**, 55–66 (2015).

27. Velcheti, V. & Schalper, K. Basic Overview of Current Immunotherapy Approaches in Cancer. *Am. Soc. Clin. Oncol. Educ. book. Am. Soc. Clin. Oncol. Annu. Meet.* **35**, 298–308 (2016).

28. Cupedo, T., Stroock, A. & Coles, M. Application of tissue engineering to the immune system: development of artificial lymph nodes. *Front. Immunol.* **3**, 343 (2012).

29. Ruddle, N. H. & Akirav, E. M. Secondary lymphoid organs: responding to genetic and environmental cues in ontogeny and the immune response. *J. Immunol.* **183**, 2205–2212 (2009).

30. Acosta Davila, J. A. & Hernandez De Los Rios, A. An Overview of Peripheral Blood Mononuclear Cells as a Model for Immunological Research of Toxoplasma gondii and Other Apicomplexan Parasites. *Frontiers in cellular and infection microbiology* **9**, 24 (2019).

31. Kishton, R. J., Sukumar, M. & Restifo, N. P. Metabolic Regulation of T Cell Longevity and Function in Tumor Immunotherapy. *Cell Metab.* **26**, 94–109 (2017).

32. Sadelain, M., Riviere, I. & Riddell, S. Therapeutic T cell engineering. *Nature* **545**, 423–431 (2017).

33. Ghassemi, S. *et al.* Reducing Ex Vivo Culture Improves the Antileukemic Activity of Chimeric Antigen Receptor (CAR) T Cells. *Cancer Immunol. Res.* **6**, 1100–1109 (2018).

34. Willard-Mack, C. L. Normal structure, function, and histology of lymph nodes. *Toxicol. Pathol.* **34**, 409–424 (2006).

35. Cyster, J. G. Chemokines, sphingosine-1-phosphate, and cell migration in secondary lymphoid organs. *Annu. Rev. Immunol.* **23**, 127–159 (2005).

36. van de Pavert, S. A. & Mebius, R. E. New insights into the development of lymphoid tissues. *Nat. Rev. Immunol.* **10**, 664–674 (2010).

37. Crivellato, E., Vacca, A. & Ribatti, D. Setting the stage: an anatomist's view of the immune system. *Trends Immunol.* **25**, 210–217 (2004).

38. Acton, S. E. & Reis e Sousa, C. Dendritic cells in remodeling of lymph nodes during immune responses. *Immunol. Rev.* **271**, 221–229 (2016).

39. Restifo, N. P., Dudley, M. E. & Rosenberg, S. A. Adoptive immunotherapy for cancer: harnessing the T cell response. *Nat. Rev. Immunol.* **12**, 269–281 (2012).

40. Rosenberg, S. A. *et al.* Durable complete responses in heavily pretreated patients with metastatic melanoma using T-cell transfer immunotherapy. *Clin. Cancer Res.* **17**, 4550–4557 (2011).

41. Robbins, P. F. *et al.* Tumor regression in patients with metastatic synovial cell sarcoma and melanoma using genetically engineered lymphocytes reactive with NY-ESO-1. *J. Clin. Oncol.* **29**, 917–924 (2011).

42. Kochenderfer, J. N. *et al.* Eradication of B-lineage cells and regression of lymphoma in a patient treated with autologous T cells genetically engineered to recognize CD19. *Blood* **116**, 4099–4102 (2010).

43. Brentjens, R. J. *et al.* Safety and persistence of adoptively transferred autologous CD19-targeted T cells in patients with relapsed or chemotherapy refractory B-cell leukemias. *Blood* **118**, 4817–4828 (2011).

44. Yang, F. *et al.* Adoptive Cellular Therapy (ACT) for Cancer Treatment BT - Progress in Cancer Immunotherapy. in (ed. Zhang, S.) 169–239 (Springer Netherlands, 2016).

45. Schmidt-Wolf, I. G. *et al.* Phase I clinical study applying autologous immunological effector cells transfected with the interleukin-2 gene in patients with metastatic renal cancer, colorectal cancer and lymphoma. *Br. J. Cancer* **81**, 1009–1016 (1999).

46. Nwangwu, C. A., Weiher, H. & Schmidt-Wolf, I. G. H. Increase of CIK cell efficacy by upregulating cell surface MICA and inhibition of NKG2D ligand shedding in multiple myeloma. *Hematol. Oncol.* **35**, 719–725 (2017).

47. Sangiolo, D. Cytokine Induced Killer Cells as Promising Immunotherapy for Solid Tumors. *J. Cancer* **2**, 363–368 (2011).

48. Gao, X. *et al.* Cytokine-Induced Killer Cells As Pharmacological Tools for Cancer Immunotherapy. *Front. Immunol* **8**, (2017).

49. Feldman, S. A., Assadipour, Y., Kriley, I., Goff, S. L. & Rosenberg, S. A. Adoptive Cell Therapy--Tumor-Infiltrating Lymphocytes, T-Cell Receptors, and Chimeric Antigen Receptors. *Semin. Oncol.* **42**, 626–639 (2015).

50. Goff, S. L. *et al.* Tumor infiltrating lymphocyte therapy for metastatic melanoma: analysis of tumors resected for TIL. *J. Immunother.* **33**, 840–847 (2010).

51. Ikeda, H. T-cell adoptive immunotherapy using tumor-infiltrating T cells and genetically engineered TCR-T cells. *Int. Immunol.* **28**, 349–353 (2016).

52. Morgan, R. A. *et al.* Cancer regression in patients after transfer of genetically engineered lymphocytes. *Science* **314**, 126–129 (2006).

53. Spear, T. T., Evavold, B. D., Baker, B. M. & Nishimura, M. I. Understanding TCR affinity, antigen specificity, and cross-reactivity to improve TCR gene-modified T cells for cancer immunotherapy. *Cancer Immunol. Immunother.* (2019).

54. Gross, G., Waks, T. & Eshhar, Z. Expression of immunoglobulin-T-cell receptor chimeric molecules as functional receptors with antibody-type specificity. *Proc. Natl. Acad. Sci. U. S. A.* **86**, 10024–10028 (1989).

55. Park, T. S., Rosenberg, S. A. & Morgan, R. A. Treating cancer with genetically engineered T cells. *Trends Biotechnol.* **29**, 550–557 (2011).

56. Davila, M. L. *et al.* Efficacy and toxicity management of 19-28z CAR T cell therapy in B cell acute lymphoblastic leukemia. *Sci. Transl. Med.* **6** (2014).

57. Porter, D. L., Levine, B. L., Kalos, M., Bagg, A. & June, C. H. Chimeric antigen receptor-modified T cells in chronic lymphoid leukemia. *N. Engl. J. Med.* **365**, 725–733 (2011).

58. Maude, S. L. *et al.* Chimeric antigen receptor T cells for sustained remissions in leukemia. *N. Engl. J. Med.* **371**, 1507–1517 (2014).

59. Sharma, P. & Kranz, D. M. Recent advances in T-cell engineering for use in immunotherapy. *F1000Research* **5**, (2016).

60. Zarour, H. M. & Ferrone, S. Cancer immunotherapy: Progress and challenges in the clinical setting. *Eur. J. Immunol.* **41**, 1510–1515 (2011).

61. Oiseth, S. & Aziz, M. Cancer immunotherapy: a brief review of the history, possibilities, and challenges ahead. *J. Cancer Metastasis Treat.* **3**, 250 (2017).

62. Song, W., Musetti, S. N. & Huang, L. Nanomaterials for cancer immunotherapy. *Biomaterials* **148**, 16–30 (2017).

63. Schuster, S. J. *et al.* Vaccination With Patient-Specific Tumor-Derived Antigen in First Remission Improves Disease-Free Survival in Follicular Lymphoma. *J. Clin. Oncol.* **29**, 2787–2794 (2011).

64. Schwartzentruber, D. J. *et al.* gp100 peptide vaccine and interleukin-2 in patients with advanced melanoma. *N. Engl. J. Med.* **364**, 2119–2127 (2011).

65. Sahin, U. & Tureci, O. Personalized vaccines for cancer immunotherapy. *Science*

359, 1355–1360 (2018).

66. Kimiz-Gebologlu, I., Gulce-Iz, S. & Biray-Avci, C. Monoclonal antibodies in cancer immunotherapy. *Mol. Biol. Rep.* **45**, 2935–2940 (2018).

67. Sathyanarayanan, V. & Neelapu, S. S. Cancer immunotherapy: Strategies for personalization and combinatorial approaches. *Mol. Oncol.* **9**, 2043–2053 (2015).

68. Oldham, R. K. & Dillman, R. O. Monoclonal antibodies in cancer therapy: 25 years of progress. *J. Clin. Oncol.* **26**, 1774–1777 (2008).

69. Malissen, B. & Bongrand, P. Early T cell activation: integrating biochemical, structural, and biophysical cues. *Annu. Rev. Immunol.* **33**, 539–561 (2015).

70. Roh, K.-H. Artificial Methods for T Cell Activation: Critical Tools in T Cell Biology and T Cell Immunotherapy. *Adv. Exp. Med. Biol.* **1064**, 207–219 (2018).

71. Delcassian, D., Sattler, S. & Dunlop, I. E. T cell immunoengineering with advanced biomaterials. *Integr. Biol. (Camb).* **9**, 211–222 (2017).

72. Dudley, M. E., Wunderlich, J. R., Shelton, T. E., Even, J. & Rosenberg, S. A. Generation of tumor-infiltrating lymphocyte cultures for use in adoptive transfer therapy for melanoma patients. *J. Immunother.* **26**, 332–342 (2003).

73. Robbins, P. F. *et al.* A pilot trial using lymphocytes genetically engineered with an NY-ESO-1-reactive T-cell receptor: long-term follow-up and correlates with response. *Clin. Cancer Res.* **21**, 1019–1027 (2015).

74. Kochenderfer, J. N. *et al.* Donor-derived CD19-targeted T cells cause regression of malignancy persisting after allogeneic hematopoietic stem cell transplantation. *Blood* **122**, 4129–4139 (2013).

75. Brudno, J. N. *et al.* Allogeneic T Cells That Express an Anti-CD19 Chimeric Antigen Receptor Induce Remissions of B-Cell Malignancies That Progress After Allogeneic Hematopoietic Stem-Cell Transplantation Without Causing Graft-Versus-Host Disease. *J. Clin. Oncol.* **34**, 1112–1121 (2016).

76. Kochenderfer, J. N. *et al.* Chemotherapy-refractory diffuse large B-cell lymphoma and indolent B-cell malignancies can be effectively treated with autologous T cells expressing an anti-CD19 chimeric antigen receptor. *J. Clin. Oncol.* **33**, 540–549 (2015).

77. Tumeh, P. C. *et al.* The impact of ex vivo clinical grade activation protocols on human T-cell phenotype and function for the generation of genetically modified cells for adoptive cell transfer therapy. *J. Immunother.* **33**, 759–768 (2010).

78. Trickett, A. & Kwan, Y. L. T cell stimulation and expansion using anti-CD3/CD28 beads. *J. Immunol. Methods* **275**, 251–255 (2003).

79. Tabdanov, E. *et al.* Micropatterning of TCR and LFA-1 ligands reveals complementary effects on cytoskeleton mechanics in T cells. *Integr. Biol.* **7**, 1272–1284 (2015).

80. Hashimoto-Tane, A. & Saito, T. Dynamic Regulation of TCR-Microclusters and the Microsynapse for T Cell Activation. *Front. Immunol.* **7**, 255 (2016).

81. Delcassian, D. *et al.* Nanoscale ligand spacing influences receptor triggering in T

cells and NK cells. *Nano Lett.* **13**, 5608–5614 (2013).

82. Matic, J., Deeg, J., Scheffold, A., Goldstein, I. & Spatz, J. P. Fine tuning and efficient T cell activation with stimulatory aCD3 nanoarrays. *Nano Lett.* **13**, 5090–5097 (2013).

83. Guasch, J., Muth, C. A., Diemer, J., Riahinezhad, H. & Spatz, J. P. Integrin-Assisted T-Cell Activation on Nanostructured Hydrogels. *Nano Lett.* **17**, 6110–6116 (2017).

84. Adutler-Lieber, S. *et al.* Substrate-bound CCL21 and ICAM1 combined with soluble IL-6 collectively augment the expansion of antigen-specific murine CD4(+) T cells. *Blood Adv.* **1**, 1016–1030 (2017).

85. Cai, H. *et al.* Full control of ligand positioning reveals spatial thresholds for T cell receptor triggering. *Nat. Nanotechnol.* **13**, 610–617 (2018).

86. Pérez del Río, E., Martinez Miguel, M., Veciana, J., Ratera, I. & Guasch, J. Artificial 3D Culture Systems for T Cell Expansion. *ACS Omega* **3**, 5273–5280 (2018).

87. Ravi, M., Paramesh, V., Kaviya, S. R., Anuradha, E. & Solomon, F. D. P. 3D cell culture systems: advantages and applications. *J. Cell. Physiol.* **230**, 16–26 (2015).

88. Caliari, S. R. & Burdick, J. A. A practical guide to hydrogels for cell culture. *Nat. Methods* **13**, 405–414 (2016).

89. Shoulders, M. D. & Raines, R. T. Collagen structure and stability. *Annu. Rev. Biochem.* **78**, 929–958 (2009).

90. Baker, E. L., Bonnecaze, R. T. & Zaman, M. H. Extracellular matrix stiffness and architecture govern intracellular rheology in cancer. *Biophys. J.* **97**, 1013–1021 (2009).

91. Baker, E. L., Srivastava, J., Yu, D., Bonnecaze, R. T. & Zaman, M. H. Cancer cell migration: integrated roles of matrix mechanics and transforming potential. *PLoS One* **6** (2011).

92. Kuo, C. K. & Tuan, R. S. Mechanoactive tenogenic differentiation of human mesenchymal stem cells. *Tissue Eng. Part A* **14**, 1615–1627 (2008).

93. Ali, M. Y., Chuang, C.-Y. & Saif, M. T. A. Reprogramming cellular phenotype by soft collagen gels. *Soft Matter* **10**, 8829–8837 (2014).

94. Kim, H.-D. *et al.* Epidermal growth factor-induced enhancement of glioblastoma cell migration in 3D arises from an intrinsic increase in speed but an extrinsic matrix- and proteolysis-dependent increase in persistence. *Mol. Biol. Cell* **19**, 4249–4259 (2008).

95. Doyle, A. D., Carvajal, N., Jin, A., Matsumoto, K. & Yamada, K. M. Local 3D matrix microenvironment regulates cell migration through spatiotemporal dynamics of contractility-dependent adhesions. *Nat. Commun.* **6**, 8720 (2015).

96. Peppas, N. A., Keys, K. B., Torres-Lugo, M. & Lowman, A. M. Poly(ethylene glycol)-containing hydrogels in drug delivery. *J. Control. Release* **62**, 81–87 (1999).

97. Drury, J. L. & Mooney, D. J. Hydrogels for tissue engineering: scaffold design variables and applications. *Biomaterials* **24**, 4337–4351 (2003).

98. Peppas, N. A., Hilt, J. Z., Khademhosseini, A. & Langer, R. Hydrogels in Biology and Medicine: From Molecular Principles to Bionanotechnology. *Adv. Mater.* **18**, 1345–1360 (2006).

99. Kloxin, A. M., Kasko, A. M., Salinas, C. N. & Anseth, K. S. Photodegradable hydrogels for dynamic tuning of physical and chemical properties. *Science* **324**, 59–63 (2009).

100. Singh, A. & Peppas, N. A. Hydrogels and scaffolds for immunomodulation. *Adv. Mater.* **26**, 6530–6541 (2014).

101. Suematsu, S. & Watanabe, T. Generation of a synthetic lymphoid tissue-like organoid in mice. *Nat. Biotechnol.* **22**, 1539–1545 (2004).

102. Okamoto, N., Chihara, R., Shimizu, C., Nishimoto, S. & Watanabe, T. Artificial lymph nodes induce potent secondary immune responses in naive and immunodeficient mice. *J. Clin. Invest.* **117**, 997–1007 (2007).

103. Tomei, A. A., Siegert, S., Britschgi, M. R., Luther, S. A. & Swartz, M. A. Fluid flow regulates stromal cell organization and CCL21 expression in a tissue-engineered lymph node microenvironment. *J. Immunol.* **183**, 4273–4283 (2009).

104. Stephan, S. B. *et al.* Biopolymer implants enhance the efficacy of adoptive T-cell therapy. *Nat. Biotechnol.* **33**, 97–101 (2015).

105. Miller, M. J., Wei, S. H., Cahalan, M. D. & Parker, I. Autonomous T cell trafficking examined in vivo with intravital two-photon microscopy. *Proc. Natl. Acad. Sci. U. S. A.* **100**, 2604–2609 (2003).

106. Stachowiak, A. N. & Irvine, D. J. Inverse opal hydrogel-collagen composite scaffolds as a supportive microenvironment for immune cell migration. *J. Biomed. Mater. Res. A* **85**, 815–828 (2008).

107. Tsao, C.-T. *et al.* Thermoreversible poly(ethylene glycol)-g-chitosan hydrogel as a therapeutic T lymphocyte depot for localized glioblastoma immunotherapy. *Biomacromolecules* **15**, 2656–2662 (2014).

108. Weiden, J. *et al.* Injectable Biomimetic Hydrogels as Tools for Efficient T Cell Expansion and Delivery. *Front. Immunol.* **9**, 2798 (2018).

109. Delalat, B. *et al.* 3D printed lattices as an activation and expansion platform for T cell therapy. *Biomaterials* **140**, 58–68 (2017).

110. Lin, H. *et al.* Automated Expansion of Primary Human T Cells in Scalable and Cell-Friendly Hydrogel Microtubes for Adoptive Immunotherapy. *Adv. Healthc. Mater.* **7**, e1701297 (2018).

111. Lee, S. W. L. *et al.* Characterizing the Role of Monocytes in T Cell Cancer Immunotherapy Using a 3D Microfluidic Model. *Front. Immunol.* **9**, 416 (2018).

112. Boussommier-Calleja, A. *et al.* The effects of monocytes on tumor cell extravasation in a 3D vascularized microfluidic model. *Biomaterials* **198**, 180–193 (2019).

113. Iyer, R. K., Bowles, P. A., Kim, H. & Dulgar-Tulloch, A. Industrializing Autologous Adoptive Immunotherapies: Manufacturing Advances and Challenges. *Front. Med.*

5, 150 (2018).

114. Vera, J. F. *et al.* Accelerated production of antigen-specific T cells for preclinical and clinical applications using gas-permeable rapid expansion cultureware (G-Rex). *J. Immunother.* **33**, 305–315 (2010).

115. Jin, J. *et al.* Simplified method of the growth of human tumor infiltrating lymphocytes in gas-permeable flasks to numbers needed for patient treatment. *J. Immunother.* **35**, 283–292 (2012).

116. Bajgain, P. *et al.* Optimizing the production of suspension cells using the G-Rex 'M' series. *Mol. Ther. Methods Clin. Dev.* **1** (2014).

117. Sadeghi, A. *et al.* Large-scale bioreactor expansion of tumor-infiltrating lymphocytes. *J. Immunol. Methods* **364**, 94–100 (2011).

118. Somerville, R. P. T., Devillier, L., Parkhurst, M. R., Rosenberg, S. A. & Dudley, M. E. Clinical scale rapid expansion of lymphocytes for adoptive cell transfer therapy in the WAVE(R) bioreactor. *J. Transl. Med.* **10** (2012).

119. Meng, Y. *et al.* Rapid expansion in the WAVE bioreactor of clinical scale cells for tumor immunotherapy. *Hum. Vaccin. Immunother.* **14**, 2516–2526 (2018).

120. Kloss, S. *et al.* Optimization of Human NK Cell Manufacturing: Fully Automated Separation, Improved Ex Vivo Expansion Using IL-21 with Autologous Feeder Cells, and Generation of Anti-CD123-CAR-Expressing Effector Cells. *Hum. Gene Ther.* **28**, 897–913 (2017).

121. Priesner, C. *et al.* Automated Enrichment, Transduction, and Expansion of Clinical-Scale CD62L(+) T Cells for Manufacturing of Gene Therapy Medicinal Products. *Hum. Gene Ther.* **27**, 860–869 (2016).

122. Mock, U. *et al.* Automated manufacturing of chimeric antigen receptor T cells for adoptive immunotherapy using CliniMACS prodigy. *Cytotherapy* **18**, 1002–1011 (2016).

123. Lock, D. *et al.* Automated Manufacturing of Potent CD20-Directed Chimeric Antigen Receptor T Cells for Clinical Use. *Hum. Gene Ther.* **28**, 914–925 (2017).

124. Zhu, F. *et al.* Closed-system manufacturing of CD19 and dual-targeted CD20/19 chimeric antigen receptor T cells using the CliniMACS Prodigy device at an academic medical center. *Cytotherapy* **20**, 394–406 (2018).

125. Muller, N. *et al.* Generation of alloreactivity-reduced donor lymphocyte products retaining memory function by fully automatic depletion of CD45RA-positive cells. *Cytotherapy* **20**, 532–542 (2018).

126. Giese, C. *et al.* A human lymph node in vitro--challenges and progress. *Artif. Organs* **30**, 803–808 (2006).

127. Seifert, M. *et al.* Crosstalk between immune cells and mesenchymal stromal cells in a 3D bioreactor system. *Int. J. Artif. Organs* **35**, 986–995 (2012).

CHAPTER 2

3D commercial scaffolds applied to CD4+ T cell expansion*

*This work has been published with the reference: Pérez del Río, E., Martinez Miguel, M., Veciana, J., Ratera, I. & Guasch, J. Artificial 3D Culture Systems for T Cell Expansion. *ACS Omega* **3**, 5273–5280 (2018).

2.1 Introduction

Taking into account what was mentioned in the introduction, it becomes evident the interest of studying the effect of different types of materials with distinct properties as a scaffold for immune cell culture. To enhance T cell proliferation of therapeutic phenotypes, we first checked 3D commercially available systems. After a bibliographic and market study, the chosen platforms for immune cell culture were Matrigel (Corning, USA) and a 3D Polystyrene Scaffold (3D Biotek, USA).

On one hand, **Matrigel** is a well-defined gelatinous protein mixture extract prepared from the Engelbreth-Holm-Swarm (EHS) mouse sarcoma, a tumor with an abundant ECM that resembles basement membranes.[1] The major components of Matrigel are laminin, collagen IV, entactin/nidogen, and heparan sulfate proteoglycans, which provide both structural and signal transduction functions.[2] It shows a stiffness of 443 Pa,[3] which is similar to other ECM-based hydrogels, such as mixtures of collagen I and laminin (60:40)[4] and softer than typical synthetic hydrogels, such as polyethylene glycol dimethacrylate.[5]

On the other hand, the **3D polystyrene scaffold** consists of layers of parallel fibers with a diameter of 300 µm, arranged at 90° and offset to each other. The resulting pore size of this structure is 400 µm, providing a 100% connectivity within its structure which allows effective exchange of nutrients and waste between the media and the cells.[6]

Thus, these two platforms, Matrigel and the 3D polystyrene scaffold, have completely different characteristics. The 3D polystyrene scaffold only provides a physical support, without any chemical stimuli, high stiffness, and a very big pore size. In contrast, Matrigel is a natural hydrogel consisting of proteins and thus chemical stimuli, low stiffness, and a low pore size. These differences allowed us to explore the influence of the 3D scaffolds under extremely different conditions, but common biomaterials for different applications. Photographs and schemes of these two platforms can be seen in figure 2.1.

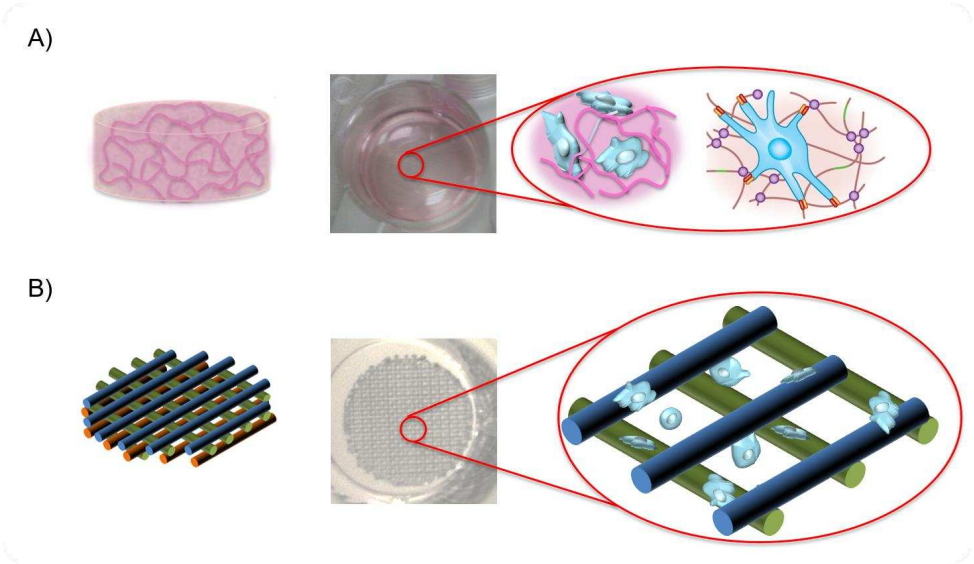

Figure 2.1 Photographs and schemes of A) Matrigel (Corning, USA) and B) Polystyrene Scaffolds (3D Biotek, USA).

Matrigel has been used in various 3D cell culture studies, mainly involving cancer cell types, such as mammary carcinoma,[7] tongue carcinoma,[8] and prostate carcinoma,[9] and also stem cells,[10] but to our knowledge, studies of T cells using Matrigel are limited to the analysis of their invasiveness and migration capacity. These assays showed that T cell migration is dependent on matrix metalloproteinase (MMP) secretion, through the correlation of MMP inhibitor's production and migration blocking in a dose-dependent manner.[11] Similarly, T lymphoblastoma cell migration was also shown to be dependent on MMPs secretion.[12] Immune cell infiltration assays were also performed to a 3D model consisting in tumor cell lines grown as floating 3D spheroids and embedded in Matrigel/collagen together with fibroblasts and immune cells, trying to mimic the active infiltration of human immune cells to a 3D tumor, for the study of the interaction between the tumor microenvironment and immune cells such as T and NK cells.[13]

Alternatively, polymer scaffolds are interesting for 3D cell cultures due to their multiple and varied fabrication techniques available[14], such as emulsion polymerization,[15] foaming,[16] phase separation,[17] electrospinning,[18] or 3D printing.[19] These techniques enable the production of scaffolds with controlled dimensions and a porous structure, both important characteristics for a suitable cell culture system. Given that plasma-treated polystyrene is an ubiquitous material for standard 2D cell culture, it is not surprising that polystyrene scaffolds have been developed to serve as 3D cell culture systems.[15–17] Such 3D polystyrene scaffolds were tested for the amplification of lymphoma cancer cells, incubating mantle cell lymphoma cells in the presence of neighboring stroma cells achieving a remarkable proliferation efficiency.[6] They were also used to study the macrophage response *in vitro* in comparison with the effects of a flat

polystyrene surface, finding that 3D nanofibrous substrates activated the intrinsic macrophage angiogenic function.[20] 3D polystyrene was also used for the study of stem cells, observing that the presence of carbonyl groups to polystyrene surfaces correlated well with successful adhesion of ECM proteins and sustaining ECM production of deposited human mesenchymal stem cells.[21] Finally, it was used as a platform for the xeno-free expansion and differentiation of induced pluripotent stem cells (hiPSCs).[22]

2.2 Objectives and strategy

The objective of this chapter was to study the influence of different 3D scaffolds to increase the T cell expansion of relevant phenotypes to contribute to the improvement of ACT. The strategy used consists of using the two platforms mentioned above, Matrigel and 3D polystyrene, to activate, expand, and tune the phenotypes of CD4+ T cells. CD4+ T cells were chosen between all the different immune cells types in order to reduce the biological variability and due to its abundance in the immune cell population. The effects of each 3D matrix in comparison with the standard static suspension cultures were analyzed, but also the differences between the two 3D systems, to better understand how the different variables and stimuli of both scaffolds affect immune culture.

2.3 CD4+ T cell activation study

As explained in chapter 1, section 1.4.1, *ex vivo* polyclonal activation of T cells has been performed by using the standard commercial artificial APCs, named Dynabeads, which are 4.5 µm diameter beads coated with the activating antibody anti-CD3 and the costimulatory antibody anti-CD28. To evaluate the effectiveness of the T cell activation, the amount of **IL-2** present in the culture media was measured. The IL-2 protein is an inflammatory cytokine responsible for multiple immunomodulatory tasks, such as the activation of T cells, trigger of natural killer cells, and inflammation.[23] Moreover, it is a very well characterized T cell growth factor that plays a crucial role in cell proliferation and determining the fate of the expanded T cells *in vitro* and *in vivo*.[24] Resting T cells do not express IL-2 receptors, but the receptors are rapidly expressed on T cells after activation. Interaction of IL-2 with the IL-2 receptor triggers T cell proliferation, and also leads to the *de novo* synthesis of IL-2 and expression of the IL-2 receptor. Synthetized IL-2 interacts on the same cells that produce it and on adjacent cells, acting through autocrine and paracrine mechanisms.[25] This means that, in principle, the higher the amount of IL-2 in the media, the more effective the activation of T cells and the greater the proliferation. Consequently, IL-2 is used in clinics to evaluate lymphocyte function. Here, it was used to evaluate the activation of CD4+ T cells in the 3D structures through a human IL-2 Quantikine enzyme-linked immunosorbent assay (ELISA) kit, together with a morphological study of the resulting cells for each condition. The results are presented below.

2.3.1 IL-2 ELISA measurements

An **ELISA** is a biochemistry assay which origins in 1971 from the hand of Engvall and Perlmann.[26] This assay allows the quantification of a ligand, normally a protein, present in a liquid sample by its immobilization in a solid-phase enzyme immunoassay and its further detection through the use of antibodies directed against the protein to measure.[27] CD4+ T cells activated with Dynabeads were cultured in three different environments, which consisted of a static suspension, 3D polystyrene scaffold, and Matrigel. To evaluate the activation of cells, which is a previous and necessary step to proliferation, the amount of the IL-2 present in the culture media was measured one day after seeding with a human IL-2 ELISA kit. A microplate pre-coated with a target-specific antibody is provided by the kit, where the IL-2 present in the sample is retained. Then, this is detected by the addition of the second antibody, and finally a substrate solution is added that reacts with the enzyme-antibody-target complex to produce a colorimetric measurable signal.

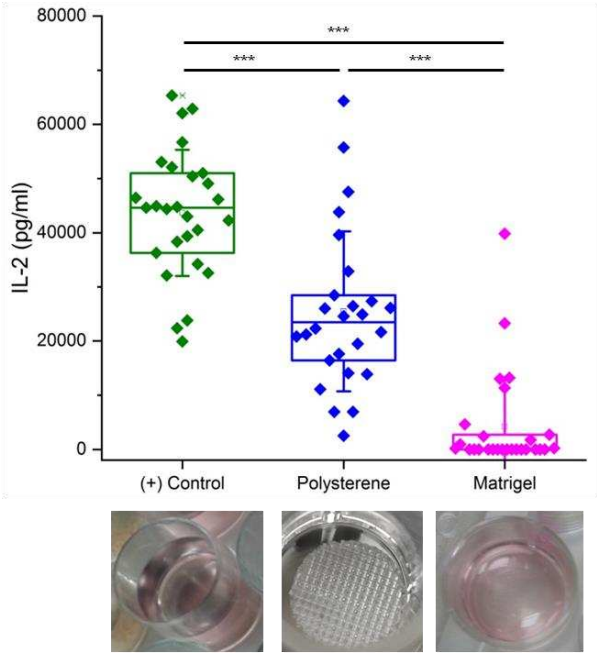

Figure 2.2 IL-2 secretion of CD4+ T cells seeded in suspension (positive control), a 3D polystyrene scaffold, and Matrigel one day after seeding. All cultures were stimulated with Dynabeads for activation. The results shown were obtained from N_{donors} = 9 and statistical significance was determined by the Mann-Whitney U test (*** $p < 0.001$).

CD4+ T cells activated with Dynabeads in suspension (positive control), i.e., without any 3D platform, showed a median value of 44.6 ng/ml of IL-2, with most measured values falling into the range between 36.3 and 51.0 ng/ml (percentiles Q-25 and Q-75), due to the intrinsic variability of primary samples. These values are significantly higher than those obtained in both the 3D polystyrene scaffold, with a median value of 23.5 ng/ml, and Matrigel, which shows negligible IL-2 results in the majority of samples. Although a real

low secretion cannot be discarded, unspecific adhesion of IL-2 to the matrices could also explain the observed results. Due to these unexpected results, more experiments were performed to evaluate the activation of T cells, like an analysis of cell morphology or the study of cell proliferation.

2.3.2 Cell Morphology

It is known that, prior to activation, cells exhibit a round morphology, while activated T cells show larger sizes and elongated shapes, compatible with the amoeboid migration mode.[28] So, various images were taken from the different cultures (negative and positive controls, 3D polystyrene, and Matrigel) by optical microscopy, in order to study the presence or not of these changes on cell morphology. The results can be seen in figure 2.3, where one representative image for each condition is presented. To quantify morphological changes, the area, perimeter, aspect radio (AR), and circularity of cells were analyzed using the FiJi (ImageJ) software.

The median area resulting of inactivated cells, i.e., without Dynabeads, was of 43.4 μm^2 (negative control), while cells activated in suspension (positive control) and in the 3D polystyrene scaffold exhibited significantly larger areas with median values of 114.8 and 109.2 μm^2, respectively. The median area of activated cells using Matrigel was of 41.3 μm^2 (figure 2.3.E). Similarly, perimeter and AR followed the tendencies observed for cell area (figures 2.3.F and 2.3.G). The median value of the cell perimeter of inactivated cells (negative control) and cells seeded in Matrigel was of 23.3 µm, while the ones of the positive control and 3D polystyrene scaffold increased to 40.2 and 37.9 µm, respectively. The AR of resting cells (negative control) was 7.3, which grew to 11.2 for cells activated in suspension (positive control) and in the 3D polystyrene scaffold. Cells activated on Matrigel showed an AR of 6.7. Alternatively, the circularity of cells, which is proportional to the area divided by the square of the perimeter, showed statistical changes in all activated cells in comparison with the negative control. Although the median values were similar (1.03 for the negative control and 1.05 for the rest of the cases), the variability of shapes was higher in the samples with activated cells, as represented by the larger box charts (figure 2.3.H). As expected, when T cells are activated, they express cell adhesion receptors that allow their spreading and adhesion to available substrates, such as vessels *in vivo*, resulting in different shapes and sizes in comparison with the completely spherical shape of the inactivated form.[29] The morphological differences observed in Matrigel compared to cells obtained in suspension or seeded in the 3D polystyrene scaffold could be explained by the truly 3D structure of Matrigel in comparison with the polystyrene,[30-32] where cells are not completely covered by the scaffold due to its large pore size. Additionally, the chemical input of Matrigel could also play a role through modifications on the phenotype obtained after proliferation.

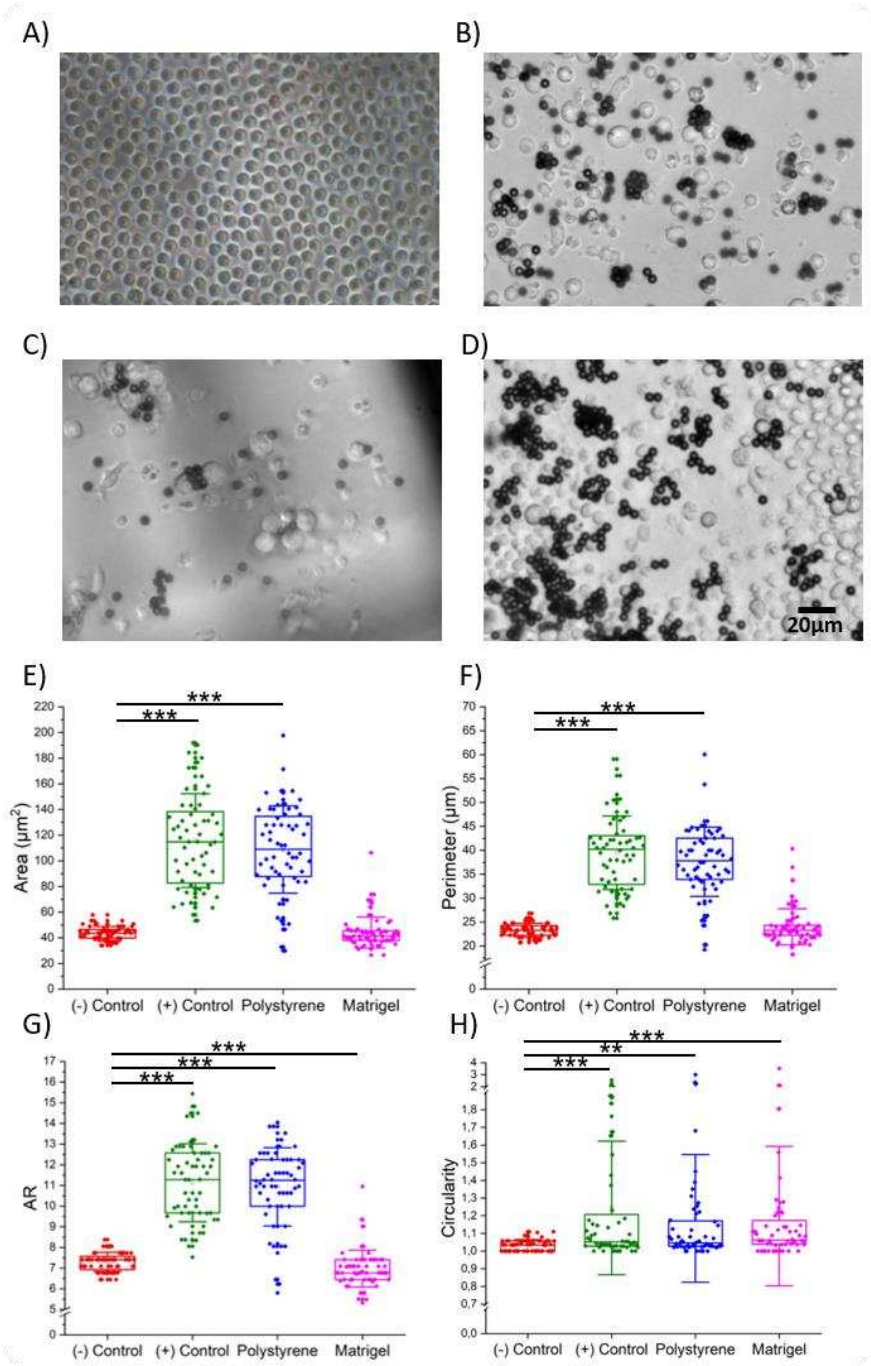

Figure 2.3 Representative optical images of CD4+ T cell cultures: A) Negative control (cells cultured without supply of Dynabeads), B) positive control (activated cells in suspension), C) in a 3D polystyrene scaffold and D) using Matrigel cells with supply of Dynabeads (dark spheres with a bright nucleus) in a 1:1 ratio for the three last environments. Analysis of cell morphometric parameters: E) Area, F) perimeter, G) aspect ratio (AR), and H) circularity were analyzed on day 2. The results shown were obtained from $N_{donors/condition} = 3$, with a minimum of $N_{cells/donor} = 20$. Statistical significance was determined by the Mann-Whitney U test (** $p < 0.01$, *** $p < 0.001$).

These results show that, although lower levels of IL-2 in suspension were measured from the samples with the 3D matrixes, cells seeded with Dynabeads acquired different conformations and sizes in comparison with inactivated cells (negative control, cells seeded without Dynabeads), suggesting that they are being properly activated.

2.4 CD4+ T cell proliferation study

Once the activation of CD4+ T cells seeded with Dynabeads in these 3D systems was confirmed, we analyzed the effect of each platform on the CD4+ T cells proliferation after five days of culture through a carboxyfluorescein succinimidyl ester (CFSE) cell proliferation kit (chapter 6, section 6.1.5).

2.4.1 CSFE analysis

CSFE is a cell permeable fluorescent staining dye that covalently binds via its succinimidyl group to intracellular molecules. Originally, it was developed as a fluorescent dye to label and track lymphocytes within animals for many months.[33] Further investigation showed that it could be also used to monitor lymphocyte proliferation, both *in vitro* and *in vivo*, due to the progressive halving of CFSE fluorescence with every completed cell division.[34] Nowadays, CFSE based tracking of the lymphocyte proliferation using flow cytometry is a powerful technique in immunology that allows to quantify the proliferation of labelled cells from 1 up to 10 divisions that cells undergo.[35]

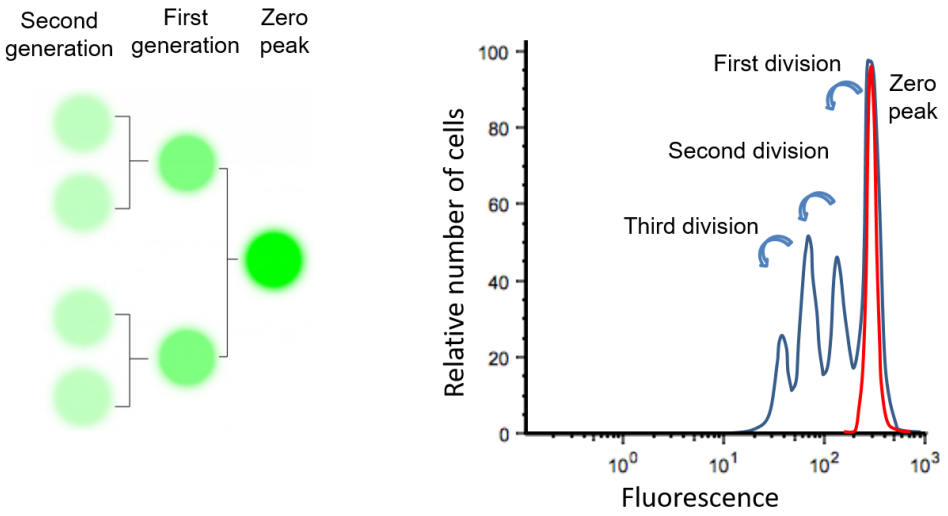

Figure 2.4 Representation of the basis behind the CSFE analysis.

This technique starts with the staining of the initial population, thus determining the maximum fluorescence, represented in figure 2.4 as the zero peak (red line). The cell populations stimulated to proliferate produce as many peaks as cell generations, reducing

the fluorescence inside the cells to half in each division as can be seen in figure 2.4 (blue line). The resulting graph is analyzed to achieve the proliferation parameters of the culture, allowing to assess T cell proliferation through the **expansion, replication, and proliferation indexes**. The expansion and replication indexes determine the fold-expansion of the whole population, and of responding cells respectively. A high value in these parameters correlates with a high quantity of cells after the proliferative process. The proliferation index is the number of divisions that cells from the original population have undergone divided by the number of divided cells. Thus, this parameter considers the number of responsive cells, i.e. a higher value correlates with a higher response to a proliferative stimulus. These three parameters are therefore relevant for cell therapy, showing how responsive the cells are to the proliferative stimulus, how much they divide after sensing this stimulus, and how many cells can finally be obtained.

2.4.2 Proliferation results

After five days of culture (figure 2.5.A), the replication index, which measures culture expansion of the responding cells, was of 19.1 for Matrigel, while the positive control and the 3D polystyrene scaffold were 12.6 and 15.1, respectively. These results indicate that the response of activated T cells was more effective in Matrigel samples than in the 3D polystyrene scaffold and the positive control. For the expansion index, Matrigel samples showed a median value of 11.2, while the suspension (positive control) exhibited an 8.9 and the 3D polystyrene scaffold an 11.1. In other words, for each million of cells seeded, Matrigel samples reached 11.2 and the 3D polystyrene scaffold 11.1 millions of cells, while in suspension 8.9 millions were obtained. Although the median value of the 3D polystyrene scaffold is similar to Matrigel, it does not show significant differences in the other indexes in comparison with the positive control as it does Matrigel. Finally, with a similar tendency than the replication index, Matrigel showed a median proliferation index value of 3.1 compared to the 2.6 and the 2.9 of suspension cells and the 3D polystyrene scaffold, respectively. Thus, the total number of divisions performed by the responding cells was significantly higher in Matrigel than in suspension.

In order to determine if the tendency observed for the 3D polystyrene to increase the CD4+ T cell proliferation parameters at day 5 improved with more time, proliferation analysis were performed at day 6 (figure 2.5.B). In this case, the replication index median increases from 19.8 to 29.8, the median value of the expansion index rises from 14.2 of the positive control to 22.1, and the proliferation index ascends from 3.1 to 3.4. In this occasion, statistically significant changes were obtained for cells seeded in 3D polystyrene scaffolds. Figure 2.5.C-D shows the diagrams of the peaks of fluorescence achieved for representative data points at days 5 and 6 respectively. The peaks corresponding to the firsts generations of proliferated cells are smaller when both Matrigel or Polystyrene are used, whereas the peaks of generations 5 are higher.

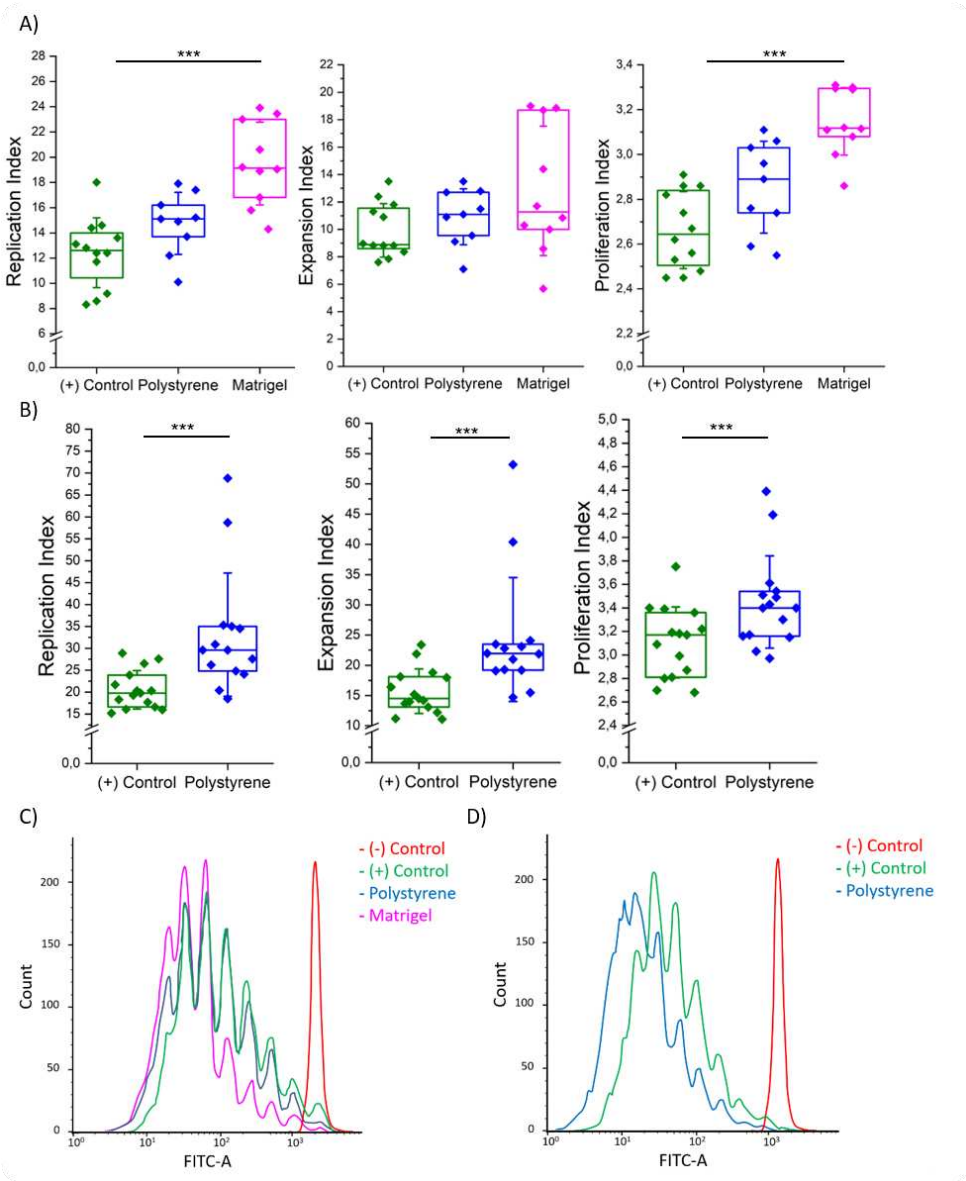

Figure 2.5 A) Raw data of the replication index (fold-expansion of the responding cells), expansion index (fold-expansion of the whole population), and proliferation index (average number of divisions among the responding cells) obtained of CD4+ T cells 5 days after seeding in Matrigel, 3D polystyrene scaffolds, and suspension (N_{donors} = 4, with a minimum of $N_{donors/condition}$ = 3). B) Proliferation analysis of CD4+ T cells 6 days after seeding in 3D polystyrene scaffolds (N_{donors} = 5). Statistical significance was determined by the Mann-Whitney U test (*** $p < 0.001$). Diagrams of the resulting CFSE fluorescence peaks of a representative data point for C) 5 days and D) 6 days of culture.

2.4.3 Normalization to the positive control

In order to reduce the influence of the intrinsic donor-to-donor variability of the samples, and make a more accurate study of the effect of each 3D platform to CD4+ T cells in comparison with the culture in suspension (positive control), the raw data previously showed (figure 2.5) were normalized to the positive control. To perform this analysis, the median value of three triplicates of each condition was calculated. Once the median value of each condition was obtained, the values of the indexes obtained for the positive control were divided by themselves, fixing their value to 1. Then, the results for the other conditions were divided by the median value of their corresponding positive control. This treatment was also used for the experiments reported in the following sections. The results of Matrigel and polystyrene after this data analysis can be seen in figure 2.6.

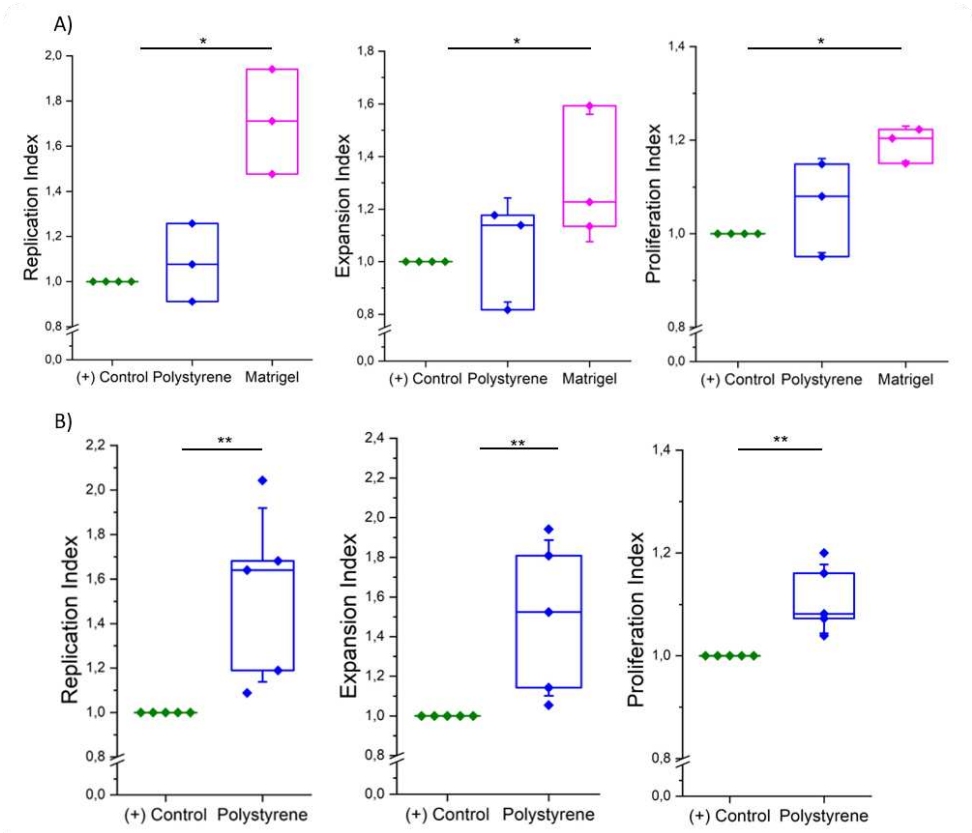

Figure 2.6 Normalized data to the positive control of the proliferation indexes achieved A) 5 days after seeding in suspension (positive control), Matrigel and 3D Polystyrene (N_{donors} = 4, with a minimum of $N_{donors/condition}$ = 3); and B) 6 days after seeding in suspension and 3D polystyrene scaffolds (N_{donors} = 5). Statistical significance was determined by the Mann-Whitney U test (* $p < 0.05$, ** $p < 0.01$).

After the normalization to the positive control, the median value of the normalized replication index obtained after 5 days of culture for Matrigel is of 1.71, i.e. an improvement of a 71% was achieved. The expansion and proliferation indexes showed median values of 1.23 and 1.20, respectively (i.e. an increase of the 23% and 20%

respectively). Thus, the tendency of the 3D polystyrene to improve the proliferation parameters is confirmed, but the statistical significance is slightly modified (figure 2.6.A). Specifically, it is increased in the expansion index and reduced in the rest. After 6 days of CD4+ T cell culture in 3D polystyrene scaffolds, the median value of the normalized replication index obtained was 1.64, whereas the expansion and proliferation indexes showed a media of 1.50 and 1.08, respectively, resulting in statistically significant results.

These results show that both 3D systems were able to increase the proliferation parameters of CD4+ T cells in comparison with cells seeded in suspension. Matrigel was able to achieve significant results in less culture time than 3D polystyrene, probably due to the presence of chemical stimuli and more adequate mechanical properties in comparison with polystyrene. Nevertheless, 3D polystyrene shows how the mere fact of having the physical effect of a 3D support can improve the proliferation of T cells. These results also suggest that the lack of IL-2 measured through ELISA was possibly not due to an inefficient activation, but to an unspecific adhesion of IL-2 on the 3D matrices.

2.5 CD4+ T cell differentiation study

To determine the phenotype of the CD4+ T cells after culture, differentiation assays were performed 5 days after seeding through the staining of two isoforms of the **cluster of differentiation 45 (CD45)**, which is a tyrosine phosphatase protein that is present in all leukocytes, with a greater expression in lymphocytes. CD45 belongs to a complex family of high molecular weight glycoproteins (180-220 kDa) and has tyrosine phosphatase activity playing an important role in the regulation of cell differentiation. The two isoforms stained were CD45RA and CD45RO, given that following mitogenic stimulation, naïve T cells gradually lose CD45RA and gain the CD45RO isoform, which is a marker for T cell memory.[36]

The percentages of T cells that express CD45RA and CD45RO prior to stimulation (negative control) are submitted to the intrinsic donor variability. In this case, they showed a low percentage of the double positive population with a median value of 14.3%, whereas the percentage of CD45RA+ ranged from 26.5 to 67.8 (percentiles Q-25 and Q-75) with a median of 53.6%, similar to CD45RO+ cells, which varied from 20.3% to 56.2% with a median value of 28.6% (figure 2.7.A-C). After stimulation, the median value of CD45RA+ cells decreased to 8.9% and 7.5% in suspension (positive control) and when using the 3D polystyrene scaffold, respectively, indicating that CD4+ T cells successfully differentiated into phenotypes other than naïve. A lower decrease was observed for cells activated in Matrigel, which showed a percentage of CD45RA+ cells of 33.0%. On the other hand, the percentage of double positive populations increased from the 14.3% of the negative control to 50.8% in the positive control, 41.2% in the 3D polystyrene scaffold, and 42.2% in Matrigel. Thus, the percentage of T cells showing both markers is significantly higher for all conditions compared to the negative control. The CD45RO+ population

remained constant with median values of 33.7% and 41.7% in the positive control and the 3D polystyrene scaffold, respectively, whereas it was reduced to 12.5% in Matrigel. The differences observed in the latter could be attributed to its chemical stimulation, absent in the other two platforms, which may promote the conservation of the CD45RA phenotype.

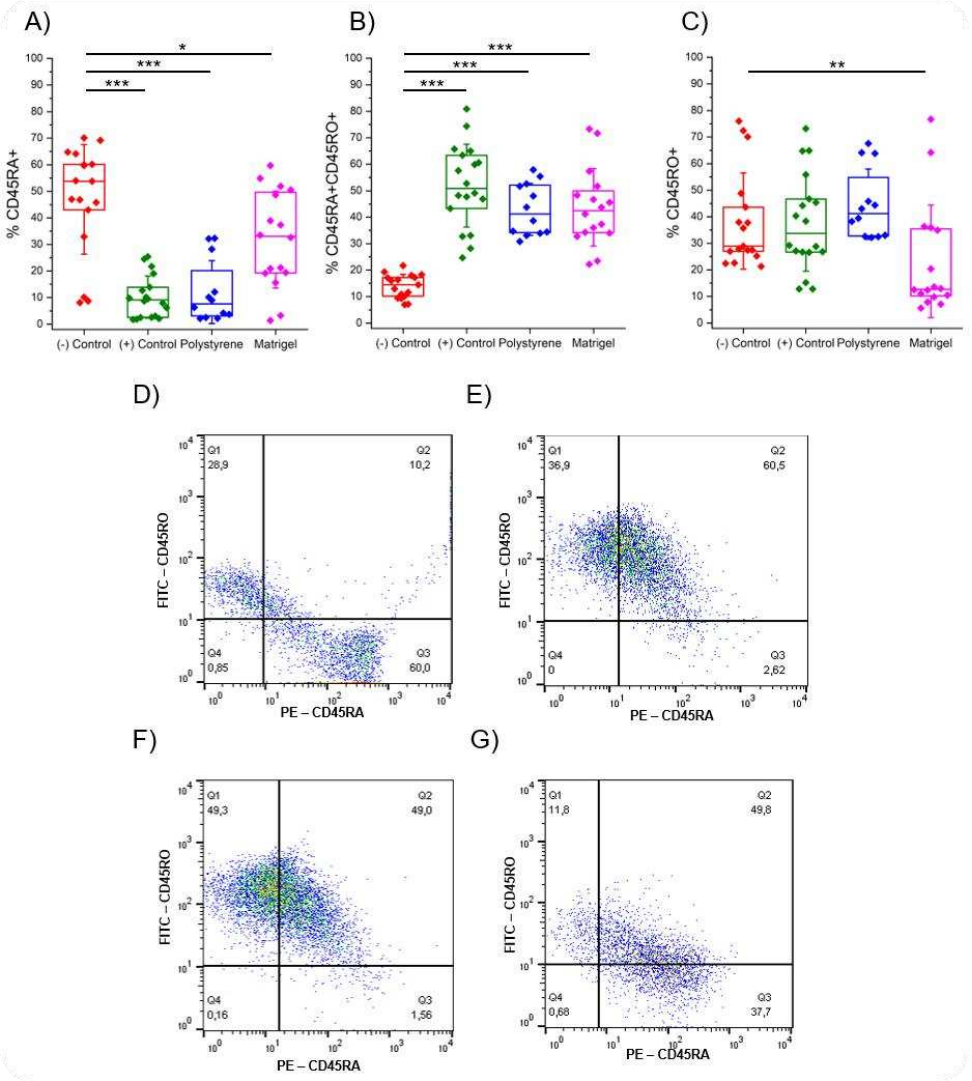

Figure 2.7 Percentage of A) CD45RA+ T cells, B) CD45+ T cells, and C) CD45RO+ CD4+ T cells in the different platforms. Representative dot plot graphs of cells in a D) negative control, E) positive control, F) 3D polystyrene scaffold and G) Matrigel 5 days after the seeding. The results shown were obtained from N_{donors} = 6, with a minimum of $N_{donors/condition}$ = 4. Statistical significance was determined by the Mann-Whitney U test (** $p < 0.01$, *** $p < 0.001$).

Finally, representative dot plots of the negative control (figure 2.7D), positive control (figure 2.7E), 3D polystyrene scaffold (figure 2.7F), and Matrigel (figure 2.7G) are shown. In this graphs each dot represents one cell analyzed by the cytometer, showing if it is CD45RO+, CD45RA+, or CD45RO+CD45RA+, and it can be easily seen the differences or similarities between the resulting populations. As can be seen in these graphs, the memory marker CD45RO appears in the 3D polystyrene scaffold and the positive control, increasing the double positive population, and drastically reducing the CD45RA phenotype. The resulting cell population of these two conditions seems to be very similar as no significant differences were observed in the studied phenotypes. Nevertheless, cells expressed higher percentages of the CD45RA marker in Matrigel, conserving the higher capacity to proliferate of naïve cells, and significantly changing the phenotype of the resulting cells.

2.6 Conclusions

In this chapter it has been proved the benefits that can be obtained from substituting typical 2D culture systems to the use of novel 3D platforms. The influence of two different 3D scaffolds (Matrigel and polystyrene) to CD4+ T cell proliferation and differentiation has been studied. It has been observed how the proliferation rates of CD4+ T cells significantly increased for all the 3D systems studied. In the case of the 3D polystyrene scaffold, which only introduces a 3D physical support in the cell culture, 6 days were required to obtain significantly different results from the positive control in comparison with the 5 days needed for Matrigel. Moreover, Matrigel, which additionally introduces a chemical input, showed promising results with interesting phenotypes, proving that a 3D matrix not only can improve CD4+ T cell proliferation, but also can tune the phenotype of the resulting cells. These observations could be exploited in the future to obtain higher percentages of cytotoxic cells capable of recognizing malignant cells and result in more effective treatments. However, Matrigel suffers from a high compositional variability, which can be explained by its natural origin and the associated batch to batch variability. Moreover, it was not designed for secondary lymphoid organ mimicking, thus significantly differing in terms of ECM composition. Thus, new 3D platforms should be designed for T cell culture to improve the current T cell expansion systems and therefore facilitate the broad use of ACT in the clinics.

2.7 References

1. Kleinman, H. K. & Martin, G. R. Matrigel: basement membrane matrix with biological activity. *Semin. Cancer Biol.* **15**, 378–386 (2005).
2. Benton, G., Arnaoutova, I., George, J., Kleinman, H. K. & Koblinski, J. Matrigel: from discovery and ECM mimicry to assays and models for cancer research. *Adv. Drug Deliv. Rev.* **79**–**80**, 3–18 (2014).
3. Soofi, S. S., Last, J. A., Liliensiek, S. J., Nealey, P. F. & Murphy, C. J. The elastic modulus of Matrigel™ as determined by atomic force microscopy. *J. Struct. Biol.* **167**, 216–219 (2009).
4. Gimenez, A., Uriarte, J. J., Vieyra, J., Navajas, D. & Alcaraz, J. Elastic properties of hydrogels and decellularized tissue sections used in mechanobiology studies probed by atomic force microscopy. *Microsc. Res. Tech.* **80**, 85–96 (2017).
5. Hwang, J. W., Noh, S. M., Kim, B. & Jung, H. W. Gelation and crosslinking characteristics of photopolymerized poly(ethylene glycol) hydrogels. *J. Appl. Polym. Sci.* **132**, (2015).
6. Caicedo-Carvajal, C. E., Liu, Q., Remache, Y., Goy, A. & Suh, K. S. Cancer Tissue Engineering: A Novel 3D Polystyrene Scaffold for In Vitro Isolation and Amplification of Lymphoma Cancer Cells from Heterogeneous Cell Mixtures. *J. Tissue Eng.* **2011**.
7. Kirshner, J., Chen, C.-J., Liu, P., Huang, J. & Shively, J. E. CEACAM1-4S, a cell-cell adhesion molecule, mediates apoptosis and reverts mammary carcinoma cells to a normal morphogenic phenotype in a 3D culture. *Proc. Natl. Acad. Sci. U. S. A.* **100**, 521–526 (2003).
8. Fischbach, C. *et al.* Engineering tumors with 3D scaffolds. *Nat. Methods* **4**, 855–860 (2007).
9. Zaman, M. H. *et al.* Migration of tumor cells in 3D matrices is governed by matrix stiffness along with cell-matrix adhesion and proteolysis. *Proc. Natl. Acad. Sci. U. S. A.* **103**, 10889–10894 (2006).
10. Terraf, P., Babaloo, H. & Kouhsari, S. M. Directed Differentiation of Dopamine-Secreting Cells from Nurr1/GPX1 Expressing Murine Embryonic Stem Cells Cultured on Matrigel-Coated PCL Scaffolds. *Mol. Neurobiol.* **54**, 1119–1128 (2017).
11. Leppert, D., Waubant, E., Galardy, R., Bunnett, N. W. & Hauser, S. L. T cell gelatinases mediate basement membrane transmigration in vitro. *J. Immunol.* **154**, 4379 LP – 4389 (1995).
12. Xia, M. *et al.* Stimulus specificity of matrix metalloproteinase dependence of human T cell migration through a model basement membrane. *J. Immunol.* **156**, 160–167 (1996).
13. Osswald, A., Hedrich, V. & Sommergruber, W. 3D-3 Tumor Models in Drug Discovery for Analysis of Immune Cell Infiltration. *Methods Mol. Biol.* **1953**, 151–162 (2019).
14. Lerman, M. J., Lembong, J., Muramoto, S., Gillen, G. & Fisher, J. P. The Evolution of Polystyrene as a Cell Culture Material. *Tissue Eng. Part B. Rev.* **24**, 359–372 (2018).

15. Chang, H., Gong, X., Zheng, C. & Wei, Z. *Preparation and characterization of porous polyacrylonitrile materials via concentrated emulsion template method*. *Asian Journal of Chemistry* **26**, (2014).

16. Sumarno, Sato, Y., Takishima, S. & Masuoka, H. Production of polystyrene microcellular foam plastics and a comparison of late- and quick-heating. *J. Appl. Polym. Sci.* **77**, 2383–2395 (2000).

17. Gutsche, A. T., Lo, H., Zurlo, J., Yager, J. & Leong, K. W. Engineering of a sugar-derivatized porous network for hepatocyte culture. *Biomaterials* **17**, 387–393 (1996).

18. Baker, S. C. *et al.* Characterisation of electrospun polystyrene scaffolds for three-dimensional in vitro biological studies. *Biomaterials* **27**, 3136–3146 (2006).

19. Fedorovich, N. E., Alblas, J., Hennink, W. E., Oner, F. C. & Dhert, W. J. A. Organ printing: the future of bone regeneration? *Trends Biotechnol.* **29**, 601–606 (2011).

20. Olkowski, R. *et al.* Three-dimensional nanofibrous polystyrene scaffolds modify macrophage phenotypes and activate macrophage angiogenic potential. *Cell Biol. Int.* **43**, 265–278 (2019).

21. Lerman, M. J. *et al.* Development of surface functionalization strategies for 3D-printed polystyrene constructs. *J. Biomed. Mater. Res. B. Appl. Biomater.* (2019).

22. Leong, M. F. *et al.* Electrospun polystyrene scaffolds as a synthetic substrate for xeno-free expansion and differentiation of human induced pluripotent stem cells. *Acta Biomater.* **46**, 266–277 (2016).

23. Roy, U. Structure and Function of an Inflammatory Cytokine, Interleukin-2, Analyzed Using the Bioinformatic Approach. *Protein J.* (2019).

24. Mahnke, Y. D., Brodie, T. M., Sallusto, F., Roederer, M. & Lugli, E. The who's who of T-cell differentiation: human memory T-cell subsets. *Eur. J. Immunol.* **43**, 2797–2809 (2013).

25. Zhang, C., Zhang, X. & Chen, X.-H. Interleukin-2 priming chemotherapy: a strategy to improve the remission of refractory/relapsed T cell acute lymphoblastic leukemia. *Med. Hypotheses* **81**, 878–880 (2013).

26. Engvall, E. & Perlmann, P. Enzyme-Linked Immunosorbent Assay, Elisa. *J. Immunol.* **109**, 129 LP – 135 (1972).

27. The enzyme-linked immunosorbent assay (ELISA). *Bull. World Health Organ.* **54**, 129–139 (1976).

28. AU - Lefort, C. T. & AU - Kim, M. Human T Lymphocyte Isolation, Culture and Analysis of Migration In Vitro. *JoVE* e2017 (2010).

29. Lammermann, T. & Germain, R. N. The multiple faces of leukocyte interstitial migration. *Semin. Immunopathol.* **36**, 227–251 (2014).

30. Sung, K. E. *et al.* Understanding the Impact of 2D and 3D Fibroblast Cultures on In Vitro Breast Cancer Models. *PLoS One* **8** (2013).

31. Ribeiro, A. *et al.* β1-integrin Cytoskeletal Signaling Regulates Sensory Neuron Response to Matrix Dimensionality. *Neuroscience* **0**, 67–78 (2013).

32. Lepzelter, D., Bates, O. & Zaman, M. Integrin Clustering in Two and Three Dimensions. *Langmuir* **28**, 5379–5386 (2012).

33. Weston, S. A. & Parish, C. R. New fluorescent dyes for lymphocyte migration studies: Analysis by flow cytometry and fluorescence microscopy. *J. Immunol. Methods* **133**, 87–97 (1990).

34. Lyons, A. B. & Parish, C. R. Determination of lymphocyte division by flow cytometry. *J. Immunol. Methods* **171**, 131–137 (1994).

35. Luzyanina, T. *et al.* Computational analysis of CFSE proliferation assay. *J. Math. Biol.* **54**, 57–89 (2007).

36. Bujan, W. *et al.* Abnormal T-cell phenotype in familial erythrophagocytic lymphohistiocytosis. *Lancet (London, England)* **342** (1993).

CHAPTER 3
Synthetic PEG–Hep hydrogels.

3.1 Introduction

As has been widely discussed in chapter 1, immunotherapy is a new treatment against cancer that is based on harnessing the immune system of patients and which has shown promising results in the last years. Thus, a lot of effort is being applied in optimizing and overcoming current limiting steps of this treatment, like immune cell activation and expansion. It has been shown the importance of introducing 3D matrixes to mimic the original ECM of cells to increase T cell proliferation and tune differentiation. The results of chapter 2 showed the potential of using a 3D platform for improving the expansion of CD4+ T cells. The benefit of only the 3D physical support could be seen due to the experiments with the 3D polystyrene scaffold, and the importance of the chemical stimuli was observed for the case of Matrigel.[1] Current bibliography supports these observations.

PEG hydrogels have been extensively studied because of their interesting physicochemical properties, chemical versatility, and biocompatibility. They can be formed under mild, cytocompatible conditions, and are easily engineered to present different functionalities such as cell adhesion and cell-mediated degradability, or different mechanical properties affecting the porosity, viscosity and stiffness.[2]

Heparin is a highly sulfated and variable glycosaminoglycan (GAG), which is highly negatively charged and an abundant component of the ECM of LNs. Heparin-functionalized hydrogels have been widely used in affinity-based protein delivery.[3] This anionic character mediates binding to various positively charged proteins which can interact with cells causing different responses such as proliferation, differentiation, and control of chemokine signaling.

PEG-Hep hydrogels have been studied for diverse applications, such as cardiovascular tissue engineering applications through the study of human aortic adventitial fibroblasts, showing improved cell adhesion to materials with the highest modulus;[4] cellularization of synthetic or autologous implants, evaluating hydrogels of different stiffness on vascular cells observing differences in attachment, proliferation, and gene expression profile associated with the hydrogel modulus;[5] and in neurobiological studies using the gel as a scaffold to demonstrate the impact of mechanical and biomolecular cues on primary nerve cells and neural stem cells.[6] However, to our knowledge, this hydrogels have never been applied to immune cell 3D culture.

In this thesis, PEG-Hep hydrogels are synthesized and studied with the objective of mimicking the physicochemical properties of the ECM of LNs, thanks to the properties of both PEG and Hep. These hydrogels are composed by maleimide-functionalized low molecular weight heparin (Hep-Mal) and a thiol-functionalized PEG multi-arm polymer.[7] The fast kinetics and specificity of the reaction between maleimide and thiols have been described,[4,5] and used in this case for the crosslinking of thiolated PEG with Hep-Mal. On one hand, PEG is responsible to imitate the physical 3D structure of the lymph nodes, due to its specific structural and mechanical properties, which can be easily regulated thanks

to its synthetic nature.[2] On the other hand, the heparin is resembling the function of the heparan sulphates naturally present in the ECM, acting as molecular sinks, storage sites, or presentation platforms to bind growth factors and chemokines.[8]

As reported in the literature and previously discussed in chapter one, there are some key parameters of any 3D platform that should be properly designed in order to achieve a proper mimicking of the LN, such as, its porosity, mechanical properties, degradability, and presence of key cell signaling molecules.[9] The pore size of the hydrogel should allow the circulation of immune cells through the inner part of the hydrogel. Previous studies showed that a pore size of 2 μm was enough to observe lymphocyte migration through the matrix, being the median size of T lymphocytes of approximately 1−2 μm of diameter when inactivated.[10] Techniques such as scanning electron microscopy (SEM) and microtomography imaging have been used to analyze the pore size of the proposed hydrogels which can be tailored by varying the amount of PEG, together with its viscosity, gelation time, and resulting stiffness.

The mechanical properties of the hydrogel are of vital importance due to its influence in both cellular behavior and tissue compatibility.[11] Moreover, most envisioned clinical applications require scaffolds that degrade into excretable or metabolizable products over time.[12] The soft nature of the lymphoid microenvironment is one of the key parameters that have to be present in the design of a 3D scaffold to be used as SLOs.[9] Interestingly, PEG-Hep hydrogels degradation has been already assessed.[7] Rheology was the chosen technique to characterize the hydrogel mechanical properties and gelation time at different compositions.

Finally, the ability of PEG-Hep hydrogels to retain positively charged molecules thanks to the role of the heparin, was confirmed with green fluorescence protein (GFP) at different concentrations and fluorescence analysis.

Following these strategies, PEG-Hep hydrogels were fully characterized and used as 3D scaffold for CD4+T cell activation, expansion, and differentiation, to study its further application into immunotherapy treatments (figure 3.1).

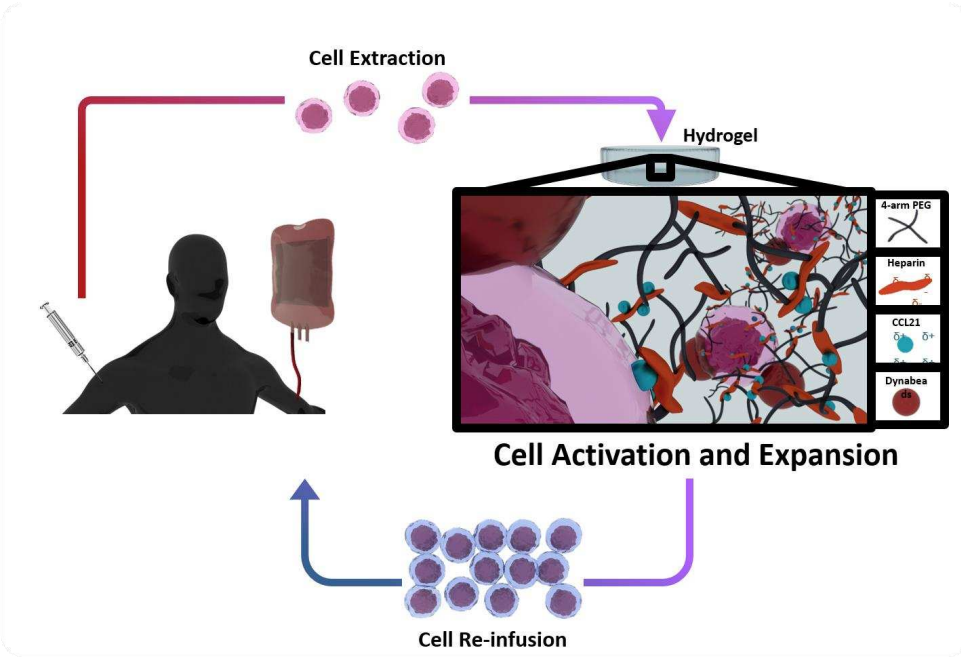

Figure 3.1 Diagram of the application of PEG-Hep hydrogels (in this case loaded with CCL21) to the expansion of immune cells.

3.2 Objectives and strategy

In this chapter PEG-Hep hydrogels are proposed for CD4+ T cell expansion, fully characterized, and studied. This material has been designed to mimic the conditions of the ECM of the SLOs, specifically the LNs, to increase CD4+ T cell proliferation and tune differentiation, given that these organs are believed to be highly efficient in promoting such cellular responses. More specifically, we had the following objectives:

1. Synthetize, design and fully characterize the proposed PEG-Hep hydrogels in order to achieve the desired properties to mimic the ECM of LNs. Hydrogels with different stiffness, porosities and loading capacities were prepared and analyzed.

2. Use of the hydrogels for CD4+ T cell culture under different conditions, studying resulting changes observed in proliferation and in the phenotypes achieved in comparison with the state-of-the-art suspension cultures.

In summary, the main objective of this chapter was to achieve high proliferation rates by using hydrogels, and obtain cytotoxic phenotypes in order to have many active cells to fight cancer.

3.3 Synthesis of Hep-Mal and PEG-Hep hydrogel formation

As has been mentioned in the introduction of this chapter, PEG-Hep hydrogels are formed by two components, 4-arm thiolated PEG and Hep-Mal. Although the PEG derivative used is commercially available (Sigma-Aldrich, USA), the heparin had to be functionalized with the maleimide prior to its use. A diagram of this functionalization process can be seen in figure 3.2.

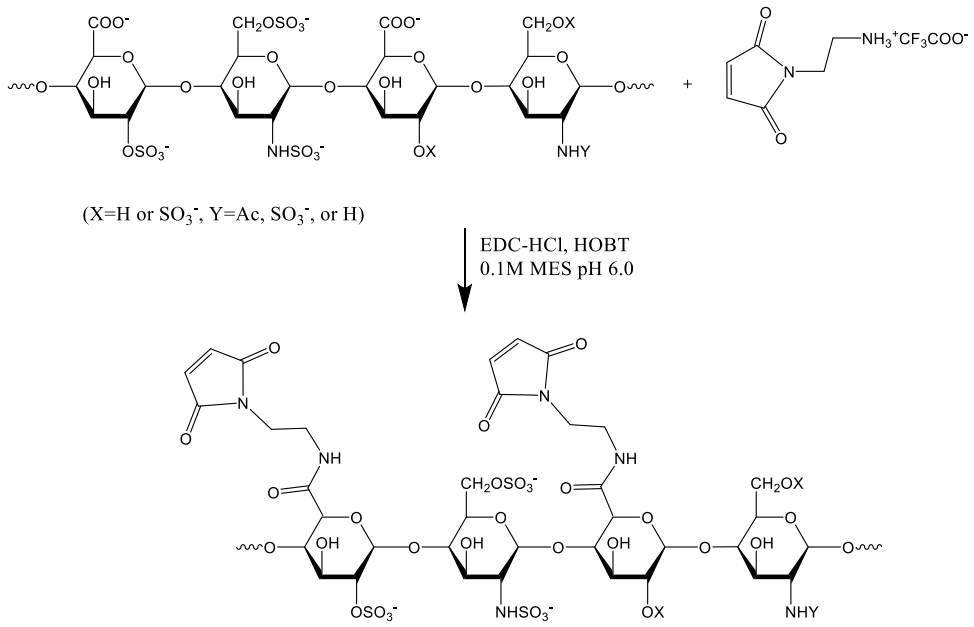

Figure 3.2 Synthesis of maleimide-functionalized heparin.

The functionalization of heparin with maleimide was based in a method previously described.[3,4] Heparin was dissolved in a solution of 0.1 M of MES buffer, together with the N-(2-aminoethyl) maleimide trifluoroacetate salt (AEM) and HOBt/EDC·HCl were added to activate the reaction (more details of this process can be found in chapter 6 section 6.2.2). The reaction was left overnight and then purified by dialysis. The resulting product was analyzed by ^{1}H-NMR spectroscopy. The result can be seen in figure 3.3.

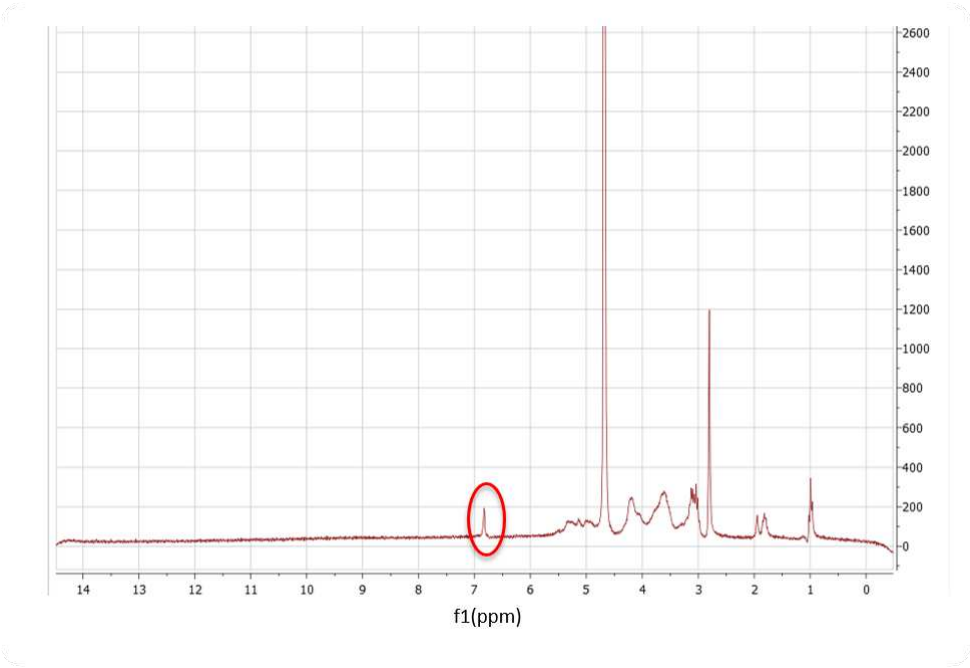

Figure 3.3 Full H-NMR spectrum of Hep functionalized with maleimide after an overnight reaction.

The maleimide linked to the heparin appears at 6.83 ppm in contrast with the free maleimide ring that has a peak at 6.86 ppm. Depending on the heparin batch, this value can slightly change its position.

Once the heparin was fully functionalized, we studied the hydrogel formation. For that, a solution of a 4-arm thiolated PEG (PEG-SH) was mixed with a solution of functionalized heparin in a proportion of 1:1.5, in phosphate buffered saline (PBS). As mentioned before, hydrogels with different mechanical properties can be obtained by varying the percentage of PEG. Thus, we prepared hydrogels with the 3%wt, 4%wt, and 6%wt of PEG, all of them with the same proportion of PEG:Hep (1:1.5). PEG-Hep hydrogels were formed through a maleimide-thiol reaction between the maleimide of the functionalized heparin, and the thiols of PEG, which result in a covalent crosslink and the consequent gelation. A diagram of this gelification mechanism can be seen in figure 3.4.A, together with the photographs of the resulting hydrogels (figure 3.4.B).

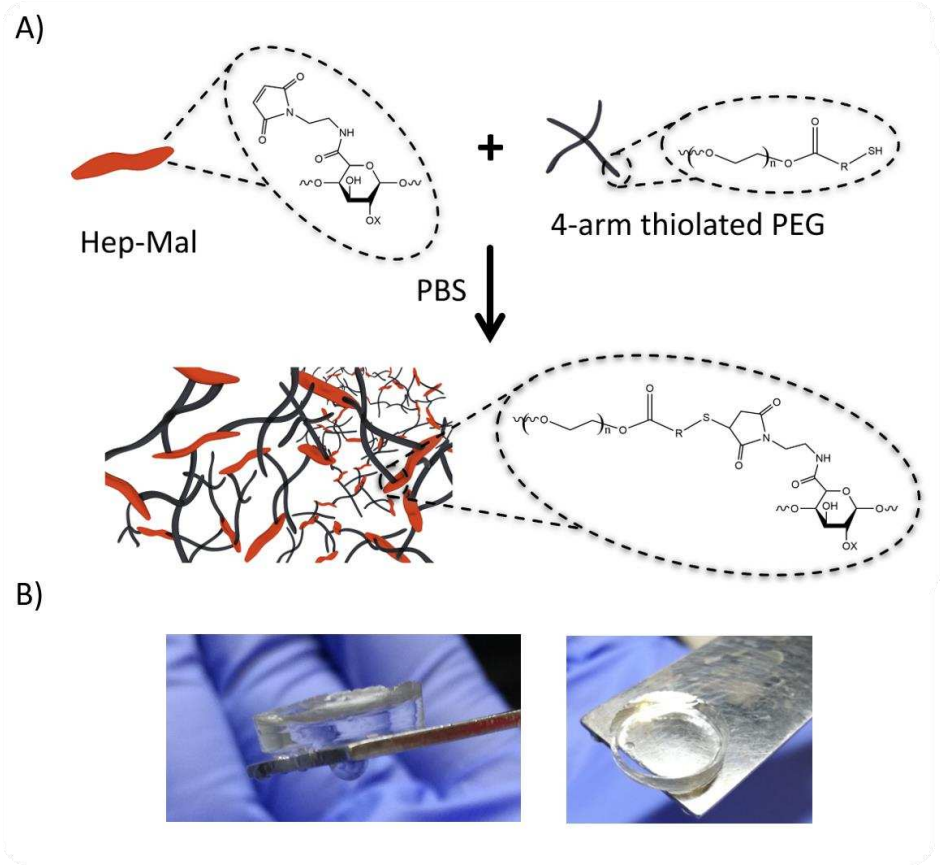

Figure 3.4 A) Schematics of PEG-Hep hydrogel formation through a maleimide-thiol reaction resulting in a covalent crosslink and gelation. B) Photographs of the resulting hydrogels.

3.4 Structural and mechanical properties of PEG-Hep hydrogels

To optimize the resulting hydrogels for immune cell culture, various experiments were performed, and its physical properties were characterized (e.g. stiffness, porosity, gelification time, and pore interconnectivity). Rheology was the technique used to characterize the gelification time and stiffness of the hydrogels. SEM was used to observe the inner structure of the hydrogel in the sections and surface. Finally, microtomography was used to obtain 3D images of the scaffold and study their pore interconnectivity.

3.4.1 Rheology

The main rheological technique to characterize hydrogels is **small-amplitude oscillatory shear (SAOS)**.[13] In SAOS, a small amount of sample is placed between parallel disks (or a cone and a disk for samples of different nature) and a small-amplitude torsional oscillation generates shear flow in the sample. SAOS is ideal for monitoring changing systems (such as the gelation of a hydrogel), since the measurement is quick and can be monitored as a

function of time. Moreover, it is also commonly used to identify the equilibrium shear modulus of a gel, Ge,[14] for gels with low stiffness, like PEG-Hep hydrogels. This modulus is the ratio of stress and strain in a balanced state where the material supports stress without deformation. To determine the Ge of a gel, the storage modulus (G') (black line of figure 3.5) and the loss modulus (G'') (grey line of figure 3.5) are measured in the linear-viscoelastic limit, and the limiting value of G' at low frequency is identified as the shear modulus. A typical linear-viscoelastic behavior of a crosslinked gel is shown in figure 3.5, where it can be seen that at high frequencies, the polymer shows a glassy behavior, while at low frequencies the gel shear modulus is observed. The transition of G' between these two regions characterizes the glass transition of the polymer.[15]

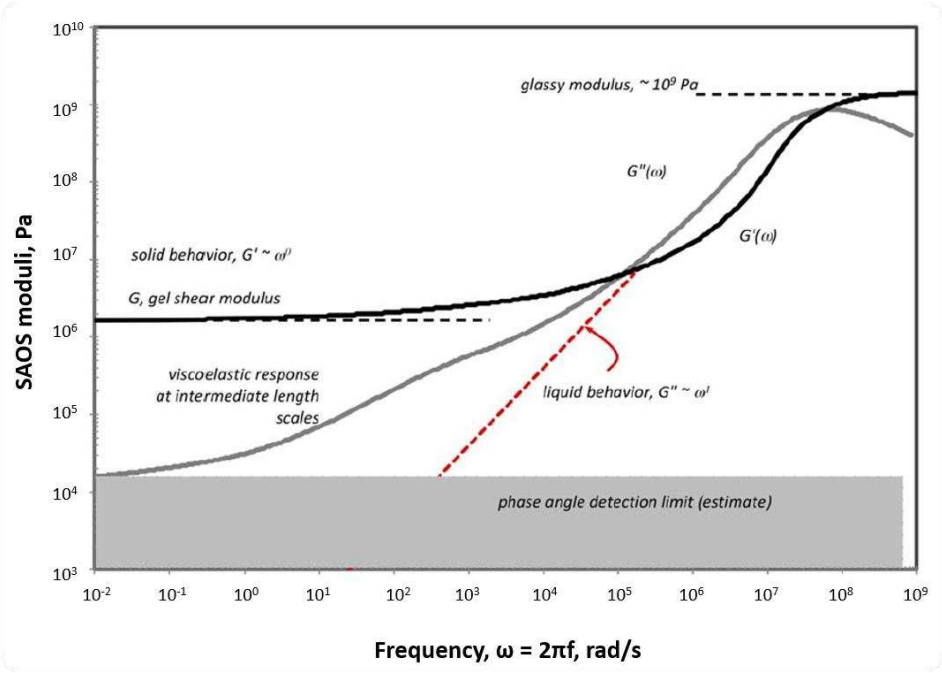

Figure 3.5 Typical linear-viscoelastic behavior of a crosslinked gel. Figure courtesy of Jonathan M. Zuidema et al.[13]

This technique requires a trial-and-error approach to find the appropriate values of strain and frequency of each gel. Thus, the measurements require strain sweeps, frequency sweeps, and time sweeps at 37°C to calibrate the range of pressure and frequency where the hydrogels maintain their viscoelastic behavior. In **strain sweeps**, G' and G'' are measured at a fixed frequency, while the pressure applied to the hydrogel increases within the range of interest. For **frequency sweeps**, the procedure is quite similar but, in this case, the pressure applied is constant and is the frequency what is changed. These two experiments show the values of pressure and frequency where the hydrogels maintain their viscoelastic behavior, and which are applied to the **time sweep**, where the changing variable is the time.

To perform these experiments, the samples with different percentages of PEG (3%wt, 4%wt, and 6%wt) were previously prepared and stored in the incubator at 37°C in Milli-Q water. Strain sweeps were performed at 37°C and a constant frequency of 1.0 Hz, while the pressure was conducted from 1 Pa to 150 Pa on fully formed hydrogels (after optimizing the range where the hydrogels maintain their viscoelastic behavior). Then, frequency sweeps were performed from 0.01 Hz to 10 Hz at a constant strength of 50 Pa. Results are shown in figure 3.6.

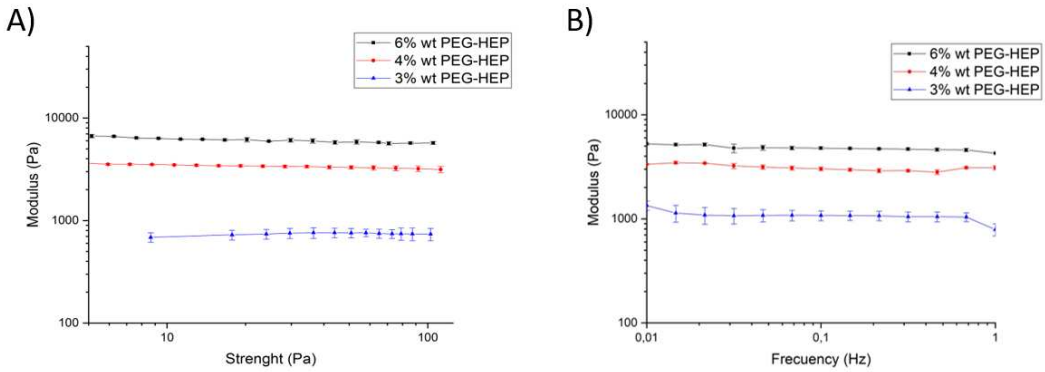

Figure 3.6 A) Strain sweeps and B) frequency sweeps of 6%wt, 4%wt, and 3%wt of PEG-Hep hydrogels.

All hydrogels showed linear behavior of G' from a strength of 10 Pa to 100 Pa. Samples of 3%wt show a G' lower than those of 4%wt and 6%wt, i.e. they can accumulate less energy in their structure without causing deformation. Thus, hydrogels with less amount of PEG are softer than those with higher amounts of PEG, as expected. The frequency sweeps were linear from 0.01 Hz to 1 Hz. Similarly, lower G' values were obtained for the 3%wt than the 4%wt and 6%wt PEG-Hep hydrogels. The values of the equilibrium shear modulus (Ge) achieved were 4.8±0.2 kPa for the 6%wt PEG-Hep hydrogel, 3.1±0.1 kPa in the case of 4%wt PEG-Hep, and 1.1±0.1 kPa for the 3%wt PEG-Hep. G'' was too small to be measured, as is to be expected for fully formed hydrogels.[13] It is worth noting that these values of Ge correspond to fully formed and completely hydrated hydrogels. This is important because this is the state in which hydrogels were applied to cell culture. Thus, these results provide reliable information about the mechanical properties of the material that cells interact with.

Time sweeps were performed for the characterization of the gelification process, performed at 50 Pa and 0.1 Hz, values in which PEG-Hep hydrogels showed to maintain their viscoelastic behavior, with the rheometer at 37°C. The 6%wt and 4%wt PEG-Hep hydrogels were stabilized after ca. 200 min, at a storage modulus of 8.2±0.5 kPa, while the 3%wt PEG-Hep hydrogel required 240 min at a storage modulus of 2.7±0.2 kPa (figure 3.7). The storage modulus values achieved are higher in comparison with the ones showed in strain and frequency sweeps, because in this case the hydrogels were not fully

formed and hydrated. In other words, here we are analyzing the gelification process and the properties of the hydrogel when this process ends, without the addition of water or any other possible treatment. This means that, without the hydration process PEG-Hep hydrogels are more compact and stiff, as expected. Although this experiment was useful to characterize the gelification process, the stiffness values relevant for immune cell culture are the ones obtained before, i.e. the ones obtained after hydrogel hydration in PBS.

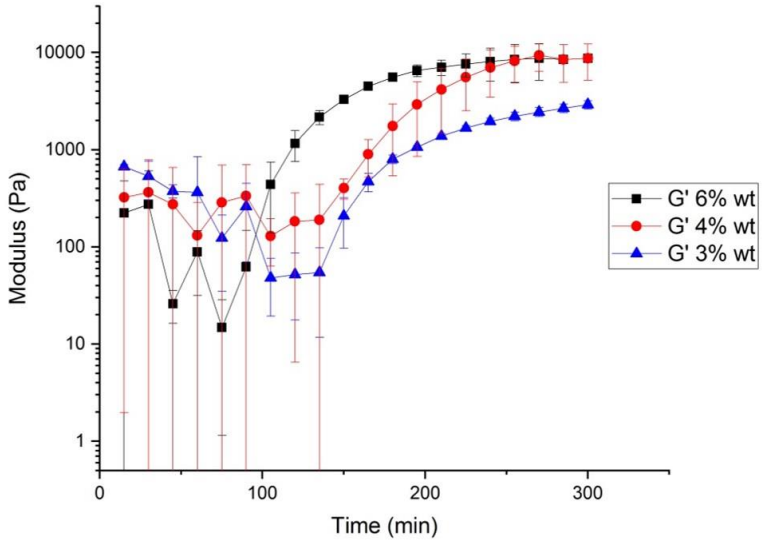

Figure 3.7 Time sweeps of 6%wt, 4%wt, and 3%wt PEG-Hep hydrogels.

3.4.2 SEM

After the rheological characterization, the pore size of fully formed and hydrated PEG-Hep hydrogels at different percentages of PEG (6%wt, 4%wt, and 3%wt) was studied by SEM imaging of their surface and section. Normally, this technique is used to analyze dry samples, however, images of the inner structure of the hydrated hydrogel could be obtained by slowly decreasing the pressure and temperature of the vacuum chamber, i.e. using the so-called ambient mode. Representative images for the surface and section of each hydrogel are shown (figure 3.8.A)

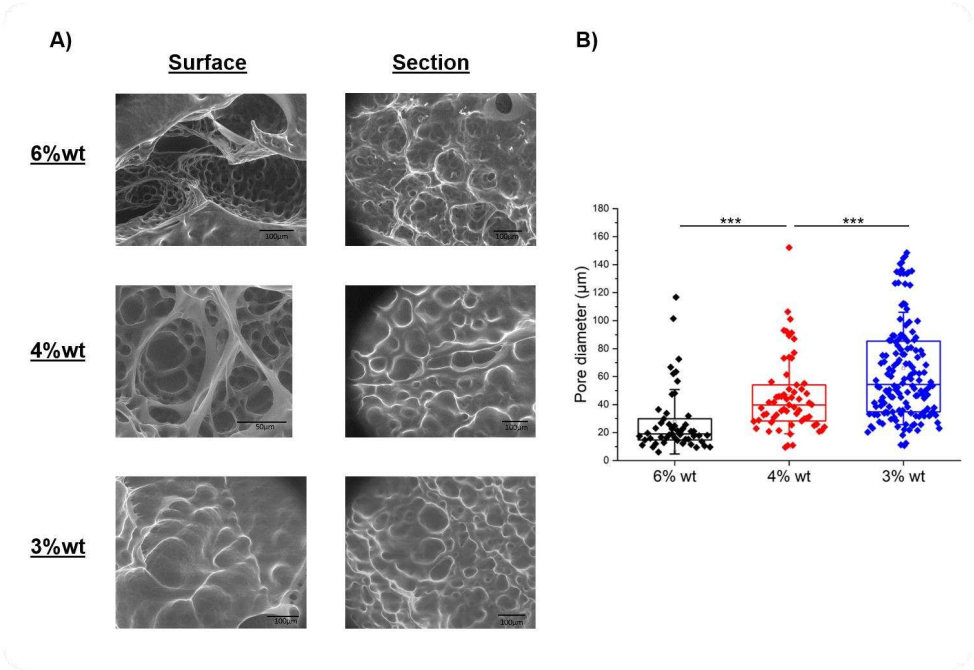

Figure 3.8 A) SEM images of the surface and section of the samples studied at different compositions of PEG (6%wt, 4%wt and 3%wt). B) Pore size evaluation of 6%wt, 4%wt, and 3%wt PEG-Hep hydrogels. The statistical significance was determined by the non-parametric Kruskal Wallis ANOVA test (*** $p < 0.001$).

The pore size the samples was analyzed using the FiJi (ImageJ) software (figure 3.8.B). The median pore size of the 6%wt PEG-Hep hydrogels resulted of 20 µm with a porosity range of 5-50 µm, which increases to 40 µm for the 4%wt hydrogels with a range of 20-75 µm, and to 55 µm with a range of 25-105 µm for the 3%wt PEG-Hep hydrogels. These results show that the lower the amount of PEG present in the sample, the higher the porosity of the hydrogel, as expected. In order to apply PEG-Hep hydrogels to immune cell culture, the 3%wt PEG-Hep hydrogel was chosen due to its porosity and mechanical properties. For a deeper study of this hydrogel, the interconnectivity of its pores was measured through 3D microtomography.

3.4.3 Microtomography

In addition to the previous characterization, 3%wt PEG-Hep hydrogels were freeze-dried and then lyophilized in order to obtain the dried 3D structure to characterize it by X-ray microtomography. The images achieved support the data obtained by SEM, and provided high quality images and videos of the internal structure of the hydrogels where the interconnectivity of the pores can be seen (figure 3.9).

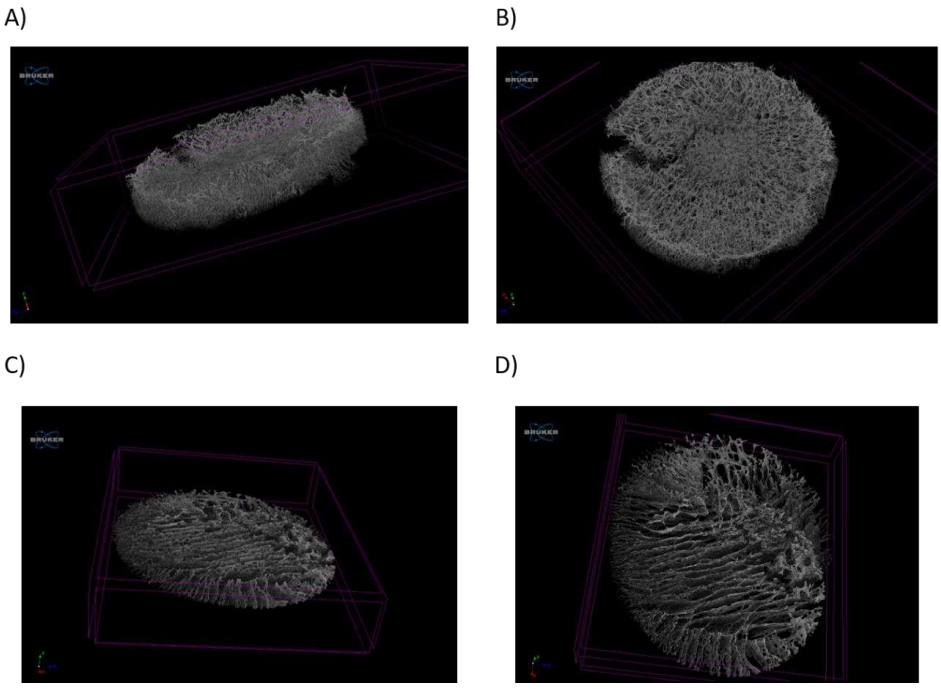

Figure 3.9 A) Lateral and B) top views of an overall 3% PEG-Hep hydrogel of 1 cm of diameter. C) and D) show the same perspectives but of a small zone of the hydrogel used to analyzed its porosity of 3.5 mm of diameter and 500 µm of height.

The percentage of the different pore sizes measured by this technique was represented and fitted to a Gaussian model (figure 3.10) with a R^2 of 0.998.

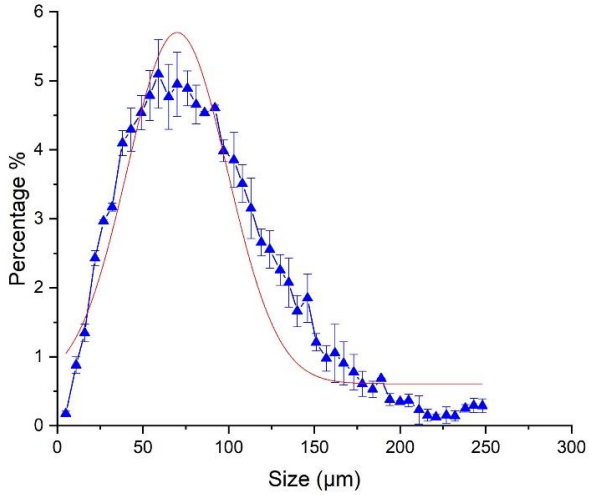

Figure 3.10 Porosity analysis of 3%wt PEG-Hep samples studied by microtomography ($N_{samples}$ = 2) and the Gaussian fitting performed.

This model fit our data to the function:

$$y = y_0 + \frac{A}{\left(\omega \cdot \sqrt{\frac{\pi}{4 \cdot \ln(2)}}\right)} \cdot e^{\left(\frac{-4 \cdot \ln(2) \cdot (x - x_C)^2}{\omega^2}\right)}$$

In this equation y_0 represents the base of the function, x_C the center, A the area, and ω, the FWHM (Full Width at Half Maximum). The values obtained applying the fitting of this function to our data are showed in the table below.

Table 3.1 Values of the Gaussian fitting applied to the porosity data achieved by microtomography for 3%wt PEG-Hep hydrogels.

Model	Gaussian
y_0	0.61 ± 0.03
x_C	69.98 ± 3.35
A	374.34 ± 33.45
ω	69.07 ± 9.24
R^2	0.998

From this analysis we can extract that most of the pores measure around 70 µm, in agreement with the data obtained by SEM, where the median pore size observed was of 55 µm.

3.5 Biofunctionalization of PEG-Hep hydrogels: Loading capacity

To confirm the ability of PEG-Hep hydrogels to attract positively charged molecules to their negatively charged heparin units, different concentrations of GFP were incubated with the hydrogels during 1 h to observe the dependency of the laoding capacity of the hydrogel with the concentration of the positively charged protein. More details of the protocol followed are explained in chapter 6, section 6.2.4.

The surface charge of the GFP used at pH 7 was calculated knowing the amino acid sequence of the protein, resulting in an estimated value of +5.6 mV (http://protcalc.sourceforge.net/ in June 2018). The surface charge of the Hep used is reported to have an aproximate value of -25 mV.[16]

As shown below, the fluorescence was retained by the hydrogel after rinsings, indicating that the GFP was trapped inside, as expected. However, even at our highest concentration of GFP available of 1 mg/ml, the fluorescence in the hydrogel was not completely saturated (figure 3.11).

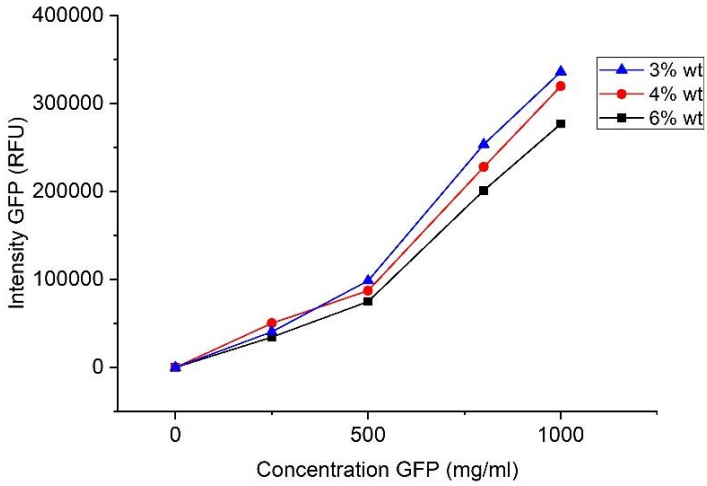

Figure 3.11 GFP loading curve of 6%wt, 4%wt and 3%wt of PEG-Hep hydrogels.

Although a higher retention capacity was expected for the 6%wt PEG-Hep hydrogels compared to the 4%wt and the 3%wt PEG-Hep hydrogels due to its higher presence of Hep in the hydrogels, the 3%wt PEG-Hep hydrogel showed the highest retention value. These results suggest that 3%wt of PEG-Hep hydrogels have a better pore interconnectivity than the rest, and thus, the GFP solution can easily reach the whole hydrogel.

3.6 Unloaded PEG-Hep hydrogels applied to CD4+ T cell culture

Once PEG-Hep hydrogels of different PEG percentages (6%wt, 4%wt, and 3%wt) were fully characterized, **3%wt PEG-Hep hydrogels** were chosen for CD4+ T cell culture, given their mechanical properties, higher porosity, and loading capacity.

As performed for the study of commercial platforms, T cell proliferation analysis were assessed through CFSE staining and flow cytometry (Chapter 2 section 2.4.1). Thus, the expansion, replication, and proliferation indexes were calculated 5 days after seeding. As a reminder, the expansion and replication indexes determine the fold-expansion of the overall culture and that of the responding cells respectively, and the proliferation index is equal to the number of divisions that cells from the original population have undergone divided by the number of divided cells.

The results of the unloaded 3%wt PEG-Hep hydrogels used as a scaffold for CD4+ T cell culture were normalized to the positive control, as showed in chapter 2 section 2.4.3, and its representation can be seen in figure 3.12.A. The media of the normalized replication index obtained was 1.25, i.e. an improvement of a 25% was achieved, whereas the expansion and proliferation indexes showed a media of 1.1 and 1.05, respectively. All three parameters showed statistically significant increases compared to the positive

controls, which corresponded to cultures in suspension with Dynabeads. The strongest difference was observed for the replication index, which indicates that the responding cells that get activated in the synthetic hydrogels proliferate more than the activated cells in suspension. A representative graph of the peaks of fluorescence obtained in the flow cytometer after culturing is shown in figure 3.12.B. It shows the displacement of the CFSE fluorescence peaks to the left in the positive control and sample compared to the negative control, indicating the new generations of cells obtained.

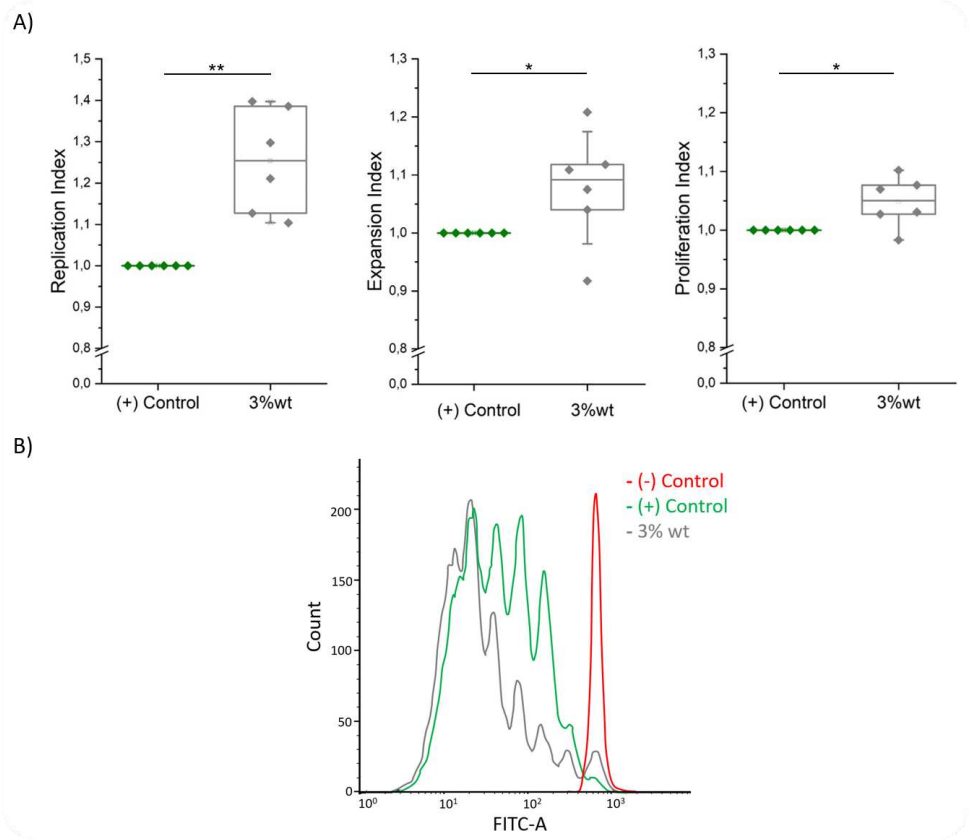

Figure 3.12 A) Normalized proliferation analysis of CD4+ T cells 5 days after seeding in unloaded PEG-Hep hydrogels (3%wt) (N_{donors} = 6). Statistical significance was determined by the Mann-Whitney U test (*p<0.05, **p<0.01). B) Diagram of the resulting CFSE fluorescence peaks of a representative data point.

These results indicate, not only that PEG-Hep hydrogels do not show any cytotoxicity for the cells, but also that the 3D physical effect of the hydrogel, even without the introduction of any chemical stimuli, already causes an improvement in CD4+ T cell proliferation, which is very promising for this material.

3.7 Study of different chemical stimuli to introduce into PEG-Hep hydrogels

Once the beneficial effect of unloaded PEG-Hep hydrogels was observed, we studied the effect of different chemical stimuli through the introduction of biomolecules into the hydrogels. For the introduction of such chemical stimuli, it was used the already proved capacity of the heparin present in the hydrogels for anchoring positively charged molecules through electrostatically interactions, mimicking the natural function of the heparin sulphates present in the ECM of the LNs.

Positively charged molecules associated with immune cell activation and expansion were studied in suspension and fixed in 2D and 3D systems to observe their effect on the proliferation and differentiation of CD4+ T cells. The proteins chosen for this purpose were the cytokines CCL21 and CCL19.

3.7.1 CCL21

Chemokine (C-C motif) ligand 21 -CCL21- is a small cytokine involved in the activation process of the immune system. It plays an important role in costimulating the expansion of CD4+ and CD8+ T cells and inducing Th1 polarization.[17] It is highly expressed in the endothelium of lymphatic vessels and LNs and interacts with T cells and mature DCs which express the chemokine receptor CCR7.[18,19]

T cells were initially activated in suspension in the presence of different concentrations of CCL21 to find the optimum amount of cytokine. The concentrations chosen were 1 ng/ml, 20 ng/ml, and 100 ng/ml. Elevated concentrations of CCL21 were avoided given their potentially inhibitory effect.[20] As can be seen in figure 3.13, no significant differences could be observed among the different CCL21 concentrations in suspension. The median values for the replication index for 100 ng/ml, 20 ng/ml, and 1 ng/ml were 1.01, 0.95, and 0.96, respectively, i.e. very similar to the positive controls. The same tendency was observed for the expansion index, with median values of 0.99, 1.02, and 0.99, and the proliferation index with values of 1.05, 1.12, and 1.00 for 100 ng/ml, 20 ng/ml, and 1 ng/ml, respectively.

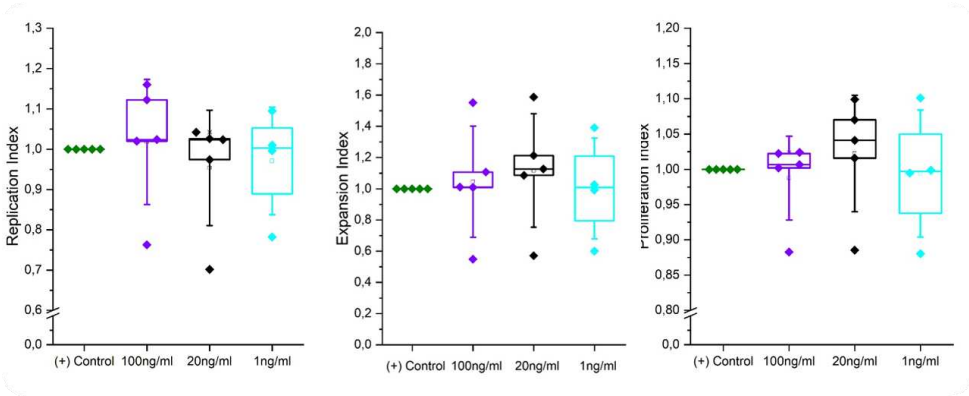

Figure 3.13 Normalized proliferation analysis of CD4+ T cells 6 days after seeding with different concentrations of CCL21 in suspension (N_{donors} = 5, with a minimum of $N_{donors/condition}$ = 4).

Nevertheless, CCL21 is known to be anchored to the stromal cells of the LNs. With the objective of mimicking such interaction, we studied the possibility of immobilizing it through its cysteine groups. Although the interaction between cysteine and Au has already been reported,[21,22] a proof of concept experiment was performed to ensure the attachment of CCL21 on Au surfaces through its domain rich in cysteines. For that, we used a surface that was functionalized with a quasi-hexagonal pattern of AuNPs only on its lower part by dip-coating, as previously reported.[23] Briefly, block copolymer micellar lithography (BCML) was used to prepare an Au-loaded micellar solution by dissolving an amphiphilic block copolymer in an apolar solvent to create reverse micelles.[24] In our case, commercial indium titanium oxide (ITO)-coated glass substrates were dip-coated with the loaded Au micellar solution obtaining AuNPs with a lateral interparticle distance of 68 ± 20 nm (figure 3.14.B). More details of the protocol used to achieve these surfaces is explained in chapter 6 section 6.2.5. These surfaces were passivated with PEG overnight and incubated with CCL21 during 1 h. After the incubation, an immunostaining (figure 3.14.C) was performed using human anti-CCL21 as primary antibody and mouse anti-human Alexa 488 as secondary antibody to observe through fluorescence where was the cytokine retained. A diagram of the experiment performed can be seen in figure 3.14.A. The immunostaining protocol used is explained in more detail in chapter 6 section 6.1.9. As can be seen below, fluorescence could only be detected in the part of the surfaces decorated with AuNPs, proving that CCL21 was fixed on their surface.

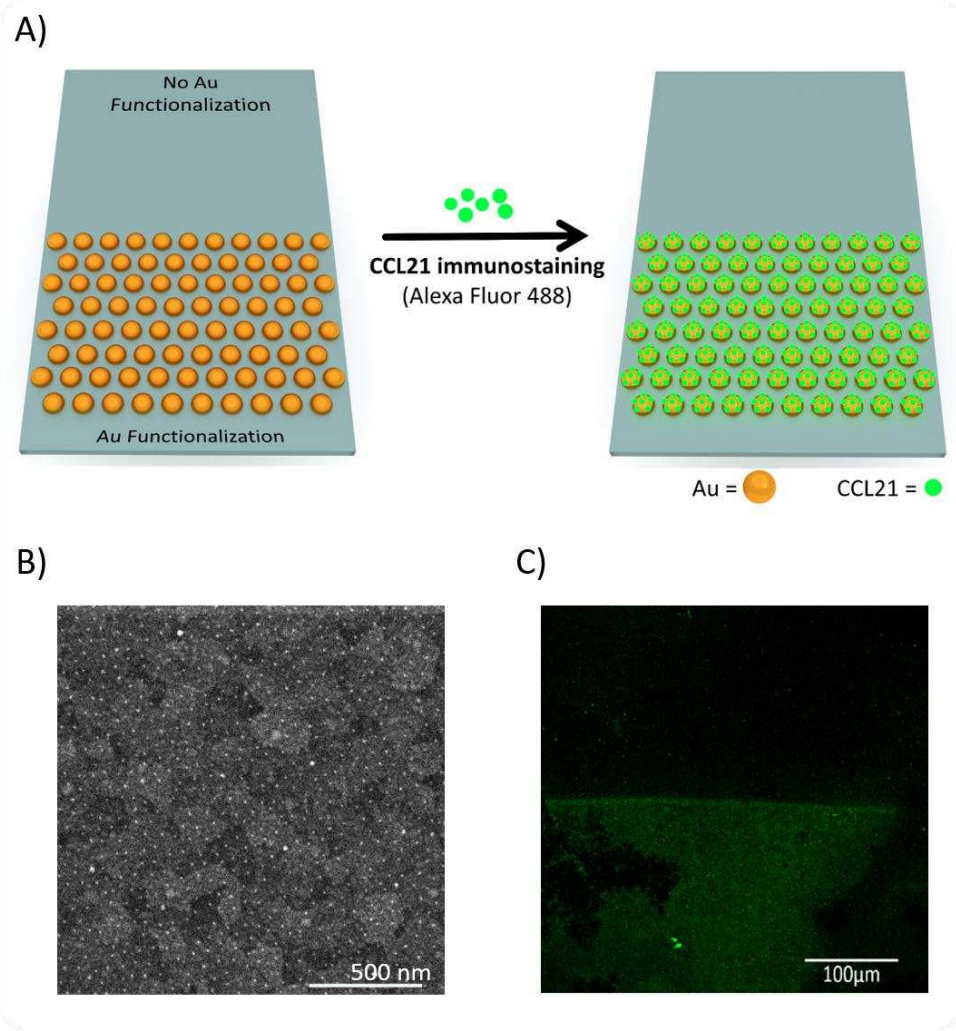

Figure 3.14 A) Scheme of the experiment performed to study the adhesion of CCL21 to gold substrates. B) SEM image of the ITO substrate with the quasi-hexagonal array of AuNPs. C) Fluorescence image of the surface decorated with AuNPs, functionalized with CCL21, immunostained with human anti-CCL21 and the secondary antibody with mouse anti-human Alexa 488, showing signal only on its lower half.

After verifying that CCL21 binds to Au, 2D planar Au surfaces were prepared as described in chapter 6, section 6.2.6, functionalized with CCL21, and used for cell culture. Specifically, the immobilization of CCL21 on Au surfaces was done at concentrations of 1 ng/ml and 20 ng/ml (figure 3.15.A) and resulted in significant changes (** $p < 0.01$) for the proliferation and expansion indexes. Specifically, the median values for the expansion index were of 1.1 and 1.16 for the concentrations of 20 ng/ml and 1 ng/ml respectively, showing an improvement of 10% and 16% in comparison with the positive control. Similarly, the proliferation index increased to 1.06 and 1.08 for each concentration. The replication index also showed a slight tendency to increase with median values of 1.06 for 20 ng/ml and 1.1 for 1 ng/ml.

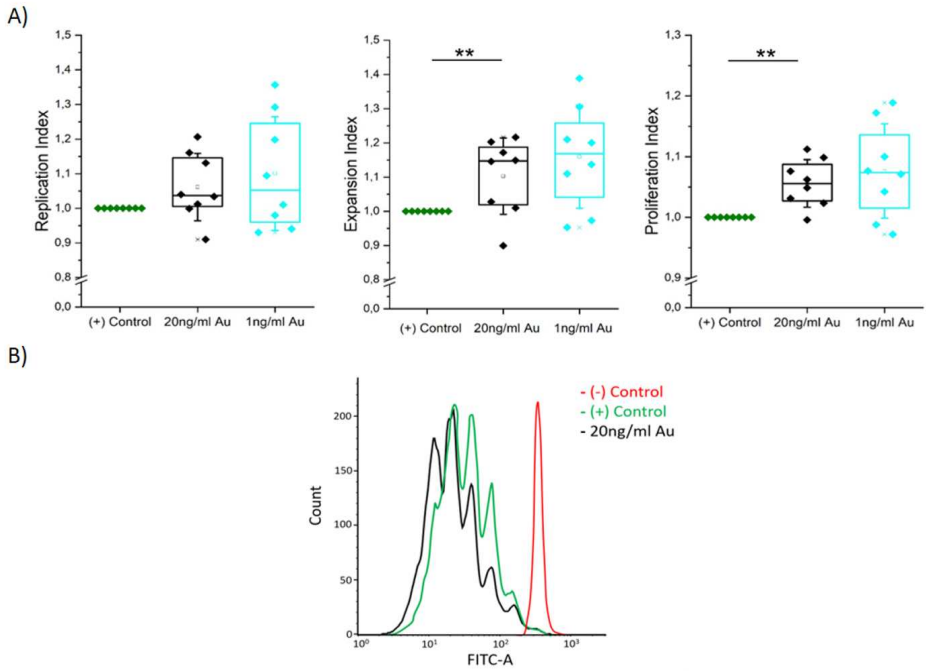

Figure 3.15 A) Normalized proliferation analysis of CD4+ T cells 6 days after seeding with different concentrations of CCL21 fixed to Au surfaces (N_{donors} = 8). Statistical significance was determined by the Mann-Whitney U test (** $p < 0.01$). B) Diagram of the resulting CFSE fluorescence peaks of a representative data point of CCL21 fixed to Au surfaces and its corresponding positive and negative control.

These results confirmed that CCL21 increases CD4+ T cell proliferation when fixed. In the next step, this cytokyne was loaded into PEG-Hep hydrogels. The study therefore evolved from a 2D to a 3D experiment; so a new optimization of the CCL21 concentration was performed. Different concentrations of CCL21 were incubated in PEG-Hep hydrogels and 100 ng/ml was identified as the concentration which led to the highest expansion results in contrast with the CCL21-immobilized on Au surfaces. This difference is most probably caused by the increase in total area available when moving from 2D to 3D biomaterials. As can be seen in figure 3.16, all the proliferation indexes were improved when using the hydrogel loaded with CCL21 in comparison with the unloaded hydrogel. For the hydrogels with 100 ng/ml of CCL21, a 30% of increase in the replication index was obtained in comparison with the positive control (1.3 of median value), while the unloaded hydrogel showed a 15% (1.15 of median value) of improvement. The proliferation and expansion indexes showed less pronounced increases with average values of 1.05 and 1.06, respectively. Again, the strongest difference was observed for the replication index, which seems to be the parameter most affected by the introduction of the 3D PEG-Hep hydrogels.

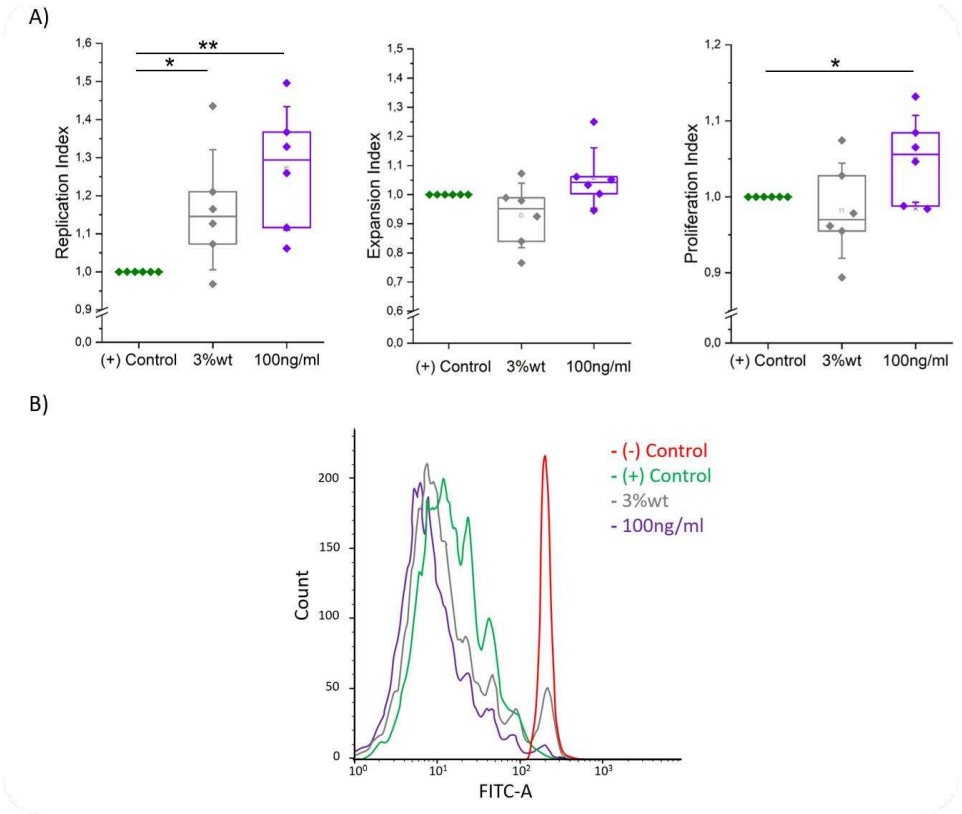

Figure 3.16 A) Normalized proliferation indexes 6 days after seeding CD4+ T cells in PEG-Hep hydrogels unloaded (3%wt) and loaded with 100 ng/ml of CCL21 (N_{donors} = 6). Statistical significance was determined by the Mann-Whitney U test (*p<0.05, **p<0.01). B) Diagram of the resulting CFSE fluorescence peaks of a representative data point.

Once verified that PEG-Hep hydrogels functionalized with CCL21 increase CD4+ T cell proliferation, differentiation assays were performed 5 days after seeding to determine the phenotype of the resulting T cells. The changes in the surface of CD4+ T cells caused by their activation result in different phenotypes, which were analyzed by flow cytometry. These phenotypes were naïve (T_N; CD45RO−/CD62L+), central memory (T_{CM}; CD45RO+/CD62L+), and effector memory (T_{EM}; CD45RO+/CD62L−).[25]

As mentioned in chapter 2, CD45RO is expressed on memory T cells. When naïve T cells become activated, they gradually lose the surface marker CD45RA and gain the CD45RO isoform.[26]

CD62L, also named L-selectin is a type I transmembrane cell adhesion molecule expressed on most circulating leukocytes, including neutrophils. L-selectin is one of three family members: L-, E- and P-selectin. Each selectin is defined according to the cell type in which it was first characterized (L = lymphocyte, E = endothelial cell, P = platelet).[27]

The percentages of CD4+ T cells that express CD45RO and CD62L prior to stimulation (negative control) are submitted to the intrinsic donor variability. As expected though, they mainly showed a T_N phenotype with a median value of 53%, whereas the T_{EM} and T_{CM} phenotypes were found in lowers percentages, being 12% and 32%, respectively (figure 3.17.A-C).

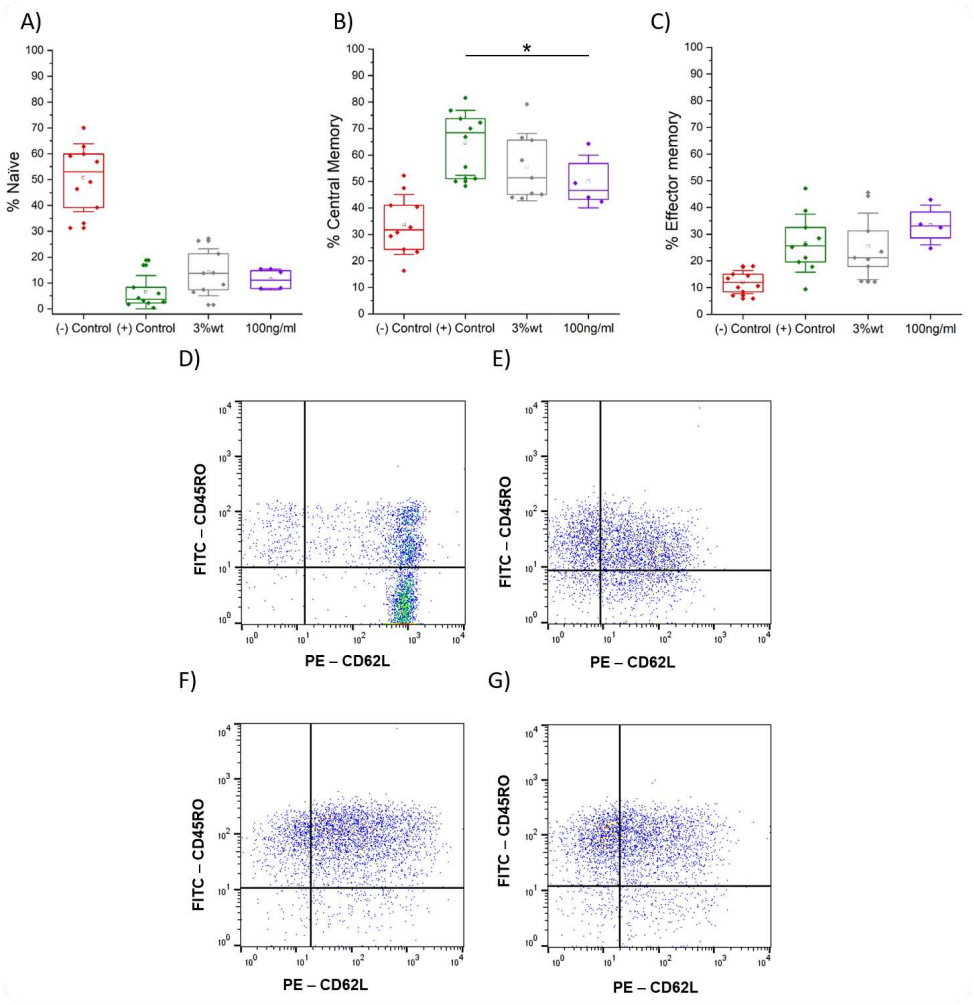

Figure 3.17 Differentiation analysis of CD4+ T cells 5 days after seeding (N_{donors} = 10, with a minimum of $N_{donors/condition}$ = 4). Percentage of A) naïve (T_N), B) central memory (T_{CM}), and C) effector memory (T_{EM}). Representative dot plot graphs of cells in a D) negative control, E) positive control, F) unloaded 3%wt PEG-Hep hydrogel, and G) 3%wt PEG-Hep hydrogel loaded with a solution of 100 ng/ml of CCL21. Statistical significance was determined by the Mann-Whitney U test (*$p<0.05$).

After stimulation, the median value of T_N cells decreased to 4% in suspension (positive control). Both unloaded and loaded (100 ng/ml of CCL21) hydrogels also exhibited a decrease of this phenotype, being the median values 14% and 11% respectively. Consequently, the T_{EM} and T_{CM} phenotypes increased in comparison with the negative

control. Specifically, the median values for the T_{CM} phenotype of the positive control, unloaded and loaded hydrogels were 68%, 51%, and 47%, respectively, thus showing lower percentages when using hydrogels. For the T_{EM} phenotype, median values raised to 26% for T cells in suspension, 21% for unloaded hydrogels, and 33% for hydrogels with 100 ng/ml of CCL21, showing an increase of effector cells for those seeded in cytokine loaded hydrogels. These results point out that PEG-Hep hydrogels can be used to modify the resulting phenotype of T cells and different chemical inputs could be studied to achieve diverse differentiation pathways. Finally, representative dot plots of the negative control, positive control, unloaded and loaded hydrogels are shown (figure 3.17.D-G). It can be seen how the resulting activated populations of cells evolve differently in suspension and in the hydrogel, although both come from the same initial population of cells.

In brief, we have seen how CCL21 improves CD4+ T cell proliferation and tune differentiation, increasing the total amount of effector T cells and decreasing the amount of central memory. Thus, it can be concluded that the capacity of PEG-Hep hydrogels for anchoring positively charged molecules opens the way to study different proteins to mimic the ECM, such as CCL19.

3.7.2 CCL19

CCL19 is a cytokine from the same family of CCL21 that interacts with the CCR7 receptor, like CCL21, resulting though in differential T cell signaling.[17] CCL21 has an extended C terminus that mediates GAG binding, whereas CCL19 lacks this domain and as such is an obligate soluble chemokine.[28] CCL19 has been found to act as a potent inducer of T cell proliferation in a DC-T cell co-culture system, although only with activated DCs.[29] Moreover, it has been identified as a key factor to increase T cell motility, conditioning T cells into a motile DC-scanning state amplifying the frequency of T cell responses.[30]

To study the effect of CCL19 on T cell activation, the cytokine was added in suspension with cells activated with Dynabeads. The same concentrations previously studied for CCL21 were used for CCL19, 100 ng/ml, 20 ng/ml, and 1 ng/ml. After 6 days of culture the proliferation results were measured (figure 3.18). In this case the highest increase of the proliferation parameters was observed for the concentration of 1 ng/ml, with median values of 1.19, 1.20, and 1.06 for the replication, expansion, and proliferation indexes, respectively.

Although no statistical changes were observed for the concentrations of 100 and 20 ng/ml of CCL19 in suspension, a tendency to increase the proliferation of CD4+ T cells can be seen for the latter. In contrast with the results observed for CCL21, where no significant differences were observed in solution, CCL19 showed its influence in suspension for the concentration of 1 ng/ml in agreement with its soluble nature.

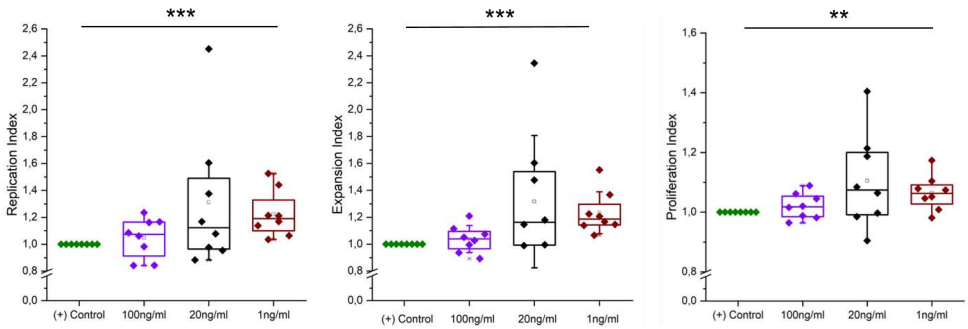

Figure 3.18 Normalized proliferation analysis of CD4+ T cells 6 days after seeding without cytokine (positive control) and with different concentrations of CCL19 in suspension (N_{donors} = 8). Statistical significance was determined by the Mann-Whitney U test (**p<0.01, ***p<0.001).

Nevertheless, we also decided to study the differences between having CCL19 in solution and anchored to the hydrogels. As shown in figure 3.19, the replication index exhibited an increase of 50% and 56% for unloaded hydrogels and loaded with 100 ng/ml of CCL19 respectively (1.5 and 1.53 of median value) compared with the positive control. A lower increase of 38% for hydrogels loaded with 20 ng/ml of CCL19 was also obtained. A similar tendency was observed for the expansion index, with average values of 1.35, 1.47, and 1.34 for unloaded, 100 ng/ml and 20 ng/ml of CCL19 respectively. Finally, the achieved proliferation index median values were 1.23, 1.20, and 1.14 respectively. Thus, all the proliferation indexes were improved in comparison with the positive control, however, no significant differences were observed between the unloaded hydrogels and the ones with CCL19, as expected given its soluble nature.

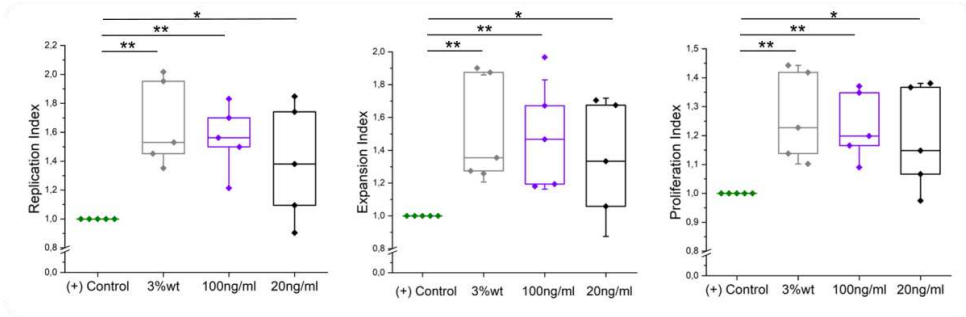

Figure 3.19 Normalized proliferation indexes 6 days after seeding CD4+ T cells in unloaded PEG-Hep hydrogels (3%wt), and in PEG-Hep hydrogels loaded with 100 ng/ml and 20 ng/ml of CCL19 (N_{donors} = 6). Statistical significance was determined by the Mann-Whitney U test (*p<0.05, **p<0.01).

3.7.3 CCL21 loaded in the hydrogel and CCL19 in solution

Once having studied CCL21 and CCL19 separately, both cytokines were used with the objective to maximize the proliferation results and mimicking the natural behavior of the LN. In agreement with the results previously obtained, the concentrations used were

100 ng/ml for both CCL21 and CCL19. However, CCL21 was loaded in the hydrogel during 1 h and CCL19 was added in solution with the media [CCL21(h) CCL19(s)]. Proliferation was measured 6 days after seeding. The results can be seen in figure 3.20.

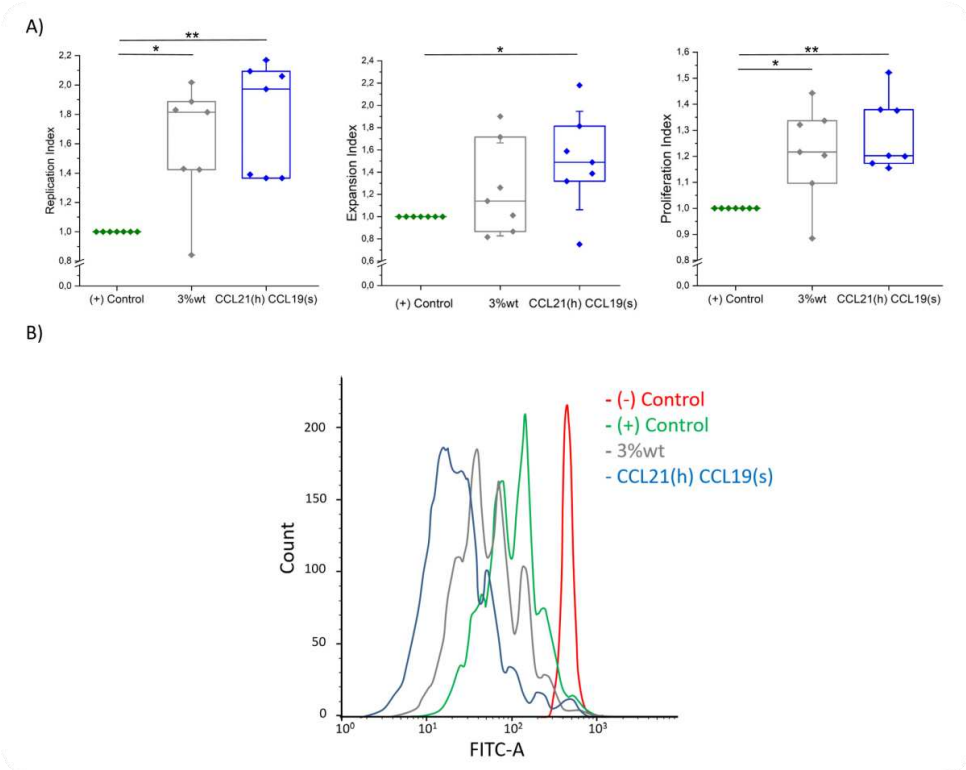

Figure 3.20 A) Normalized proliferation indexes 6 days after seeding CD4+ T cells in unloaded PEG-Hep hydrogels (3%wt) and in PEG-Hep hydrogels loaded with 100 ng/ml of CCL21 and with 100 ng/ml of CCL19 in solution (N_{donors} = 6). Statistical significance was determined by the Mann-Whitney U test (*p<0.05, **p<0.01). B) Diagram of the resulting CFSE fluorescence peaks of a representative data point.

Hydrogels loaded with 100 ng/ml of CCL21 and 100 ng/ml of CCL19 in solution showed to duplicate the replication index (2 of median value) in comparison with the positive control, improving also the unloaded hydrogel, which had a median value of 1.8. The expansion index was also improved obtaining average values of 1.5 for the hydrogel with cytokines and 1.13 for the unloaded hydrogel. Finally, the proliferation index obtained similar median values, 1.21 and 1.20 respectively, showing higher statistical significance in the case of the hydrogel with CCL21 and CCL19. These results show the benefits of resembling the natural environment of cells as accurate as possible, thus achieving higher proliferation rates than the ones observed only with one of the cytokines or with the unloaded hydrogel.

3.8 Summary and conclusions/perspectives

In this chapter we presented the synthesis and characterization of PEG-Hep hydrogels and their optimization to mimic the ECM of the LNs. Such hydrogels were used for CD4+ T cell expansion and differentiation.

More specifically, we presented the successful optimization of the reaction between heparin and maleimide (Hep-Mal. Then, PEG-Hep hydrogels with different percentages of PEG were efficiently produced (6%wt, 4%wt, and 3%wt) by mixing the Hep-Mal and thiolated 4-arm PEG. The mechanical properties of the resulting hydrogels were measured by rheology. Briefly, high values of hydrogel stiffness were related with high percentages of PEG. The porosity was analyzed by different techniques that showed that the lower the amount of PEG in the samples the higher the pore sizes and the interconnectivity obtained. Finally, the capacity of the hydrogel to retain positively charged molecules due to electrostatic interactions with the heparin was proven through fluorescence measurements using GFP as a positively charged model protein. All the data resulting from this characterization evidenced that the 3%wt PEG-Hep hydrogels were the most suitable for CD4+ T cell culture.

The use of PEG-Hep hydrogels to culture CD4+ T cells showed an increase in the proliferation of CD4+ T cells, and modification of the resulting phenotypes, even without the addition of any chemical stimuli. Moving a step forward, the cytokine CCL21 was anchored to the heparin present in the hydrogel to promote CD4+ T cell proliferation. First, it was proven that CCL21 induces CD4+ T cell proliferation when is fixed, but has no effect when is in suspension. Thus, PEG-Hep hydrogels were pre-incubated with CCL21 and afterwards used for CD4+ T cell culture. Higher proliferation results than the ones observed with unloaded hydrogels were obtained, proving the versatility of this platform to introduce different chemical factors. The same study was performed with CCL19, although in this case significant differences were observed when having the cytokine in solution. The highest proliferation parameters obtained were achieved with the combination of both cytokines, the CCL21 loaded in the hydrogel and CCL19 added in solution to the media, mimicking their original state in the LN. This system proved to have the potential to be further developed and explored towards the fabrication of artificial LNs, and could help surpassing one of the most challenging limitations of current immunotherapies, which is producing large amounts of T cells with therapeutic phenotypes.

3.9 References

1. Pérez del Río, E., Martinez Miguel, M., Veciana, J., Ratera, I. & Guasch, J. Artificial 3D Culture Systems for T Cell Expansion. *ACS Omega* **3**, 5273–5280 (2018).
2. Wang, H., Cai, L., Paul, A., Enejder, A. & Heilshorn, S. C. Hybrid elastin-like polypeptide-polyethylene glycol (ELP-PEG) hydrogels with improved transparency and independent control of matrix mechanics and cell ligand density. *Biomacromolecules* **15**, 3421–3428 (2014).
3. Nie, T., Baldwin, A., Yamaguchi, N. & Kiick, K. L. Production of heparin-functionalized hydrogels for the development of responsive and controlled growth factor delivery systems. *J. Control. Release* **122**, 287–296 (2007).
4. Nie, T., Akins, R. E. J. & Kiick, K. L. Production of heparin-containing hydrogels for modulating cell responses. *Acta Biomater.* **5**, 865–875 (2009).
5. Robinson, K. G. *et al.* Differential effects of substrate modulus on human vascular endothelial, smooth muscle, and fibroblastic cells. *J. Biomed. Mater. Res. A* **100**, 1356–1367 (2012).
6. Freudenberg, U. *et al.* A star-PEG–heparin hydrogel platform to aid cell replacement therapies for neurodegenerative diseases. *Biomaterials* **30**, 5049–5060 (2009).
7. Baldwin, A. D. & Kiick, K. L. Reversible maleimide-thiol adducts yield glutathione-sensitive poly(ethylene glycol)-heparin hydrogels. *Polym. Chem.* **4**, 133–143 (2013).
8. Lammermann, T. & Sixt, M. The microanatomy of T-cell responses. *Immunol. Rev.* **221**, 26–43 (2008).
9. Singh, A. & Peppas, N. A. Hydrogels and scaffolds for immunomodulation. *Adv. Mater.* **26**, 6530–6541 (2014).
10. Tsao, C.-T. *et al.* Thermoreversible poly(ethylene glycol)-g-chitosan hydrogel as a therapeutic T lymphocyte depot for localized glioblastoma immunotherapy. *Biomacromolecules* **15**, 2656–2662 (2014).
11. Kloxin, A. M., Kloxin, C. J., Bowman, C. N. & Anseth, K. S. Mechanical properties of cellularly responsive hydrogels and their experimental determination. *Adv. Mater.* **22**, 3484–3494 (2010).
12. Irvine, D. J., Stachowiak, A. N. & Hori, Y. Lymphoid tissue engineering: invoking lymphoid tissue neogenesis in immunotherapy and models of immunity. *Semin. Immunol.* **20**, 137–146 (2008).
13. Zuidema, J. M., Rivet, C. J., Gilbert, R. J. & Morrison, F. A. A protocol for rheological characterization of hydrogels for tissue engineering strategies. *J. Biomed. Mater. Res. B. Appl. Biomater.* **102**, 1063–1073 (2014).
14. Ross-Murphy, S. B. & Shatwell, K. P. Polysaccharide strong and weak gels. *Biorheology* **30**, 217–227 (1993).
15. Ferry, J. D. *Viscoelastic Properties of Polymers*. *3rd Edition. John Wiley, New York* (1980).

16. Liang, Y. & Kiick, K. L. Heparin-functionalized polymeric biomaterials in tissue engineering and drug delivery applications. *Acta Biomater.* **10**, 1588–1600 (2014).

17. Flanagan, K., Moroziewicz, D., Kwak, H., Horig, H. & Kaufman, H. L. The lymphoid chemokine CCL21 costimulates naive T cell expansion and Th1 polarization of non-regulatory CD4+ T cells. *Cell. Immunol.* **231**, 75–84 (2004).

18. Sokol, C. L. & Luster, A. D. The chemokine system in innate immunity. *Cold Spring Harb. Perspect. Biol.* **7** (2015).

19. Shi, M., Chen, D., Yang, D. & Liu, X.-Y. CCL21-CCR7 promotes the lymph node metastasis of esophageal squamous cell carcinoma by up-regulating MUC1. *J. Exp. Clin. Cancer Res.* **34** (2015).

20. Ziegler, E. *et al.* CCR7 signaling inhibits T cell proliferation. *J. Immunol.* **179**, 6485–6493 (2007).

21. Caprile, L. *et al.* Interaction of l-cysteine with naked gold nanoparticles supported on HOPG: a high resolution XPS investigation. *Nanoscale* **4**, 7727–7734 (2012).

22. Tkachenko, A., Xie, H., Franzen, S. & Feldheim, D. L. Assembly and characterization of biomolecule-gold nanoparticle conjugates and their use in intracellular imaging. *Methods Mol. Biol.* **303**, 85–99 (2005).

23. Cavalcanti-Adam, E. A. *et al.* Cell spreading and focal adhesion dynamics are regulated by spacing of integrin ligands. *Biophys. J.* **92**, 2964–2974 (2007).

24. Guasch, J. *et al.* Synthesis of Binary Nanopatterns on Hydrogels for Initiating Cellular Responses. *Chem. Mater.* **28**, 1806–1815 (2016).

25. Sommermeyer, D. *et al.* Chimeric antigen receptor-modified T cells derived from defined CD8+ and CD4+ subsets confer superior antitumor reactivity in vivo. *Leukemia* **30**, 492–500 (2016).

26. Bujan, W. *et al.* Abnormal T-cell phenotype in familial erythrophagocytic lymphohistiocytosis. *Lancet (London, England)* **342** (1993).

27. Ivetic, A. A head-to-tail view of L-selectin and its impact on neutrophil behaviour. *Cell Tissue Res.* **371**, 437–453 (2018).

28. Murphy, P. M. Double duty for CCL21 in dendritic cell trafficking. *Immunity* **32**, 590–592 (2010).

29. Marsland, B. J. *et al.* CCL19 and CCL21 induce a potent proinflammatory differentiation program in licensed dendritic cells. *Immunity* **22**, 493–505 (2005).

30. Kaiser, A., Donnadieu, E., Abastado, J.-P., Trautmann, A. & Nardin, A. CC chemokine ligand 19 secreted by mature dendritic cells increases naive T cell scanning behavior and their response to rare cognate antigen. *J. Immunol.* **175**, 2349–2356 (2005).

CHAPTER 4
Expansion of PBMCs in 3D systems

4.1 Introduction

PBMCs are a cell population whose composition is donor-dependent, but approximately is formed by an 80% of T and B cells, 10% NK cells, and 10% monocytes. A diagram of the cells present in this population can be seen in Chapter 1, figure 1.1. These blood cells play an important role in the immune response which preserves the host's homeostasis, fight infection, and cope with intruders.[1] They have been used for immunotherapy to treat patients with problems such as cancer or infectious diseases.[2]

Payne et al.[3] studied the clinical applicability of a cellular reprogramming protocol using PBMCs of breast cancer patients expanded *ex vivo*. They reported that the combined proteins bryostatin 1 and ionomycin, together with the cytokines IL-2, IL-7, and IL-15 could expand and reprogram tumor-sensitized PBMCs, achieving cells resistant to myeloid-derived suppressor cells (MDSC), and with a predominantly CD62L+ memory T cell phenotype. These results suggest that NK T cells may protect T cells from MDSC suppression via an NKG2D-dependent signaling pathway, although further investigation is required.[3] Preclinical studies showed that reprogrammed memory T cells persisted in animals after complete rejection of the tumor.[4] Currently this is one of the major goals of Immunotherapy, because it would allow not only to overcome the tumor, but also to avoid any possible relapse. This research exemplifies one of the advantages of working with PBMCs, which is the synergy between the different cells that integrate the PBMC population influencing both proliferation and differentiation pathways. However, using populations with different types of cells, as PBMCs, increases the number of variables present in the study.

PBMC-derived models have also shown excellent preclinical results to study immune checkpoint inhibitors, as described by Shouheng Lin et al.[5] This model consisted of human lung cancer cells implanted in mice followed by an injection of human PBMCs. After four weeks the efficacy could be evaluated, showing accurate results in terms of PD-L1/PD-1 signaling,[5] which is a pathway that has been successfully exploited to elicit positive responses in lung cancer patients in some clinical trials.[6,7]

Somerville et al.[8] studied PBMC expansion in a WAVE® bioreactor (figure 1.8.C of chapter 1). Through the use of this system, gene modified cells were generated with comparable properties to a gas permeable static bags, thus simplifying the process of rapidly expanding tumor reactive lymphocytes. Cellular and immunological analysis suggested that the WAVE bioreactor may be a preferred method of cell expansion for some cell subsets or phenotypes, such as the CD8+CD62L+ and CD62+ cells.[8] This study shows the impact that the method of expansion can have not only in the efficiency of cell proliferation, but also in the resulting phenotypes.

Additionally, PBMCs are the precursor cell population of different types of purified cells used in ACT, such as T cells.[3–5,9] The purification of such cells might also have an influence on the clinical results, as shown in CIK cells, whose biological activity changed when purified using a blood cell separator (apheresis method) or a Ficoll lymphocyte separation medium (Ficoll method).[10]

Another immunotherapy that has been widely studied using PBMCs is the addition of T cell bispecific antibodies (TCBs) that target an antigen on the tumor cells and recruit immune cells for the lysis of the former. Different TCBs have been studied in order to cause potent tumor killing activity reducing the toxicities derived from cytokine release.[11-13] For example, there are antibodies that target the receptor tyrosine kinase HER2, which is a tumor-associated antigen of approximately the 25% of breast cancers.[14]

To explore the potential of 3D systems throughout the field of immunotherapy, PBMCs were cultured in the 3D platforms previously mentioned.

4.2 Objectives and strategy

As has been mentioned, primary human PBMCs are usually the source of relevant therapeutic T cell subsets such as CD4+ and CD8+ T cells. They are isolated and can be expanded ex vivo using different approaches, however, current expansion systems should be improved in order to efficiently expand large quantities of cells. Depending of the chosen system it would be possible not only to increase the number of obtained cells, but also to manipulate the differentiation pathways of seeded cells affecting the phenotype of the resulting expanded cells.

With the objective of study new 3D platforms for PBMC expansion that allow to tune cell differentiation, two different 3D systems have been studied: 3D polystyrene scaffolds and PEG-Hep synthetic hydrogels, as previously done with CD4+ T cells. The techniques to measure proliferation and study the resulting phenotypes are the ones previously described in chapters 2 and 3. Moreover, in this chapter the cytotoxic capability of the cultured PBMCs was studied through a co-culture of the resulting PBMCs with cancerous cells in the presence of bispecific antibodies in collaboration with Prof. J. Arribas from the Vall d'Hebron Institute of Oncology (VHIO, Spain).

4.3 PBMC culture in 3D polystyrene scaffolds

We first explored the possibility of culturing PBMCs in a commercially available 3D polystyrene scaffold, before assessing their proliferation in our recently synthetized PEG-Hep hydrogels.

4.3.1 Proliferation analysis

As performed for CD4+ T cells in chapter 2.4, the expansion, proliferation, and replication indexes of PBMCs seeded in 3D Polystyrene Scaffolds (3D Biotek, USA) (figure 2.1.B, chapter 2) were evaluated 5 days after seeding. A graphical representation of the obtained numeric results, and a diagram of the peaks of fluorescence achieved with the CFSE staining for a representative point are shown in the figure below.

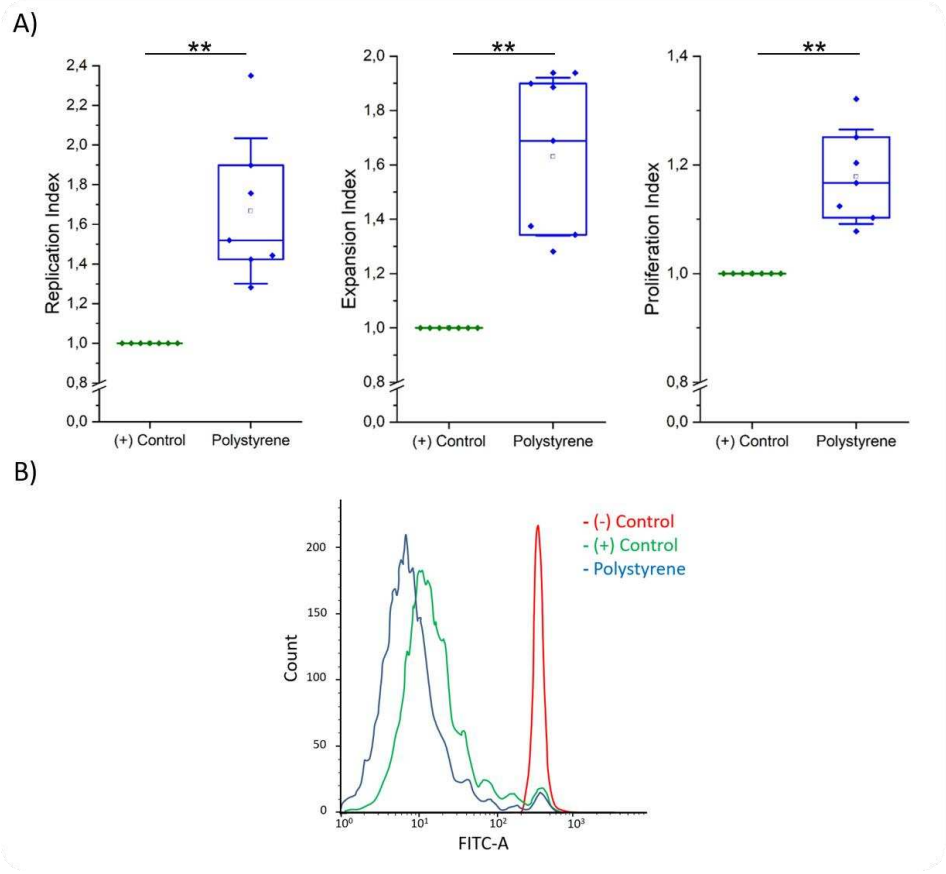

Figure 4.1 A) Normalized proliferation analysis of PBMCs 5 days after activation with Dynabeads and seeding in suspension (positive control) and in 3D polystyrene scaffolds (N_{donors} = 7). B) Diagram of the resulting CFSE fluorescence peaks of a representative data point. The negative control corresponds to PBMCs seeded in suspension without Dynabeads. Statistical significance was determined by the Mann-Whitney U test (**$p < 0.01$).

The resulting data indicates that all the parameters increased after 5 days of culture. The higher increase was observed for the expansion index, with a median value of 1.68, i.e. an improvement of a 68% was achieved. The replication and proliferation indexes showed a media of 1.52 and 1.17, respectively.

In contrast with the results obtained for the CD4+ T cells seeded on 3D polystyrene scaffolds, statistically significant results were obtained after 5 days for all the proliferation parameters studied. Moreover, higher proliferation rates were achieved in comparison with the CD4+ T cell experiments due to the presence of all the different types of cell populations that compose the PBMCs. The interactions between cells such as T cells with monocytes present in the PBMCs, enhance the proliferative stimulus.[15] However, the use of PBMCs also increase the variability of the results, affecting the reproducibility of the experiments due to the presence of many different types of cells in the same culture and the lack of control of their proportions due to their donor-dependent nature.

As previously mentioned, polystyrene scaffolds not only present an excellent connectivity with open size pores that allow the adequate diffusion of cells and nutrients, but also present a mechanically strong structure.[16] According to these results, it seems that the 3D stiff structure of these 3D polystyrene scaffolds is beneficial for PBMC overall proliferation, although they could be improved, for example, by adding chemical stimuli.

4.3.2 Differentiation analysis

Once proven that the 3D polystyrene scaffolds increased PBMC proliferation, the CD3+CD4+ and CD3+CD8+ proportions after expansion were analyzed to study if the presence of the scaffold affected the proportion of these populations. This experiment was performed following the protocol used to analyze the quality of PBMCs after purification described in chapter 6.1.2.

The median percentage of CD4+ T cells in the negative control was of 67.3%, while in the positive control increased to 72.8%. The value obtained with the 3D polystyrene scaffold was of 69.0%. These results show that after activation, the percentage of CD3+CD4+ T cells increased, however, the presence of the 3D polystyrene scaffold, slightly reduced the percentage of these cells.

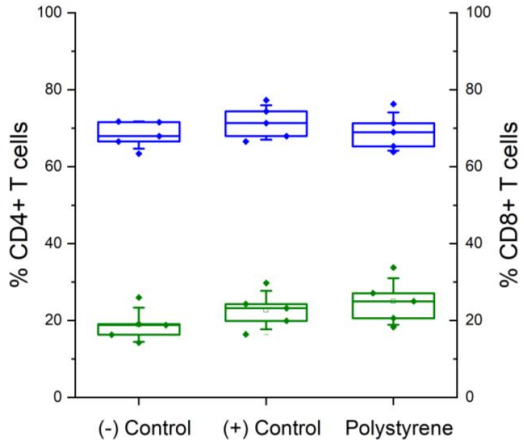

Figure 4.2 Percentage of CD3+CD4+ and CD3+CD8+ T cell subsets within PBMCs. The box plots summarize the percentage of CD4+ (blue) and CD8+ (green) T cells within PBMCs (N_{donors} = 6) cultured in suspension with (positive control) and without (negative control) Dynabeads, as well as cells expanded with Dynabeads in a 3D polystyrene scaffold. Statistical significance was determined by the Mann-Whitney U test (*p < 0.05).

The median percentage of the CD3+CD8+ phenotype in the negative control was of 18.9%, which increased after activation to 21.5% in the positive control and 25.0% for T cells seeded in the 3D polystyrene scaffold, as shown in figure 4.2. Thus, it seems that the 3D polystyrene scaffold, although only provides 3D mechanical support without any chemical stimuli, favors the CD3+CD8+ proportion 5 days after T cell activation. This information is very valuable as CD8+ T cells are the subset of choice in many ACT applications, because of their effector cytotoxic function and enhanced antitumor activity.[17] It is also worth mentioning that in general terms, the higher percentage of CD4+ than CD8+ T cells in the PBMCs agrees with the reported 2:1 ratio found in peripheral blood.[18]

As previously mentioned, CD45RO is a surface protein expressed by human leukocytes and used as a marker of memory T cells.[19] CD62L, also named L-selectin is a type I transmembrane cell adhesion molecule expressed on most circulating leukocytes.[20]

In this case the population under study is PBMCs, which, as said, is mainly composed of CD4+ and CD8+ T cells (~80%), but it also has cells of different nature. Consequently, we did not use the T_N, $T_{CM,}$ or T_{EM} terminology, but the presence or absence of the relevant markers (CD45RO−/CD62L+, CD45RO+/CD62L+, and CD45RO+/CD62L−).

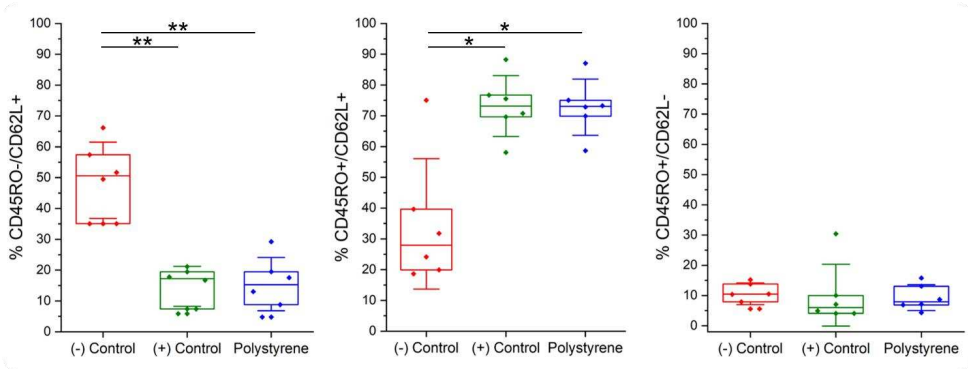

Figure 4.3 Differentiation analysis of PBMCs 5 days after seeding showing the percentages of CD45RO−/CD62L+, CD45RO+/CD62L+, and CD45RO+/CD62L+. The controls consist of cells seeded in suspension with (positive control) and without (negative control) Dynabeads. The sample cells were activated with Dynabeads and seeded in 3D polystyrene scaffolds (N_{donors} = 6). Statistical significance was determined by the Mann-Whitney U test (*p<0.05, **p<0.01).

The resulting phenotypes analysed with this procedure barely changed for cells activated in suspension and in the 3D polystyrene scaffolds. The percentage of CD45RO−/CD62L+ cells decreased from a mean value of 50.6% for the inactivated cells (or negative control) to 17.1% for cells activated in suspension (or positive control) and 15.1% for cells seeded and activated in 3D polystyrene scaffolds. These values resulted in a significant decrease of this phenotype for activated cells, but no significant differences were observed due to the effect of the 3D system. CD45RO+/CD62L+ cells increased from a mean percentage of 28.1% in the negative control, to a mean value of 73.1% in both the positive control and 3D polystyrene scaffold. Finally, no significant change was observed for CD45RO+/CD62L+ cells, i.e. similar median values of 10.7%, 6.2%, and 8.2% were obtained for the negative and positive controls and polystyrene, respectively. These results show that although the proliferation indexes obtained for PBMCs expanded in 3D polystyrene scaffolds were higher than for PBMCs expanded in suspension, the resulting phenotypes are similar for both conditions.

4.3.3 Analysis of the killing capacity

To study the cytotoxic capacity of the phenotypes obtained after the activation and expansion of PBMCs under different conditions, the resulting cells were cultured together with MKN45, a carcinoembryonic antigen (CEA)-expressing tumor cell line of human gastric adenocarcinoma, with the objective of study the capacity of the resulting PBMCs to kill these tumoral cells, in collaboration with Prof. J. Arribas (VHIO, Spain). Additionally, we added an IgG-based TCB, which recognizes the CEA present in this cell line and recruit immune cells due to interaction with the CD3 marker. A scheme of this experiment is shown in figure 4.4.

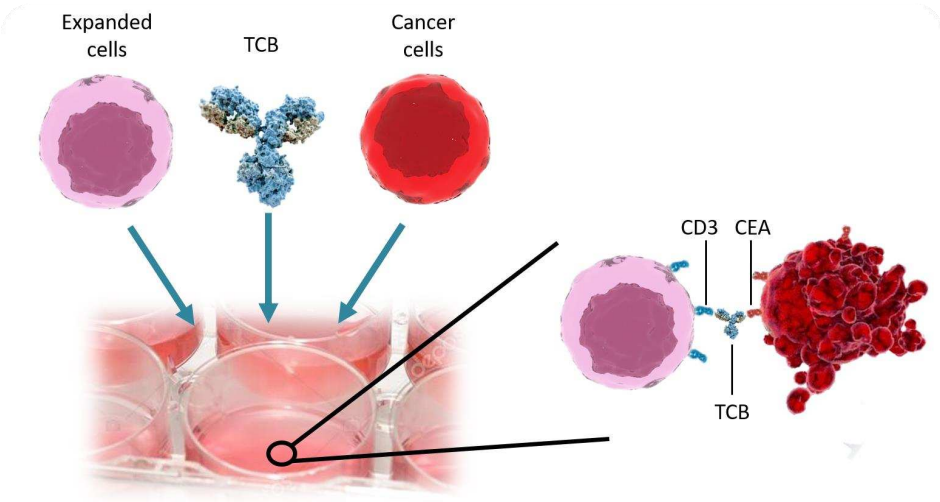

Figure 4.4 Co-culture of expanded PBMCs together with a TCB that recognizes the CEA present in this cell line and recruits immune cells due to interactions with the CD3 domain, causing the death of the cancer cells.

This CEA-TCB is a novel approach for the treatment of CEA-expressing solid tumors, which has already been proven to cause the secretion of cytotoxic granules and tumor cell lysis.[22] To ensure that there is no intrinsic T cell killing prior to adding the CEA-TCB to the cell culture (PBMCs were polyclonally activated and not directed against CEA), the first step consisted of culturing PBMCs activated in suspension with MKN45 cells.

With this objective, first we compared PBMCS cultured in our standard complete RPMI media (20% of FBS and 1% of P/S) with PBMCs cultured in RPMI with "human serum (HS)" consisting of 10% of HS, 10 mM of HEPES, and 30 IU/ml of IL-2, which was the protocol used by Prof. J. Arribas laboratory to ensure the inactivity of PBMCs prior to TCB addition. In both cases, PBMCs were expanded using Dynabeads for 5 days and then co-cultured with MKN45 in HS medium during 2 days without the addition of the TCB. The results can be seen in the figure below.

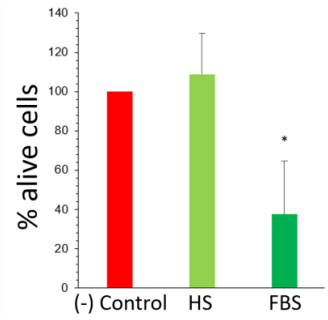

Figure 4.5 Cytotoxicity study of cultured PBMCs against MNK45 cells without TCB. The PBMCs were non-activated (negative control) and activated PBMCs in suspension with Dynabeads using either HS or FBS media (N_{donors} = 2).

Although no killing capacity was expected, PBMCs expanded in RPMI with FBS showed inner killing capacity. In order to avoid interferences in the cytotoxic studies, and study the killing capacity of resulting PBMCs caused exclusively by the presence of the TCB and different phenotypes, we substituted the FBS-containing media by the HS one.

Consequently, we assessed the influence of such medium in the proliferation of PBMCs without the addition of any 3D system during 6 days of culture. The results obtained are shown in figure 4.6. The proliferation parameters studied did not show any significant difference between PBMCs seeded in one supplemented medium or the other, with the exception of the expansion index. This index showed a slight decrease when cells were cultured in RPMI supplemented with HS, falling their median normalized values from 1.00 to 0.83. The median values for the replication and proliferation indexes were 1.06 and 0.93 respectively.

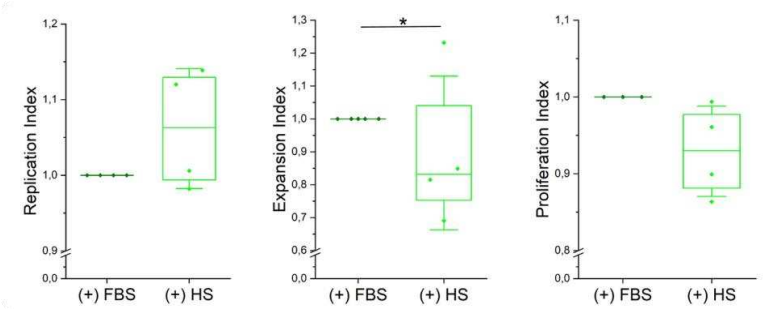

Figure 4.6 Proliferation study of the effect of FBS and HS used as supplements of the RPMI media after 6 days of culture. Analysis was made with N_{donors} = 4. Statistical significance was determined with Mann-Whitney U test (*p<0.05).

In addition to the proliferation study, the resulting phenotypes of cells were studied for the different media following the system previously used (section 4.3.2). The CD45RO−/CD62L+ cells showed median values of 52.60% and 48.20% for the negative control when using FBS and HS, respectively, whereas values of 33.40% and 26.12% were obtained for the positive control. As shown in figure 4.7, no significant changes were achieved for these cells. Similarly, the CD45RO+/CD62L+ cells did not result in

significant changes either with a 22.80% and 26.34% for the inactivated cells as well as a 55.04% and 48.20% for activated cells for FBS and HS-based media, respectively. However, the CD45RO+/CD62L− PBMCs showed a significant increase in their phenotype for activated cells cultured in RPMI supplemented with HS, from a 6.03% of the media supplemented with FBS to a 17.30%. These results show that, with the exception of a slight increase of the CD45RO+/CD62L- population, no significant changes were observed by changing the supplement of the media in terms of proliferation.

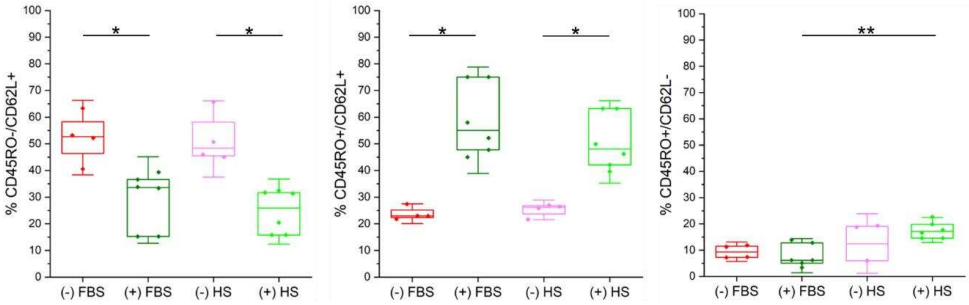

Figure 4.7 PBMC differentiation analysis when cultured in negative and positive controls, supplemented with either FBS or HS. The results shown were obtained 5 days after seeding, from $N_{donors} = 6$ with a minimum of $N_{donors/condition} = 4$. Statistical significance was determined with Mann– Whitney U test (*p<0.05, **p<0.01).

Once proven that HS could be used without major changes in proliferation and differentiation, the killing capacity of PBMCs cultured with HS in suspension and in 3D polystyrene scaffolds, without the addition of the TCB was studied (figure 4.8).

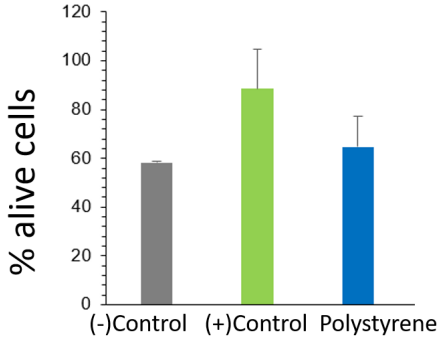

Figure 4.8 Cytotoxicity study of cultured PBMCs against MNK45 cells without TCB. The PBMCs were non-activated (negative control) and activated PBMCs in suspension and 3D polystyrene scaffolds with Dynabeads using HS medium ($N_{donors} = 2$).

As no basal killing capacity was observed in this case, the TCB was added. Different concentrations of the antibody were used to study the cytotoxic capacity of the expanded PBMCs measuring the number of malignant cells resting in the culture after 2 days of co-culture. All conditions (positive and negative controls and PBMCs seeded in 3D polystyrene) were seeded at the same cell concentration, thus the number of cells

obtained after expansion is not relevant in this experiment. In contrast, the phenotypes obtained are crucial to induce cytotoxic capacity in combination with the TCB. More information of this experiment and its protocol can be found in chapter 6 section 6.1.10. The achieved results can be seen in figure 4.9.

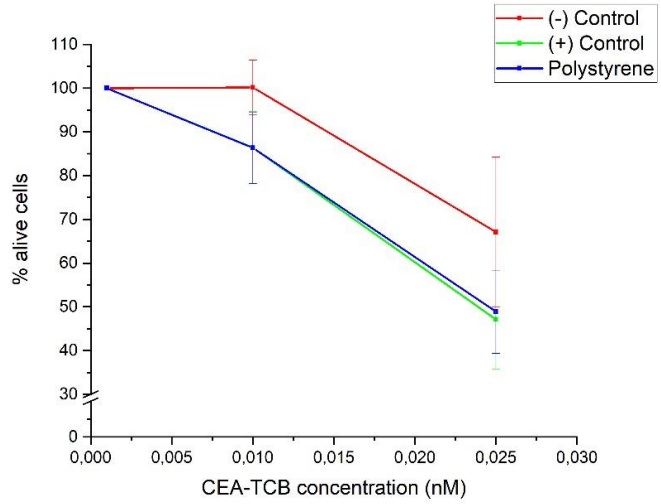

Figure 4.9 Cytotoxicity study of cultured PBMCs against MNK45 cells with TCB at different concentrations. The PBMCs were non-activated (negative control), activated in suspension (positive control) or activated in 3D polystyrene scaffolds (N_{donors} = 5).

The concentrations used of targeting CEA-TCB were 0.001 nM, 0.01 nM, and 0.025 nM. Inactivated PBMCs did not show any killing capacity for antibody concentrations of 0.001 nM and 0.01 nM. However, at a concentration of CEA-TCB of 0.025 nM, T cells seem to be affected by the capacity of the antibody, killing cancer cells and decreasing this population to a median value of 67.1% MKN45 survival. When using cells from the positive control and cells expanded in 3D polystyrene scaffolds, the MKN45 survival dropped from a 100% at a concentration of 0.001 nM of antibody to 86.3% at 0.01 nM for both cases. Moreover, the survival rates further decreased reaching values of 49.3% and 47.2% at 0.025 nM CEA-TCB for the positive control and the 3D polystyrene scaffold, respectively. These results are in agreement with our hypothesis that PBMCs expanded in suspension (positive control) and in 3D polystyrene scaffolds would show similar killing capacities giving their similar resulting phenotypes.

4.4 PBMC culture in PEG-Hep hydrogels

After proving that the increase observed in CD4+ T cell proliferation when using 3D polystyrene scaffolds in comparison with standard suspensions (chapter 2.4) could be extrapolated to PBMCs, PEG-Hep hydrogels were studied with the same purpose. The protocols of hydrogel preparation (chapter 6.2.3) and seeding (chapter 6.1.6) used for CD4+ T cells were also applied to PBMCs.

4.4.1 Proliferation analysis

Proliferation was measured 5 days after cell seeding in unloaded and loaded hydrogels with 100 ng/ml of CCL21. The obtained results can be seen in figure 4.10. PBMCs exhibited lower median values than the positive control for all the indexes studied. Specifically, the replication index showed no statistically significant difference with media normalized values of 0.93 for the unloaded PEG-Hep hydrogels and 0.88 for the ones loaded with CCL21. However, the expansion index showed statistical relevance with median normalized values of 0.84 and 0.73 for unloaded and loaded hydrogels, respectively. Finally, the proliferation index also exhibited slight reductions for the unloaded PEG-Hep hydrogels with a median value of 0.95 and loaded with cytokine, with a higher decrease to 0.92. Unfortunately, the tendency observed for CD4+ T cells seeded in PEG-Hep hydrogels of increased cell expansion (chapter 3.7.1, figure 3.15) could not be thus reproduced with PBMCs.

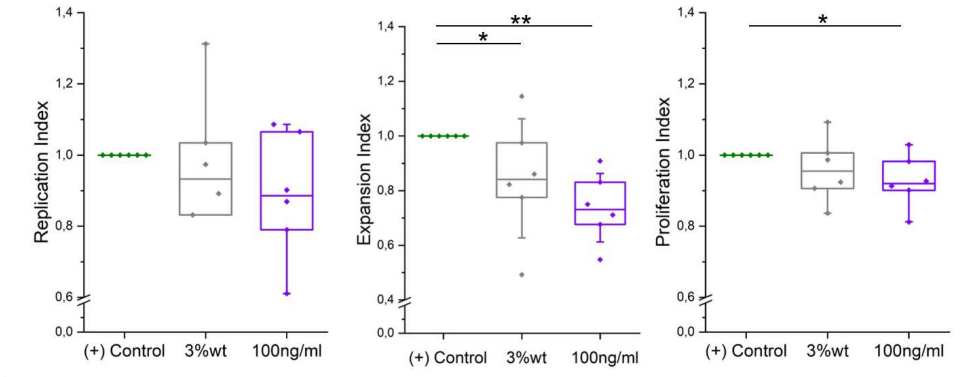

Figure 4.10 Normalized proliferation indexes of PBMCs after 5 days of expansion in suspension, and using PEG-Hep hydrogels unloaded (3%wt) and loaded with 100 ng/ml of CCL21 (N_{donors} = 6). Statistical significance was determined by the Mann-Whitney U test (*p<0.05, **p<0.01).

Given these results, we repeated these experiments 6 days after seeding to study if longer culturing times were needed to appreciate a beneficial effect. The protocols used were the same than the ones used in the previous experiments.

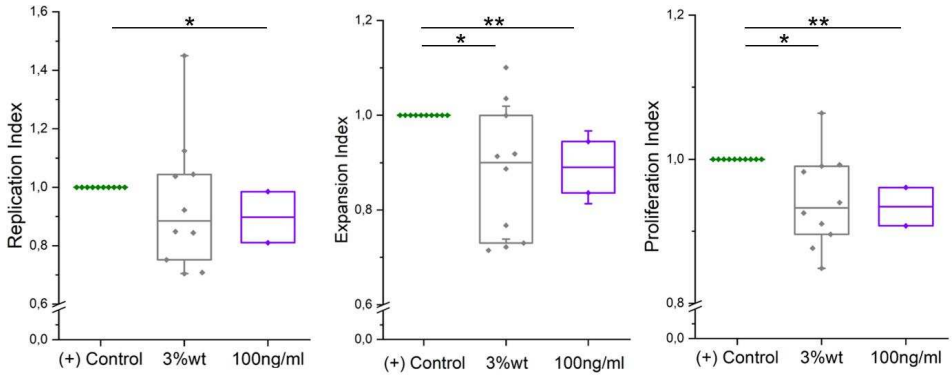

Figure 4.11 Normalized proliferation indexes of PBMCs after 6 days of expansion in suspension, and using PEG-Hep hydrogels unloaded (3%wt) and loaded with 100 ng/ml of CCL21 (N_{donors} = 10, with a minimum of $N_{donors/condition}$ = 2). Statistical significance was determined by the Mann-Whitney U test (*p<0.05, **p<0.01).

Nevertheless, as showed in figure 4.11, similar results were achieved 6 days after seeding. Namely, the replication, expansion, and proliferation indexes of PBMCs seeded in 3%wt PEG-Hep hydrogels decreased a 12%, 10%, and 7%, with median values of 0.88, 0.90, and 0.93, respectively. Moreover, very large ranges and high variability were obtained with percentiles Q-25 and Q-75 of 0.75 and 1.05 for the replication index, 0.73 and 1.00 for the expansion index, and 0.90 and 1.00 for the proliferation index. Similar data were obtained for PEG-Hep hydrogels loaded with 100 ng/ml of cytokine with median values of 0.90 for replication and expansion indexes, and 0.94 for the proliferation index. In this last case, only two donors were used due to the observed inefficiency to improve the proliferation parameters. As it was obtained for 5 days of culture the proliferation parameters could not be improved.

4.4.2 Differentiation analysis

The resulting phenotypes of PBMCs seeded in PEG-Hep hydrogels were also studied to discriminate between CD45RO−/CD62L+, CD45RO+/CD62L+, and CD45RO+/CD62L− cells (Figure 4.12).

The CD45RO−/CD62L+ phenotype significantly decreased from a mean value of 52.8% for the negative control, to 6.7% and 7.4% for the positive control and hydrogel. The percentage of CD45RO+/CD62L+ cells increased from a median percentage of 29.7% for inactivated cells to 69.8% and 56.4% for PBMCs activated in suspension and in the hydrogel. On the other hand, the CD45RO+/CD62L- population increased significantly from an 8.9% of the negative control to a 19.0% of the positive control and a 31.2% for the PBMCs seeded in PEG-Hep hydrogels.

In this case thus, not only differences could be observed in the resulting phenotypes of activated and inactivated cells, but also in PBMCs activated in suspension and in 3D PEG-Hep hydrogels.

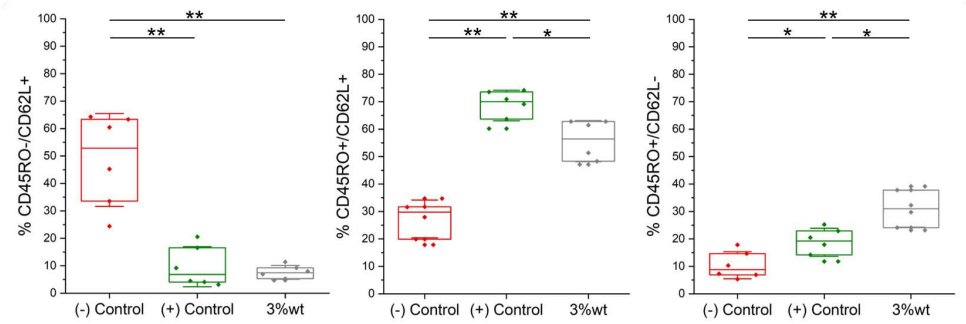

Figure 4.12 Differentiation analysis of PBMCs activated with Dynabeads and cultured in suspension and PEG-Hep hydrogels (N_{donors} = 6). Statistical significance was determined by the Mann-Whitney U test (*p<0.05, **p<0.01).

In summary, these results showed that, although the proliferation parameter could not be improved for PBMCs with the use of PEG-Hep hydrogels, they affected the differentiation pathways taken by the cells, allowing to tune the resulting phenotypes. Taking into account that T cell differentiate in a linear direction from T_N to T_{CM} to T_{EM},[23] rather than branching from different early subtypes, we assume that the higher percentage of CD45RO+/CD62L- (corresponding to T_{EM}) means that the resulting cells were more differentiated from the initial population. In future experiments, we will further optimize the physicochemical conditions of the hydrogels to promote the differentiation into T_{CM}, which has been proved to be the preferable phenotype for therapy success.[24,25]

4.5 Summary and conclusions

In this chapter PBMCs were used to study their expansion and differentiation capacities when cultured in different 3D systems with the objective to use them for experiments with patients in collaboration with Prof. J. Arribas (VHIO, Spain). It was proven that the use of 3D polystyrene scaffolds increased PBMC proliferation, achieving significantly higher values of expansion, proliferation, and replication indexes 5 days after seeding. Also, the resulting phenotypes from this platform were analyzed. Although no significant changes were observed through the analysis of the CD45RO and CD62L markers, the CD3+CD8+ T cells were favored over the CD3+CD4+ T cells. The cytotoxic assays demonstrated the same killing capacity of MKN45 cells by PBMCs expanded in suspension than in the 3D scaffolds when using the targeting CEA-TCB (once HS was implemented in our protocol as the medium supplement to avoid interferences with the intrinsic killing capacity of PBMCs acquired by the use of FBS). We suggest that these results can be explained by the functional phenotypes after the culture despite the increased CD3+CD8+ population.

In any case, the improvement of the proliferation makes the 3D polystyrene scaffolds a good option for PBMC activation and expansion. However, the unfeasibility of introducing a chemical input in these 3D structures, prevents a further proliferation improvement and a tune in the resulting phenotypes.

The use of PEG-Hep synthetic hydrogels to culture PBMCs enabled the introduction of such chemical input to the culture. However, it resulted in a proliferation decrease 5 and 6 days after seeding for both unloaded and loaded hydrogels (with 100 ng/ml of CCL21). Moreover, the scaffold resulted in a significantly higher percentage of CD45RO+/CD62L- cell population (effector memory phenotype, T_{EM}, for T cells) accompanied by a decrease in the percentage of CD45RO+/CD62L+ (central memory phenotype, T_{CM}, for T cells). These phenotypes were also obtained with the pure CD4+ T cell population. Given the linear differentiation pathway followed by T cells previously reported,[23] we hypothesize that the higher percentage of T_{EM} could be reduced together with the culture time. Moreover, other chemical stimuli, such as the combination of immobilized CCL21 and soluble CCL19, could be studied in order to obtain the desired phenotypes.

4.6 References

1. Acosta Davila, J. A. & Hernandez De Los Rios, A. An Overview of Peripheral Blood Mononuclear Cells as a Model for Immunological Research of Toxoplasma gondii and Other Apicomplexan Parasites. *Frontiers in cellular and infection microbiology* **9**, 24 (2019).
2. Heo, Y. J., Son, C. H., Chung, J.-S., Park, Y.-S. & Son, J. H. The cryopreservation of high concentrated PBMC for dendritic cell (DC)-based cancer immunotherapy. *Cryobiology* **58**, 203–209 (2009).
3. Payne, K. K. *et al.* Peripheral blood mononuclear cells of patients with breast cancer can be reprogrammed to enhance anti-HER-2/neu reactivity and overcome myeloid-derived suppressor cells. *Breast Cancer Res. Treat.* **142**, 45–57 (2013).
4. Kmieciak, M. *et al.* Activated NKT cells and NK cells render T cells resistant to myeloid-derived suppressor cells and result in an effective adoptive cellular therapy against breast cancer in the FVBN202 transgenic mouse. *J. Immunol.* **187**, 708–717 (2011).
5. Lin, S. *et al.* Establishment of peripheral blood mononuclear cell-derived humanized lung cancer mouse models for studying efficacy of PD-L1/PD-1 targeted immunotherapy. *MAbs* **10**, 1301–1311 (2018).
6. Garon, E. B. *et al.* Pembrolizumab for the treatment of non-small-cell lung cancer. *N. Engl. J. Med.* **372**, 2018–2028 (2015).
7. Chakravarti, N. & Prieto, V. G. Predictive factors of activity of anti-programmed death-1/programmed death ligand-1 drugs: immunohistochemistry analysis. *Transl. lung cancer Res.* **4**, 743–751 (2015).
8. Somerville, R. P. T., Devillier, L., Parkhurst, M. R., Rosenberg, S. A. & Dudley, M. E. Clinical scale rapid expansion of lymphocytes for adoptive cell transfer therapy in the WAVE(R) bioreactor. *J. Transl. Med.* **10**, (2012).
9. Petersen, C. T. *et al.* Improving T-cell expansion and function for adoptive T-cell therapy using ex vivo treatment with PI3Kdelta inhibitors and VIP antagonists. *Blood Adv.* **2**, 210–223 (2018).
10. Liu, H. *et al.* Comparative study of different procedures for the separation of peripheral blood mononuclear cells in cytokine-induced killer cell immunotherapy for hepatocarcinoma. *Tumour Biol.* **36**, 2299–2307 (2015).
11. Trinklein, N. D. *et al.* Efficient tumor killing and minimal cytokine release with novel T-cell agonist bispecific antibodies. *MAbs* **11**, 639–652 (2019).
12. Fu, M. *et al.* Therapeutic Bispecific T-Cell Engager Antibody Targeting the Transferrin Receptor. *Front. Immunol.* **10**, (2019).
13. Zeidler, R. *et al.* Simultaneous activation of T cells and accessory cells by a new class of intact bispecific antibody results in efficient tumor cell killing. *J. Immunol.* **163**, 1246–1252 (1999).
14. Rius Ruiz, I. *et al.* p95HER2-T cell bispecific antibody for breast cancer treatment. *Sci. Transl. Med.* **10**, (2018).

15. Blasco, E. *et al.* Proliferative response of human CD4+ T lymphocytes stimulated by the lectin jacalin. *Eur. J. Immunol.* **25**, 2010–2018 (1995).

16. Caicedo-Carvajal, C. E., Liu, Q., Remache, Y., Goy, A. & Suh, K. S. Cancer Tissue Engineering: A Novel 3D Polystyrene Scaffold for In Vitro Isolation and Amplification of Lymphoma Cancer Cells from Heterogeneous Cell Mixtures. *J. Tissue Eng.* (2011).

17. Jackson, S. R., Yuan, J. & Teague, R. M. Targeting CD8+ T-cell tolerance for cancer immunotherapy. *Immunotherapy* **6**, 833–852 (2014).

18. Verhoeckx K, Cotter P, López-Expósito I, Kleiveland C, Lea T, Mackie A, Requena T, Swiatecka D, W. H. *The Impact of Food Bioactives on Health: in vitro and ex vivo models. Chapter 16. PBMC-Derived T Cells*. (2015).

19. Valentine, M. *et al.* Expression of the memory marker CD45RO on helper T cells in macaques. *PLoS One* **8** (2013).

20. Ivetic, A. A head-to-tail view of L-selectin and its impact on neutrophil behaviour. *Cell Tissue Res.* **371**, 437–453 (2018).

21. Sommermeyer, D. *et al.* Chimeric antigen receptor-modified T cells derived from defined CD8+ and CD4+ subsets confer superior antitumor reactivity in vivo. *Leukemia* **30**, 492–500 (2016).

22. Bacac, M. *et al.* A Novel Carcinoembryonic Antigen T-Cell Bispecific Antibody (CEA TCB) for the Treatment of Solid Tumors. *Clin. Cancer Res.* **22**, 3286–3297 (2016).

23. Durek, P. *et al.* Epigenomic Profiling of Human CD4(+) T Cells Supports a Linear Differentiation Model and Highlights Molecular Regulators of Memory Development. *Immunity* **45**, 1148–1161 (2016).

24. Ghassemi, S. *et al.* Reducing Ex Vivo Culture Improves the Antileukemic Activity of Chimeric Antigen Receptor (CAR) T Cells. *Cancer Immunol. Res.* **6**, 1100–1109 (2018).

25. Sadelain, M., Riviere, I. & Riddell, S. Therapeutic T cell engineering. *Nature* **545**, 423–431 (2017).

CHAPTER 5
PEG–Hep hydrogels for 3D Printing

5.1. Introduction

3D printing is a technique that consists of producing 3D objects with precisely designed geometries in a layer by layer approach. Moreover, this fabrication method is compatible with different materials, and thus, there are different inks that can be used, ranging from polymers to metals, including ceramics and organic molecules. This system represents a promising technology in various fields due to its notable advantages including a high degree of automation and accurate control of complex structures, especially in biomedical engineering.[1]

Nowadays, **3D printing technologies** can be divided into four major categories, namely vat photopolymerization-based printing, powder-based printing, droplet-based printing, and extrusion-based printing.[2] Vat photopolymerization-based printing technologies uses a vat of a liquid photopolymer such as resins, out of which the model is constructed layer by layer, while an ultraviolet (UV) light is used to cure or harden the resin where required. Inside this category, there are the stereolithography, direct light processing, and continuous liquid interface production techniques.[3,4] The powder-based printing technology uses localized heating to fuse the materials utilized, which usually are polyamide, alumide, titanium, and rubber-like materials. Techniques such as selective laser sintering, direct metal laser sintering, selective laser melting, multijet fusion, and electron beam melting, belong to this category.[5] In droplet-based printing technologies such as multijet modeling, laser-induced forward transfer, and wax deposition modeling, liquid droplets are ejected onto a substrate to form a layer by layer construct.[6,7] Finally, the extrusion-based printing, which includes fused deposition modeling and direct ink writing, uses printable materials that are extruded from a nozzle and deposited in filaments layer by layer on a platform to form a 3D construct.[8,9] A scheme of this technique can be seen in figure 5.1. This last technique is the most popular method in biomedicine, especially for cell-laden 3D constructs, because of the wide range of printable materials that can be used including cells, as well as its simplicity.[10]

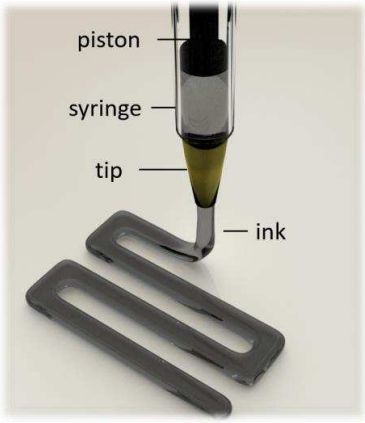

Figure 5.1 Diagram of a typical extrusion-based printing technique.

In this field, 3D printing has been used for different applications such as tissue engineering, pharmacokinetic analysis, and basic cell biology studies. For example, implants and scaffolds have been created for regenerative medicine[11] or artificial tissues have been produced with the objective of replicating the structures of native tissues by precisely depositing biological factors and cell-laden biomaterials.[12–15] An ideal bioink to ensure the correct functionality of bioprinted tissues and organs should possess certain mechanical and biological properties. Regarding the physical properties, the material should have adequate structural strength and stiffness, preferably in a tunable and dynamic manner through an adjustable gelation and stabilization process. The porosity is a key parameter of the material, because it affects cellular responses such as migration, but also the robustness and strength of the material. Additionally, the bioink must be obviously biocompatible and should be processed under cell-friendly conditions, i.e. no toxic agents, neutral pH, and room temperature processes. Depending on the application, it should also present some biodegradability, allow chemical modifications to satisfy tissue-specific needs, and have potential for large-scale production.[11,16–18] Bioinks may be made from natural polymers (such as collagen, fibrinogen, alginate, gelatin, etc.), synthetic biomaterials (such as PEG, poly (vinyl alcohol), etc.), or combinations of both.[19] For example, Matrigel was studied mixed with alginate to improve its printability for vascularization studies, revealing that the types of materials and their ratios are critical parameters to adjust when developing an optimum bioink.[20]

5.2 Objectives and strategy

Due to the beneficial effects showed by PEG-Hep hydrogels for T cell expansion (chapter 3) and in order to move one step forward in the study of the potential of this material for different applications, these hydrogels were analyzed as bioink for 3D printing in collaboration with Dr. Miguel Timoneda from the Institute of Bioengineering of Catalonia (IBEC, Spain). To achieve this, the gelification process of PEG-Hep hydrogels was optimized and adjusted to the 3D printer requirements. Then, the resulting scaffolds were studied for immune cell culturing. Both CD4+ T cells and PBMCs were used to study the potential of the 3D printing technique, which also opens the way to new applications such as cell-laden PEG-Hep hydrogels that we started to explore.

5.3 PEG-Hep hydrogels as bioink for 3D printing

To use PEG-Hep hydrogels as bioink, the gelification process had to be optimized to obtain well defined pre-designed 3D scaffolds for cell culture in a 3D Discovery printer from RegenHU Biosystem Architects (Switzerland). In this case, the printed structure chosen was a basic one, which is commonly used by our collaborators in IBEC to evaluate new materials, consisting of a grid with a separation of 1.5 mm between its lines and of 4 layers of height. A diagram of this structure can be seen in figure 5.1.

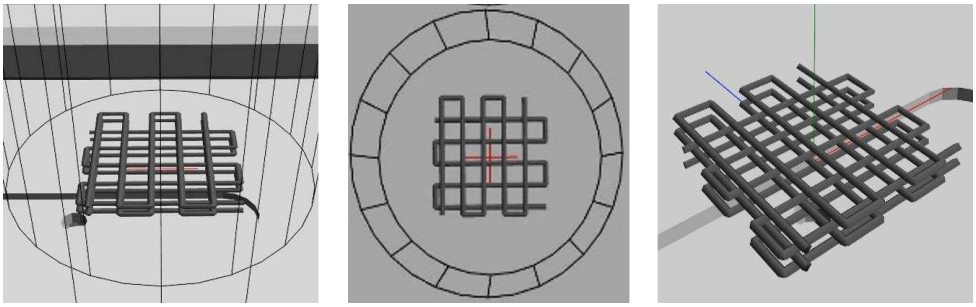

Figure 5.2 Schematic images of the scaffold designed to optimize the use of PEG-Hep hydrogels as bioink.

With this purpose, 3%wt PEG-Hep hydrogels were prepared in PBS as usual, following the protocol explained in chapter 6.2.3. Once the solutions with both reagents (PEG and Hep) were mixed and heated up to 37°C, the resulting mixture was analyzed as bioink for 3D printing at different times. 3 h after the beginning of the gelification, the sample remained liquid impeding its printing. Nevertheless, the first printings could be performed after 3.5 h, when the sample had enough consistency. As shown in figure 5.2.A, the resulting scaffolds had though a very low rigidity and no differentiated lines were achieved in the printed grid. To improve that, samples were stored overnight under two conditions, at room temperature and in the incubator at 37°C, and the experiment was repeated after 24 h of gelation. The material stored at room temperature showed optimal properties for its printing, obtaining quite well defined scaffolds, as it can be seen in figure 5.2.B. Nevertheless, samples stored at 37°C inside the incubator got very dried, making the printing heterogeneous and difficult, and the resulting scaffolds were not adequate for cell culture (figure 5.2.C). Additionally, different pressures of extrusion and tips for the printing were tested. After the corresponding optimization experiments, it was found that the optimum extrusion pressure was of 1.2 bars by using a conic tip with an inner diameter of 27 G (0.36 mm).

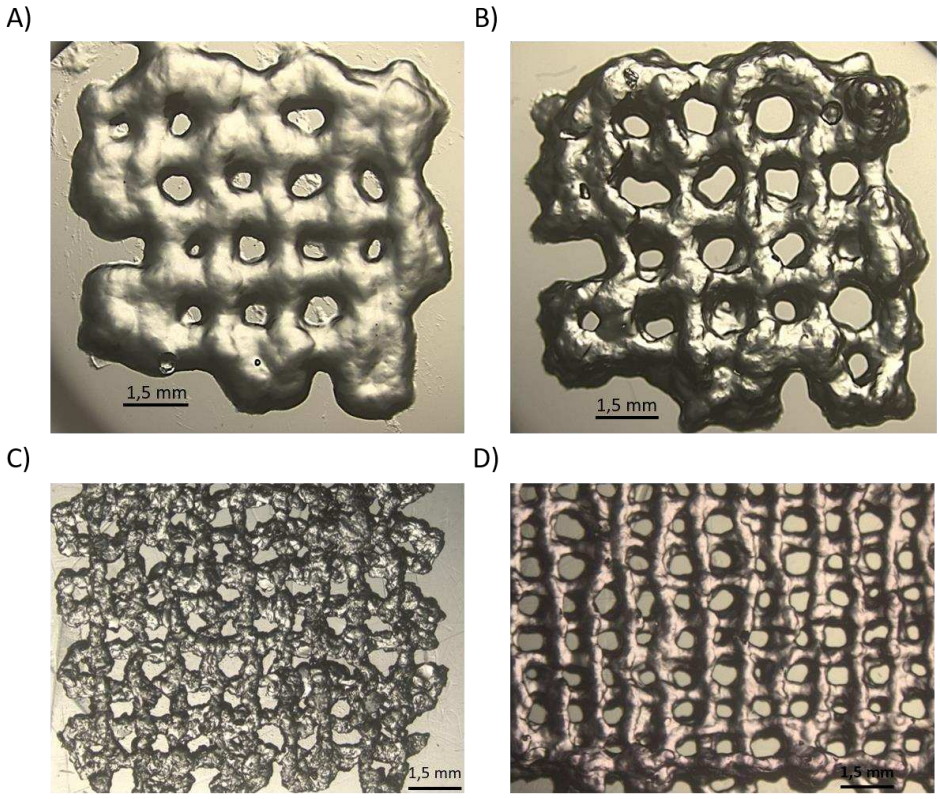

Figure 5.3 Microscope images of the resulting scaffolds printed with a 3%wt PEG-Hep hydrogel after A) 3.5 hours of gelation, B) one day at room temperature, and C) one day incubated at 37°C. D) Microscope images of scaffolds printed with 3%wt PEG-Hep hydrogels made in DMEM media instead of PBS.

In order to assess the use of PEG-Hep hydrogels for cell-laden experiments, we tried to prepare these hydrogels in culture media instead of PBS as usual. Unexpectedly, the gelation was immediate, probably due to the catalysis of the gelification reaction through some of the components present in the cell media, and the resulting gel could be properly printed (figure 5.2.D). Thus, this strategy could be used in the future to introduce cells inside the hydrogel through cell-laden experiments.

5.4 PEG-Hep printed scaffolds for CD4+ T cell expansion

Once it was demonstrated that 3%wt PEG-Hep hydrogels could be used as bioink and the protocol was optimized, 3D layered structures were printed to observe their effect on CD4+ T cell culturing and ensure their (bio)compatibility.

Initially, we assessed the printing in a 96 well plate (WP) as these are the ones that we usually employ. It was technically impossible due to the intrinsic resolution of the used 3D printer. Consequently, we discarded the possibility of directly printing on a 96 WP and we printed the scaffolds in the larger wells of the 24 WP (figure 5.3).

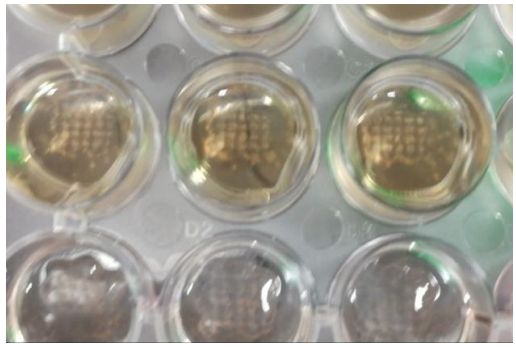

Figure 5.4 Photographs of the printed scaffolds in the 24WP with CD4+ T cells.

Given the price of the material and that the printed superficial area was higher than in the non-printed hydrogels, it was decided to print scaffolds of 4 and 6 layers with 1.5 mm of separation between the lines of the grid, using ~35 and ~50 µg of material, respectively, as a starting point to evaluate the potential usefulness of the printing process. Although we maintained the cell concentration of the seeded CD4+ T cells at 10^6 cells/ml as in the previous experiments (chapters 2-4), the total volume of media had to be scaled up ten times, from 100 µl to 1 ml due to the larger size of the well. Consequently, the number of cells/µg of material was lower than in the previous experiments where each hydrogel weighted ~50 µg. The results obtained in this chapter are therefore not quantitatively comparable to the ones obtained in the previous chapters.

We first evaluated unloaded printed hydrogels and after we incubated the scaffolds with 100 ng/ml of CCL21 as in the previous studies, given that the protein was considered small enough to successfully penetrate the hydrogel. Thus, it is supposed to be equally distributed in both printed and non-printed systems.

5.4.1 Unloaded printed hydrogels

Unloaded printed scaffolds of 4 and 6 layers were cultured with CD4+ T cells activated with Dynabeads during 6 days. Afterwards, the replication, expansion, and proliferation indexes were measured by flow cytometry as usually and compared with the ones obtained for cells seeded in suspension (positive control). The results were normalized to the positive control, as showed in chapter 2 section 2.4.3.

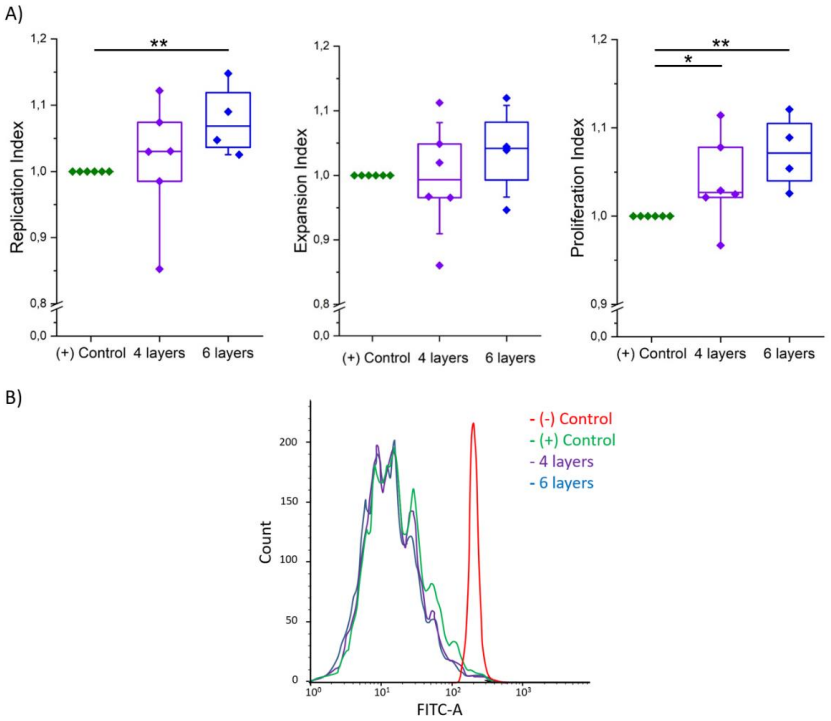

Figure 5.5 A) Normalized proliferation analysis of CD4+ T cells seeded in suspension (positive control), and unloaded printed PEG-Hep hydrogels of 4 and 6 layers of height, 6 days after seeding (N_{donors} = 6). Statistical significance was determined by the Mann-Whitney U test (*p<0.05, **p<0.01). B) Diagram of the resulting CFSE fluorescence peaks of a representative data point for all the conditions.

The PEG-Hep scaffold printed with a height of 4 layers exhibited a slight tendency to increase the proliferation parameters in comparison with the positive control, obtaining normalized values of 1.03 for the replication and proliferation indexes. The only significant change obtained was in the proliferation index. On the other hand, the PEG-Hep scaffolds printed with 6 layers of height showed higher and statistically significant proliferation parameters, improving the replication and proliferation index a 7% (1.07 as a result of their normalized value), and the expansion index a 4%. It can be therefore concluded that the amount of hydrogel used has an influence on cell proliferation, improving the proliferation parameters with higher amounts of material, i.e. higher number of layers. Thus, the presence of a 3D printed scaffold improves T cell proliferation in comparison to expansion in suspension. The representative graph of the

CFSE peaks obtained (figure 5.4.B) shows lower differences than in previous cases, given that the material/cell proportion has decreased ten times compared to previous experiments. Because of that, it can be concluded that the amount of printed material used could be further increased in order to improve the proliferation indexes.

To determine if the phenotype of the resulting T cells was affected, the differentiation assay explained in chapter 3 section 3.7, was here performed again with scaffolds of 4 and 6 layers. Thus, the resulting CD4+ T cell populations were classified in naïve (T_N; CD45RO−/CD62L+), central memory (T_{CM}; CD45RO+/CD62L+), and effector memory (T_{EM}; CD45RO+/CD62L−)[21] 5 days after seeding. The results achieved are shown in the figure below.

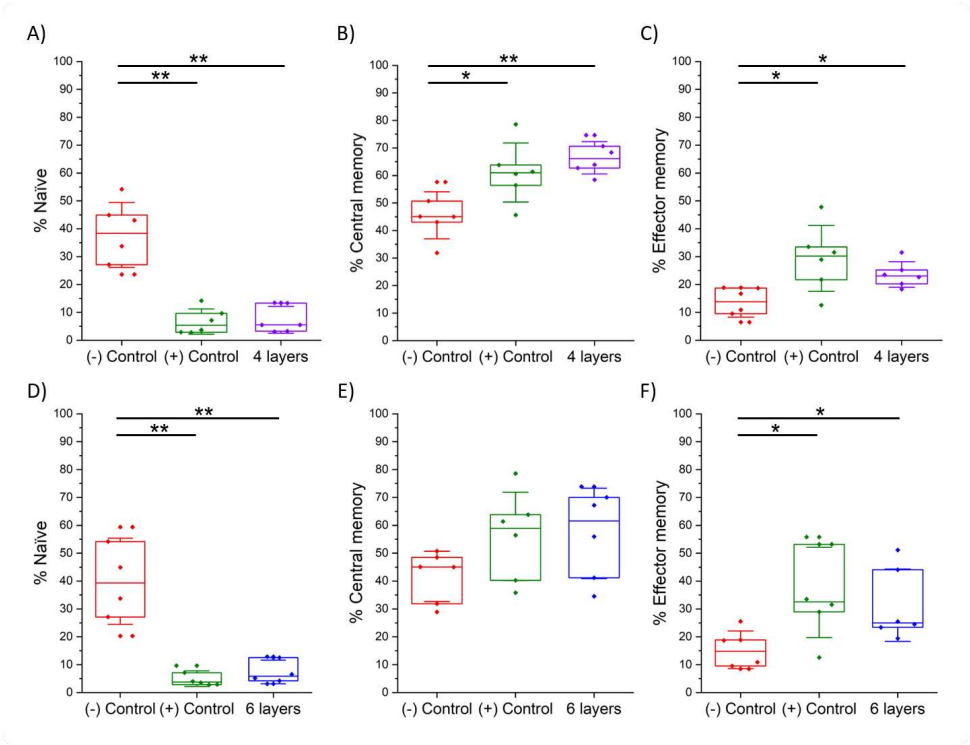

Figure 5.6 Differentiation analysis of CD4+ T cells seeded in unloaded printed PEG-Hep hydrogels of 4 and 6 layers of height with their respective controls (N_{donors} = 6). Percentage of A) and D) naïve (T_N), B) and E) central memory (T_{CM}), and C) and F) effector memory (T_{EM}).

For the 4 layers scaffolds (figure 5.5.A-C), a statistically significant increase of the percentage of T_{CM}, which is a cytotoxic phenotype associated with positive responses in clinics, was observed corresponding with a decrease in the T_{EM}. The median value of T_{CM} raised from the 45% of the negative control, to the 61% of the positive control and 66% for the 4 layers printed hydrogels. On the other hand, the T_{EM} mean values augmented for CD4+ T cells activated in suspension from a 14% of the negative control to a 30%, while this increase was lower for cells seeded in the printed hydrogel, with a mean value of 23%. The naïve cells decreased from a 39% of the inactivated cells to a 5% and 6% of

cells activated in suspension and in hydrogels, respectively. However, no significant changes were observed between cells activated in suspension or using a scaffold in this population. Although the same tendency was observed for scaffolds with 6 layers, the achieved differences were less pronounced, especially for the T_{CM}. Interestingly, these results differ from the ones obtained for non-printed PEG-Hep hydrogels in chapter 3 section 3.7, where the T_{EM} phenotype increased and the T_{CM} decreased. Thus, the use of printed hydrogels provides an advantage over non-printed ones.

5.4.2 Printed hydrogels loaded with CCL21

As previously done for non-printed hydrogels, a solution of 100 ng/ml of CCL21 was incubated during 1 h prior cell to seeding to decorate the printed scaffolds and study its effect on CD4+ T cell proliferation. In addition, a control consisting of a non-printed hydrogel (N.P. 3%wt) was added using the same mass of sample than in the 6 layers printed hydrogel (~50 µg) to evaluate the effect of the printing. The quantitative achieved results can be seen in figure 5.6.A, whereas figure 5.6.B shows a representative CSFE diagram of the analyzed samples.

The replication index improved a 3% and 10% (which mean values of 1.03 and 1.10) when using unloaded and loaded printed hydrogels, respectively, in comparison with the positive control. The expansion index showed no significant changes for the unloaded gels, slightly increasing its mean value from 1 to 1.06 with the addition of the cytokine. Finally, the same tendency was obtained for the proliferation index with mean values of 1.05 and 1.08 for unloaded and loaded hydrogels, respectively. Once again, all the proliferation indexes improved when using the hydrogel loaded with CCL21 in comparison with the unloaded hydrogel and the positive control. Unexpectedly, the non-printed PEG-Hep hydrogels improved all the proliferation indexes a 15% (i.e. mean values of 1.15) compared to the positive control, although these changes were only statistically relevant in the case of the proliferation index. Moreover, higher mean proliferation rates than both unloaded and loaded printed scaffolds were obtained.
These results evidenced that the used non-printed hydrogels already allow a good transfer of cells, nutrients, and gases, which are in agreement with the positive results obtained when using T cells. Nevertheless, preliminary experiments with thicker hydrogels (i.e. with a higher material/cell ratio) have shown problems, which we believe to be able to solve with 3D printed scaffolds. Consequently, further experiments will be performed in order to assess the advantages of 3D printing.

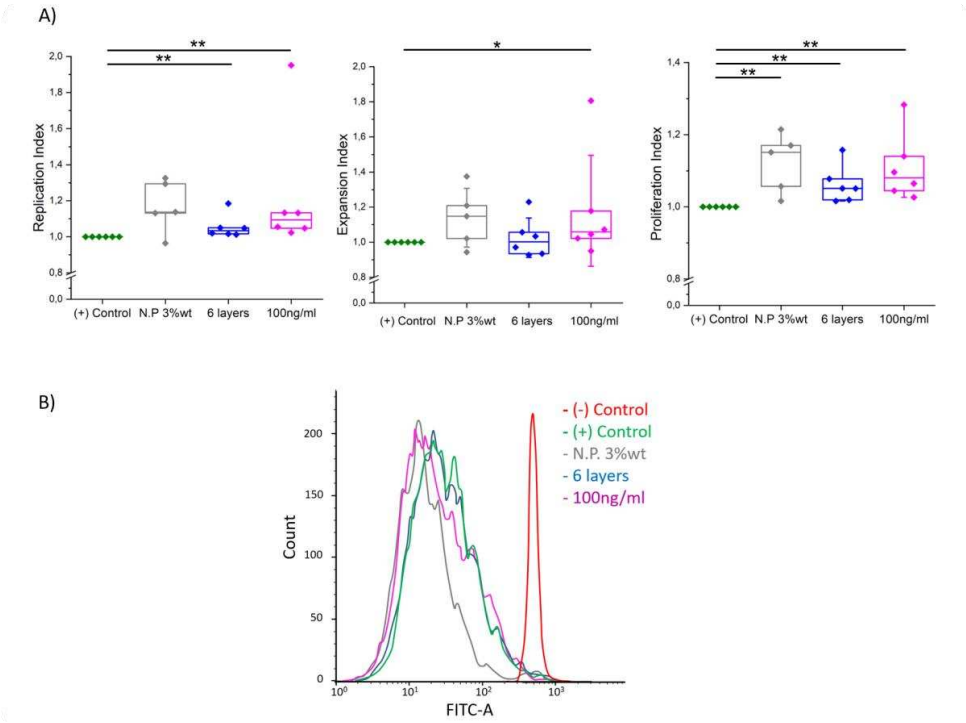

Figure 5.7 A) Normalized proliferation indexes 6 days after seeding CD4+ T cells in suspension (positive control), non-printed PEG-Hep hydrogels (N.P. 3%wt) as well as 6-layer printed PEG hydrogels unloaded and loaded with 100 ng/ml of CCL21 (N_{donors} = 6). Statistical significance was determined by the Mann-Whitney U test (*p<0.05, **p<0.01). B) Diagram of the resulting CFSE fluorescence peaks of a representative data point.

5.5 PEG-Hep printed scaffolds for PBMCs expansion

Although the PEG-Hep hydrogels could not improve the proliferation of PBMCs, as seen in chapter 4.4.1, we decided to study the effect of the 3D printing to this material on the PBMCs culture, to study the effect of the increase in surface area. With this objective PBMCs were seeded in PEG-Hep printed scaffolds of 4 and 6 layers, as previously performed with CD4+ T cells.

5.5.1 Unloaded printed hydrogels

PBMCs were cultured during 6 days with the same scaffolds previously used for the expansion of CD4+ T cells. However, a high variability of the results was again observed, especially for the replication and expansion indexes (figure 5.7). The replication index showed values between 0.78 and 1.04 for scaffolds of 4 layers (percentiles Q-25 and Q-75) with a median value of 0.90, and 0.81 to 1.03 for scaffolds of 6 layers with a median value of 0.93. Nevertheless, no significant differences could be detected. Similar data were obtained for the expansion index with median values of 0.89 and 0.90, and a range between 0.76 to 1.08, and 0.8 to 0.93, for scaffolds of 4 and 6 layers respectively.

In this case though, the results obtained with the printed 6 layer scaffolds were significantly lower than the positive control. Finally, the proliferation index showed lower variability, but the median values were still lower than the normalized positive control (0.96 and 0.95, respectively).

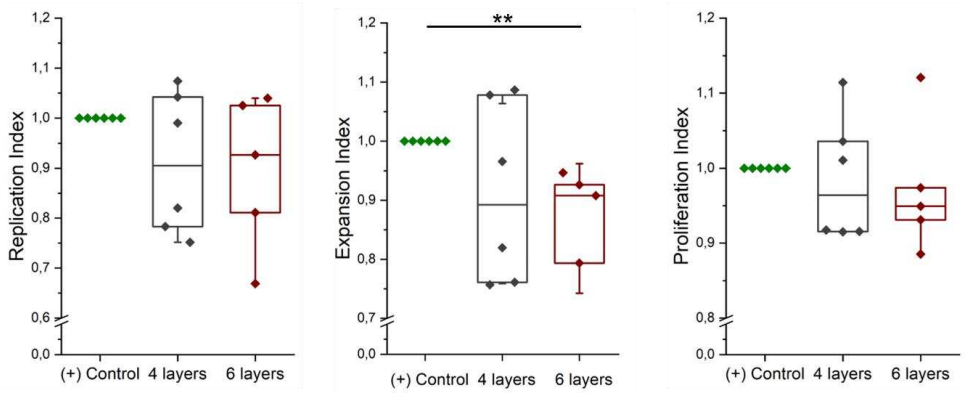

Figure 5.8 Normalized proliferation indexes of PBMCs seeded in 3D printed scaffolds of PEG-Hep hydrogels of 4 and 6 layers. Statistical significance was determined by the Mann-Whitney U test (**p<0.01).

These results show that, as observed in chapter 4 section 4.4.1, the proliferation of PBMCs does not improve in either printed and non-printed hydrogels. These results suggest that this material might not be the most adequate one for this cell population, although further optimization could be done to change this situation.

The resulting phenotypes (CD45RO−/CD62L+, CD45RO+/CD62L+, and CD45RO+/CD62L−) were also analyzed following the same procedure used in chapter 4 section 4.3.2. The results can be seen in the figure below.

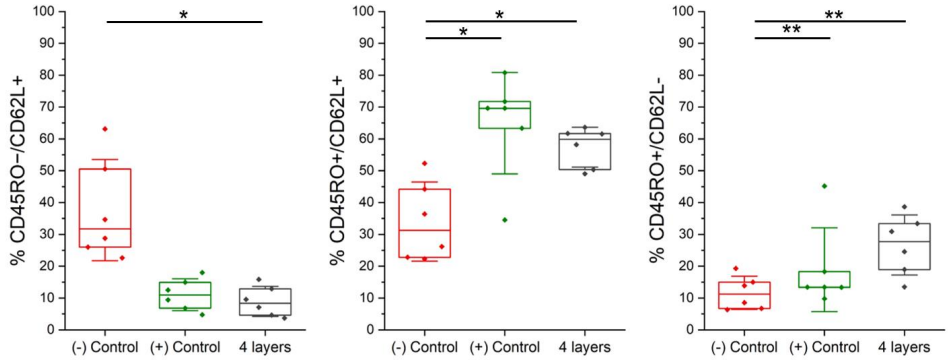

Figure 5.9 Differentiation analysis of inactivated (negative control) and activated (positive control) PBMCs cultured in suspension, and 4 layer printed 3%wt PEG-Hep hydrogels (N_{donors} = 6). Statistical significance was determined by the Mann-Whitney U test (*p<0.05, **p<0.01).

The resulting phenotypes of PBMCs seeded in 3D printed gels changed in comparison with those expanded in suspension, as was previously reported for non-printed

hydrogels in chapter 4 section 4.4.2. The CD45RO−/CD62L+ cells, corresponding with the naïve phenotype of T cells, show a significant decrease when comparing non-activated (negative control) with activated cells, and no differences were observed between the positive control and the printed hydrogel. The mean values were 31.64% for the negative control, 10.87% for the positive control, and 8.23% for the 4 layers printed hydrogel. The mean values of the double positive population were 31.18% for the negative control, which significantly increased to 69.84% for the positive control and 59.68% for the case of PBMCs seeded in printed hydrogels. Finally, the CD45RO+/CD62L- cells slightly increased from 11.09% of the negative control to 13.75% of the positive control, and augmented even more, to a 27.65%, in the printed hydrogels. The tendency here observed is the same than the one obtained for PBMCs seeded in non-printed hydrogels, which consists of a decrease in the CD45RO+/CD62L+ population accompanied by an increase in the CD45RO+/CD62L- cells. These results indicate that the resulting PBMCs were more differentiated than the initial population, as expected. In contrast to CD4+ T cells, the resulting phenotypes of PBMCs are comparable for both, printed and non-printed hydrogels.

5.5.2 Analysis of the killing capacity

The PBMCs that resulted from 5 days of culture in printed PEG-Hep hydrogels were seeded together with the tumor cell line MKN45 and different concentrations of a TCB (0.001 nM, 0.01 nM, and 0.025 nM), which recognizes the CEA present in this cell line, as was previously done to study the cytotoxic capacity of PBMCs expanded in 3D polystyrene scaffolds in chapter 4 section 4.3.3. The achieved results can be seen in the figure below. More information of this experiment and its protocol can be seen in chapter 6 section 6.1.10.

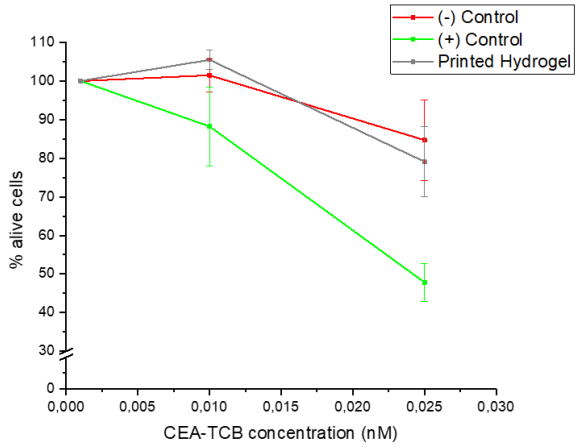

Figure 5.10 Cytotoxicity study of expanded PBMCs for non-activated cells (negative control), activated PBMCs in suspension (positive control), and PBMCs expanded in the 3D printed hydrogel (N_{donors} = 2).

Starting from the 100% of MKN45 survival at a concentration of 0.001 nM of antibody, a decrease to an 88% was obtained at a concentration of 0.01 nM for the positive control, while no further cell death could be measured in the negative control or printed scaffolds. Finally, the antibody concentration of 0.025 nM resulted in a percentage of alive cells of a 48%. However, the MKN45 survival in the culture where the PBMCs were expanded in the printed scaffold, was only slightly lower than the one observed in the negative control, with mean values of 80% and 85%, respectively (figure 5.9). Thus, PBMCs cultured in the printed hydrogels showed a lower killing capacity than those expanded in suspension. These results can be explained by the decrease in the CD45RO+CD62L+ phenotype (T_{CM} for the T cells) obtained in the printed hydrogels in comparison with the positive control.[22,23]

5.6 Conclusions

In this chapter it has been shown that after an adequate optimization of the gelification process, 3%wt PEG-Hep hydrogels can be successfully used as an ink for 3D printing. Thus, 3D scaffolds were obtained with PEG and Hep diluted in both, PBS and cell culture media, opening the way to a wide range of applications, including cell-laden experiments. In our case, PEG-Hep hydrogels were printed in a basic grid structure, obtaining 3D scaffolds that were used for the culture of CD4+ T cells and PBMCs.

The proliferation of CD4+ T cells increased when cells were incubated in printed scaffolds in comparison with the positive control, observing even higher rates for scaffolds of 6 layers. We suggest that this increase is produced by the presence of a higher amount of material, being therefore the number of layers one of the multiple variables that could be optimized. Additionally, these scaffolds also resulted in an increase of the percentage of T_{CM} cells obtained after 5 days of incubation, which is known to be a phenotype associated with high cytotoxicity and effectiveness in immunotherapies. Interestingly, the increase of the percentage of T_{CM} cells differ from the results previously obtained for non-printed hydrogels in chapter 3 section 3.7, where the T_{EM} phenotype was promoted. CCL21 was also studied as a chemical stimulus for the printed hydrogels, observing the expected CD4+ T cell proliferation increase. Besides, non-printed samples formed with the same mass of material than the printed hydrogels were used to study the beneficial effect of the 3D printing. Unexpectedly, these samples showed higher proliferation rates than the printed ones.

On the other hand, 3D printed hydrogels did not improve PBMC proliferation, in agreement with the results reported in chapter 4 section 4.4.1. The resulting phenotypes were not affected either by the printing processability, obtaining the tendency previously observed for non-printed hydrogels consisting of a decrease of the phenotype CD45RO+/CD62L+ and an increase of the CD45RO+/CD62L- population. Not surprisingly, these phenotypes possessed less cytotoxic capacity than PBMCs expanded in suspension.

In summary, the differences observed in the proliferation rates using printed hydrogels, with and without cytokine, were lower than expected. Thus, further experiments will be performed to optimize the use of PEG-Hep hydrogels as bioink for 3D printing and assess its advantages.

5.7 References

1. Mandrycky, C., Wang, Z., Kim, K. & Kim, D.-H. 3D bioprinting for engineering complex tissues. *Biotechnol. Adv.* **34**, 422–434 (2016).
2. Liaw, C.-Y. & Guvendiren, M. Current and emerging applications of 3D printing in medicine. *Biofabrication* **9** (2017).
3. Billiet, T., Vandenhaute, M., Schelfhout, J., Van Vlierberghe, S. & Dubruel, P. A review of trends and limitations in hydrogel-rapid prototyping for tissue engineering. *Biomaterials* **33**, 6020–6041 (2012).
4. Tumbleston, J. R. *et al.* Continuous liquid interface production of 3D objects. *Science.* **347**, 1349 – 1352 (2015).
5. Shirazi, S. F. S. *et al.* A review on powder-based additive manufacturing for tissue engineering: selective laser sintering and inkjet 3D printing. *Sci. Technol. Adv. Mater.* **16**, 33502 (2015).
6. Ozbolat, I. T. Scaffold-Based or Scaffold-Free Bioprinting: Competing or Complementing Approaches? *J. Nanotechnol. Eng. Med.* **6**, (2015).
7. Do, A.-V., Khorsand, B., Geary, S. M. & Salem, A. K. 3D Printing of Scaffolds for Tissue Regeneration Applications. *Adv. Healthc. Mater.* **4** (2015).
8. Lewis, J. A. Direct Ink Writing of 3D Functional Materials. *Adv. Funct. Mater.* **16**, 2193–2204 (2006).
9. Kaufui V. Wong, A. H. A review of additive manufacturing. *AIP Conference Proceedings* **1980**, (2018).
10. Placone, J. K. & Engler, A. J. Recent Advances in Extrusion-Based 3D Printing for Biomedical Applications. *Adv. Healthc. Mater.* **7** (2018).
11. Kumar, A. *et al.* Low temperature additive manufacturing of three dimensional scaffolds for bone-tissue engineering applications: Processing related challenges and property assessment. *Mater. Sci. Eng. R Reports* **103**, 1–39 (2016).
12. Luo, Y., Lin, X. & Huang, P. 3D Bioprinting of Artificial Tissues: Construction of Biomimetic Microstructures. *Macromol. Biosci.* **18** (2018).
13. Leijten, J. *et al.* Spatially and Temporally Controlled Hydrogels for Tissue Engineering. *Mater. Sci. Eng. R. Rep.* **119**, 1–35 (2017).
14. Bajaj, P., Schweller, R. M., Khademhosseini, A., West, J. L. & Bashir, R. 3D biofabrication strategies for tissue engineering and regenerative medicine. *Annu. Rev. Biomed. Eng.* **16**, 247–276 (2014).
15. Luo, Y., Luo, G., Gelinsky, M., Huang, P. & Ruan, C. 3D bioprinting scaffold using alginate/polyvinyl alcohol bioinks. *Mater. Lett.* **189**, 295–298 (2017).
16. Luo, Y., Wei, X. & Huang, P. 3D bioprinting of hydrogel-based biomimetic microenvironments. *J. Biomed. Mater. Res. B. Appl. Biomater.* **107**, 1695–1705 (2019).
17. Liu, F. *et al.* Natural Polymers for Organ 3D Bioprinting. *Polymers (Basel).* **10**

(2018).

18. Loo, Y. *et al.* Peptide Bioink: Self-Assembling Nanofibrous Scaffolds for Three-Dimensional Organotypic Cultures. *Nano Lett.* **15**, 6919–6925 (2015).

19. Gungor-Ozkerim, P. S., Inci, I., Zhang, Y. S., Khademhosseini, A. & Dokmeci, M. R. Bioinks for 3D bioprinting: an overview. *Biomater. Sci.* **6**, 915–946 (2018).

20. Poldervaart, M. T. *et al.* Prolonged presence of VEGF promotes vascularization in 3D bioprinted scaffolds with defined architecture. *J. Control. Release* **184**, 58–66 (2014).

21. Sommermeyer, D. *et al.* Chimeric antigen receptor-modified T cells derived from defined CD8+ and CD4+ subsets confer superior antitumor reactivity in vivo. *Leukemia* **30**, 492–500 (2016).

22. Ghassemi, S. *et al.* Reducing Ex Vivo Culture Improves the Antileukemic Activity of Chimeric Antigen Receptor (CAR) T Cells. *Cancer Immunol. Res.* **6**, 1100–1109 (2018).

23. Hashimoto, K. *et al.* Single-cell transcriptomics reveals expansion of cytotoxic CD4 T cells in supercentenarians. *Proc. Natl. Acad. Sci.* **116** (2019).

CHAPTER 6
Experimental methods

6.1 Biological techniques

In this section all the different biological techniques that were used are explained.

6.1.1 PBMCs isolation

PBMCs were obtained through a purification process of buffy coats of healthy adult donors obtained from "Banc de Sang i Teixits" (Barcelona, Spain) after the approval of the "Ethics Committee on Animal and Human Experimentation" of the Autonomous University of Barcelona (No. 3511). The buffy coat is the fraction of an anticoagulated blood sample that contains most of the white blood cells and platelets.

PBMCs were separated by density gradient centrifugation using Ficoll. All procedures were performed under sterile conditions. The blood was diluted with the pre-warmed Dulbecco's phosphate-buffered saline (DPBS) with 2 mM of EDTA at 37ºC in a proportion of 1:4. This diluted blood was slowly placed over the Ficoll keeping the 2 phases separated, in a proportion 2:1, and centrifuged during 20 min at 300 g (1500 rpm) and 20°C. Photographs and schemes of the sample after the centrifugation can be seen in figure 6.1.

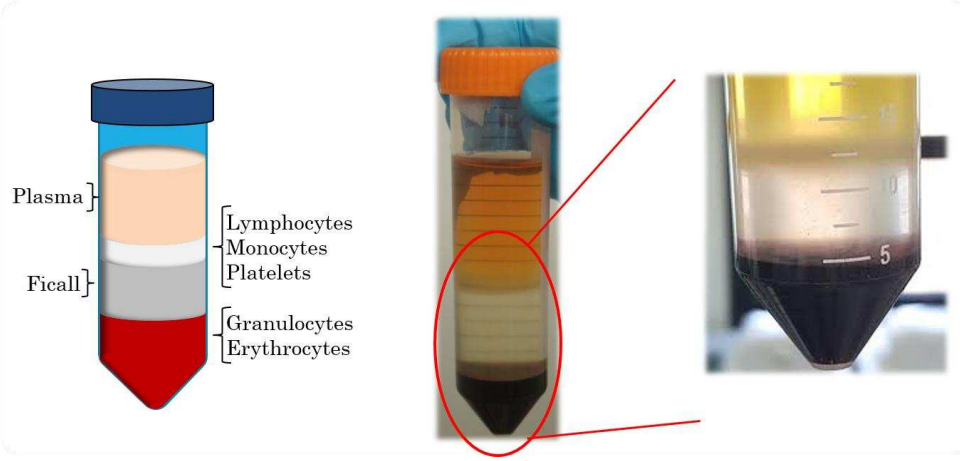

Figure 6.1 Schemes and photographs of the different phases resulting after the centrifugation of the blood with Ficoll.

Once the sample was centrifuged the upper part or supernatant was removed, and the white phase between the supernatant (plasma) and the Ficoll was recovered. This white phase was cleaned three times with DPBS with 2 mM of EDTA and centrifuged at 300 g. Then, the achieved cells were counted with a Neubauer chamber (Hirschmann). Until this step the process is shared for obtaining PBMCs and CD4+ T cells.

The protocol to purify the CD4+ T cells is presented in the section below (6.1.3 CD4+ T cell purification). For the purification of PBMCs, the resulting cells were resuspended with Red Blood Cell Lysing Buffer to eliminate resting red cells. Pictures of the pellet after and before the addition of this product can be seen in figure 6.2. Cells were incubated in ice with this product for 5 min and then neutralized with RPMI with 20% of FBS and 1% of P/S. Then, they were centrifuged, again at 300 g during 10 min, resuspended in the same media used for neutralization and re-counted.

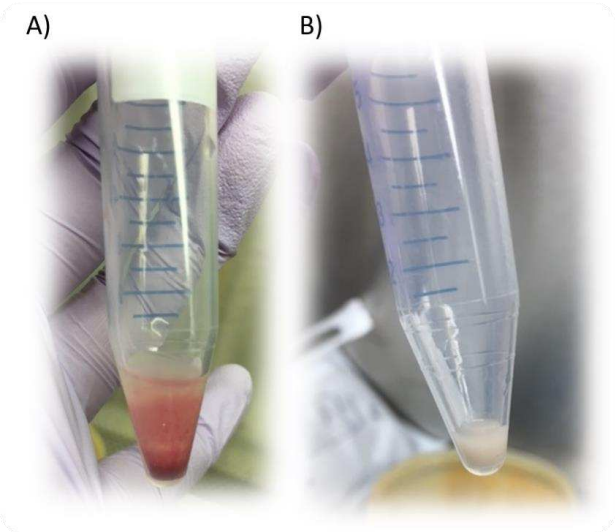

Figure 6.2 Photographs of the resulting pellet A) before and B) after the addition of the Red Blood Cell Lysing Buffer

6.1.2 PBMCs quality control

The proportion of CD3+ CD4+ and CD3+ CD8+ of each population of PBMCs obtained was measured by flow cytometry. To determine this donor dependent parameter three samples of 10^5 cells in 50 µl of PBS with 0.1% of FBS were stained. The first one was incubated with 2.5 µl of antihuman CD3 FITC and antihuman CD4 PE, the second one with 2.5 µl of antihuman CD3 FITC and antihuman CD8 PE, and the last one with 2.5 µl mouse IgG2a control PE-conjugated and mouse IgG1 control FITC-conjugated for the negative control. All antibodies were acquired from Immunotools GmbH (Germany). After the addition of the antibodies, the cells were incubated during 30 min at 0°C in the dark. Then, the samples were washed with PBS with 0.1% of FBS and centrifuged for 6 min at 22°C and 1800 rpm to remove the excess of antibodies. After carefully removing the supernatant, 500 µl of PBS with 0.1% of FBS were added to the samples and they were placed in tubes for flow cytometry.

6.1.3 CD4+ T cell purification

Primary human CD4+ T cells were obtained through a purification process of PBMCs (see section 6.1.1) from healthy adult donors, as explained before. Once the PBMCs were obtained, a CD4+ T cell isolation kit purchased from Miltenyi Biotec (Germany) was employed. This kit contains a biotin-antibody cocktail with antibodies against CD8, CD14, CD15, CD16, CD19, CD36, CD56, CD123, TCR γ/δ, and CD235a (Glycophorin A), which is used to label non-CD4+ cells, i.e., CD8+ T cells, monocytes, neutrophils, eosinophils, B cells, dendritic cells, NK cells, granulocytes, γ/δ T cells, or erythroid cells. The other component of the kit is a CD4+ T Cell MicroBead Cocktail, which are magnetic microbeads conjugated to the monoclonal anti-biotin, which retain all the labeled cells. The suspension obtained after incubation with the two cocktails is added on a LS column, properly placed in a magnet. The matrix of the LS columns is composed of ferromagnetic spheres, which are covered with a cell-friendly coating allowing a fast and gentle separation of cells. Thus, the magnetically labelled cells stay in the column, while the resulting CD4+ T cells are collected after passing through the column.

6.1.4 CD4+ T cell purity assay

Once the CD4+ T cells were obtained, their quality was analyzed by flow cytometry. To determine their purity, the staining protocol followed was the same than in the case of the PBMCs but in this case only two samples were necessary. The first one with antihuman CD3 FITC and antihuman CD4 PE, and the other one, with the negative control. Only samples that were at least 90% positive for both CD3+ and CD4+ by flow cytometry (usually CD3+CD4+ T cells > 95%) were used for experiments. Viability was constantly above 80% (usual viability > 90%).

6.1.5 CSFE staining. Proliferation assay

To study the proliferation of cells, they were stained with a CellTrace CFSE cell proliferation kit provided by Thermo Fisher Scientific, before their seeding. Carboxyfluorescein succinimidyl ester (CFSE) is a long lasting dye well retained within labelled cells. For the staining, 1 µL of CFSE stock solution was diluted in 99 µL of PBS with 5% of FBS. Cells were diluted in PBS up to a final volume of 900 µL, put in contact with 100 µL of the diluted CFSE solution through rapid agitation, and incubated for 5 min at room temperature in the dark. After the incubation, 10 ml of ice cold PBS with 5% of FBS were added to quench the staining. Then, the medium was extracted and cells were resuspended in the corresponding media at the desired concentration.

6.1.6 Cell seeding and culture

Cells were seeded on 96 WP, except for the experiments performed with 3D printing, which required 24WP as explained in chapter 5. The culture media used was Roswell Park Memorial Institute (RPMI) medium with 10% FBS and 1% P/S for CD4+ T cells and RPMI with 20% FBS and 1% P/S for PBMCs for all studies, except those focused on cytotoxicity evaluation where RPMI where RPMI with 10% of HS, 10 mM of HEPES, and 30 IU/ml of IL-2 was employed as explained in chapter 4, section 4.3.3. The cell seeding concentration was of 10^6 cells/ml in all the cases with the exception of the proliferation studies of 3D printing experiments, where a concentration of $5 \cdot 10^5$ cells/ml was used. The activation of cells was induced by commercial Dynabeads in a 1:1 ratio, as suggested by the manufacturer (Invitrogen, Thermo Fisher Scientific, USA). For all the hydrogels studied, cells were seeded with Dynabeads on top of a previously formed hydrogel, given their capacity to penetrate and migrate through it. For the 3D polystyrene scaffolds, a 15 µL drop of a concentrated cell suspension was seeded on top of the scaffold, incubated during 3 h at 37 °C, and finally the corresponding medium was added. Positive controls were done by seeding the cells in suspension, as well as negative controls, which did not include Dynabeads.

6.1.7 CD4+ T cell activation study

The amount of IL-2 present in the media was used to evaluate the activation of cells. Cultures were evaluated 1 day after seeding by measuring the secreted IL-2. The supernatant of the cell cultures was recovered and the IL-2 concentration was determined by a human IL-2 Quantikine ELISA (R&D Systems, USA) following the instructions of the manufacturer.

Additionally, activation was also qualitatively assessed through cell morphology using optical microscopy, which was performed in a Nikon Eclipse TE2000-E (Nikon, Japan), and the images acquired were treated with FiJi (ImageJ).

6.1.8 Differentiation analysis

The phenotypes resulting after 5 days of culture were analyzed by cell staining with different antibodies depending on the populations under study. Two different differentiation experiments were performed, CD45RO/RA and CD62L/CD45RO.

The first experiment was performed with the antibodies antihuman CD45RA PE and antihuman CD45RO FITC, with mouse IgG2a control PE-conjugated and mouse IgG1 control FITC-conjugated as negative control. All these antibodies were provided by Immunotools GmbH (Germany). In the samples where cells were activated, Dynabeads were removed with a magnet before the staining. Then, cells were centrifuged, suspended in PBS with 0.1% of FBS, and the antibodies were added (2.5 µl as in the

other staining protocols) and incubated for 30 min at 0°C. Afterward, they were washed and analyzed by flow cytometry.

The analysis with antihuman CD45RO FITC and antihuman CD62L PE required the purchase of CD62L PE and its control from BioLegend (USA). In this case, the protocol was the same than before, with the only difference that 1 µl of the CD62L PE antibody and its control was enough to obtain good measurements.

6.1.9 Immunostaining of CCL21 in glass surfaces functionalized with Au NPs

To prove that CCL21 could bind to Au, 100 µl of CCL21 at 10 µg/ml were incubated on the desired substrates in a PBS solution for 1 h at room temperature. The chosen substrates were glass surfaces half-functionalized with Au NPs, with the objective of clearly seeing the difference between the part with and without Au in the same sample. After 1 h of incubation the surfaces were washed three times with PBS during 5 min each wash, to remove all the cytokine that could not bind the surface, and ensure the quality of the experiment.

Once the samples were ready, the staining protocol was performed. For that, the substrates were incubated with a solution of 10 µg/ml of the primary antibody mouse anti-human CCL21 (Invitrogen, USA) in PBS for 1 h at room temperature. This antibody binds to every CCL21 protein present in the samples. The same washing procedure mentioned before was applied after this incubation for the removal of the excess of antibody. After that, a secondary antibody, goat anti-mouse Alexa 488 (Invitrogen, USA), which binds to the first antibody and provides fluorescence, was added in a solution of PBS with 1% of BSA at a concentration of 10 µg/ml. The incubation time was again of 1 h at room temperature, but in this case, the sample was covered with aluminum foil, to avoid fluorescence quenching. Finally, samples were washed during 10 min on a shaker, and prepared for imaging. The fluorescence microscope used was an Olympus BX51 with U-RFL-T reflected fluorescence system (Olympus, Japan).

6.1.10 Expanded PBMCs, co-culture of MKN45, and targeting CEA-TCB

To study the cytotoxicity of PBMCs expanded under different conditions, they were cultured together with tumoral MKN45 cells and the targeting CEA-TCB. MKN45 is a cell line of human gastric adenocarcinoma established from the poorly differentiated adenocarcinoma of the stomach (medullary type) of a 62-year-old woman which was purchased from ATCC (USA). TCBs are engineered molecules that include, within a single entity, binding sites to the TCR and to tumor-associated or tumor-specific antigens.[1] CEA-TCB is an antibody which has the capacity to link T cells to the MKN45 cells, with the objective to destroy the malignant cells.

Prior to the co-culture of both cell types and the antibody, MKN45 cells were cultured in RPMI with 10% HS and 2mM of glutathione, and stained with CSFE as previously described (Section 6.1.5). Once the desired PBMCs were expanded they were

co-cultured in a ratio effector:target of 1:1, and the targeting CEA-TCB antibody was added in three different concentrations, 0.001 nM, 0.01 nM, and 0.025 nM. The plates were incubated for 48 h and then cells were analyzed by flow cytometry. Thus, fluorescent cells were counted and the amounts of live and dead cells were obtained, allowing to establish the efficacy of the treatment.

6.2 Chemical techniques and materials

6.2.1 Materials

A modified green fluorescence protein (GFP) was synthesized as described elsewhere[2] by our collaborator Dra. Elena García-Fruitós in IRTA (Institute of Agrifood Research and Technology). Low molecular weight heparin was purchased from Fisher Scientific (Fisher BioReagents, Spain). Poly(ethylene oxide) 4-arm thiol terminated (Mn 10000 g/mol), N-(2-aminoethyl) maleimide trifluoroacetate salt (AEM), 1-hydroxybenzotriazole hydrate (HOBT), N-(3-dimethylamino-propyl)-N'-ethylcarbodiimide hydrochloride (EDC·HCl), 2-(N-morpholino) ethanesulfonic acid (MES), and the rest of the products not otherwise specified were purchased from Sigma-Aldrich (USA).

6.2.2 Synthesis of heparin functionalized with maleimide

The functionalization of heparin with maleimide was based in a method previously described.[3,4] For 100 mg (0.02 mmol) of heparin dissolved in a solution of 0.1M MES, 20.6 mg of HOBT (0.15 mmol), 20.6 mg of AEM (0.08 mmol), and 20.6 mg of EDC·HCl (0.11 mmol) were used. To ensure maximum yield, the reaction was left overnight. The product was purified by dialysis (MWCO 1000) against 500 ml of deionized water for 6-15 h during the first step, and 500 ml of MilliQ (MQ) water during the second and last steps. Once the product was purified, it was lyophilized, and characterized by nuclear magnetic resonance (^{1}H-NMR) spectroscopy in a Bruker Avance-III of 400MHz equipment.

6.2.3 PEG-Hep hydrogel formation

To prepare PEG-Hep hydrogels, a solution of 4-arm thiolated PEG (PEG-SH) was mixed with a solution of functionalized heparin in a proportion of 1:1.5, both PBS. For such calculation, five maleimide groups per molecule of heparin were estimated to react with the four thiol groups of PEG.[4] Different concentrations in weight of PEG were used (6%wt, 4%wt, and 3%wt) to obtain different types of hydrogels. Once the solutions were mixed, they were kept in the incubator at 37°C during at least 1 h to produce the gel. Negative controls consisting of solutions of only one of the reactants at relevant concentrations confirmed that the hydrogel formation is caused by the reaction between the thiol groups of the 4-arm PEG and the maleimide of the functionalized heparin.

6.2.4 Loading capacity

3%wt PEG-Hep hydrogels were loaded with solutions of GFP at different concentrations during 1 h. After that, the supernatant was removed and the hydrogels were washed three times with PBS. The fluorescence of the supernatant, washing PBS, and hydrogels was measured in each step with a Victor 3 Multioption plate reader (Perkin Elmer, USA).

6.2.5 Preparation of nanostructured surfaces for CCL21 immobilization on Au

Nanostructures were prepared by block copolymer micellar lithography (BCML) as previously described in literature.[8] As explained in chapter 3 section 3.7.1, BCML consists of dissolving an amphiphilic block copolymer in an apolar solvent to create reverse micelles, which can be loaded with a metallic precursor. In our case, 40 mg of polystyrene (x)-2-vinylpyridine (y) (PS(106)-P2VP(75); Polymer Source Inc., Canada) were dissolved in 20 ml of a dry solution of o-toluene at room temperature and stirred for 24 h. Then, 19.54 mg of gold (III) chloride trihydrate (Sigma-Aldrich, USA) were added to the block copolymer micellar solution and stirred for 48 h. This inorganic metal complex was dissolved into the polar micellar cores, where it loses a proton that binds to the nitrogen atom of the P2VP chain, stabilizing the micelles. Commercial indium titanium oxide (ITO)-coated glass substrates (20 mm x 15 mm Ossila Ltd, UK) were dip-coated with the Au-loaded micellar solution at a constant velocity of 110 mm/min and then plasma treated with oxygen plasma (150 W, 0.15 mbar, 45 min) using a microwave gas plasma system (210 PVA TePla, Germany) to obtain quasi-hexagonally ordered AuNPs with lateral interparticle distances of 68 ± 20 nm. After that, the ITO surface was passivated with 50 mg of PEG-silane (Prochimia, Poland), 20 µl milliQ water, and 2 ml triethylamine (Sigma Aldrich, USA) in 20 ml toluene overnight at 80°C. Then, it was functionalized with CCL21 (Sigma Aldrich, USA; concentration 10 µg/ml) during 1 h at room temperature by means of the cysteine groups of the cytokine.

6.2.6 Preparation of CCL21-functionalized planar Au surfaces

The function of CCL21 and its effect in T cell proliferation was studied in suspension and immobilized on Au surfaces to analyze the influence of fixing this cytokine on CD4+ T cell proliferation. To prepare these samples, glass surfaces were properly washed with piranha and coated with 3 nm of titanium and 10 nm of gold in an evaporation System Auto 306, Boc Edwards. The resulting Au surfaces were fixed to the bottom of the well plates with a special glue named picodent twinsil speed (Picodent, Germany). Once the device was ready CCL21 was incubated during 1 h at the desired concentration.

6.3 Physical techniques

6.3.1 Rheology

The small-amplitude oscillatory shear (SAOS) technique was used to characterize the linear-viscoelastic regime (LVE) of the hydrogels. It consists of a small-amplitude torsional oscillation that generates a shear flow in the sample and requires a trial-and-error approach to find the appropriate values of strain and frequency of each gel.[7] The equipment used was a Rheometer HAAKE RheoStress RS600 (Thermo Electron Corporation) with a rotor of 10 mm of diameter (figure 6.3). The experiments performed were strain sweeps, frequency sweeps, and time sweeps at 37°C to calibrate the range of pressure and frequency where the hydrogels maintain their viscoelastic behavior, characterize the gelification process, and achieve the value of the gel equilibrium shear modulus (Ge). To perform the strain and frequency sweeps, samples were previously prepared, i.e. completely gelified, and stored in the incubator at 37°C in MQ water. For the time sweeps, 200 µl of sample were needed to characterize the gelification process. In this experiment, the reactants to form the hydrogel (4-arm thiolated PEG and Hep functionalized with maleimide) were mixed in PBS and immediately placed under the center of the rotor, to characterize the whole gelification process, from the liquid state to the gel.

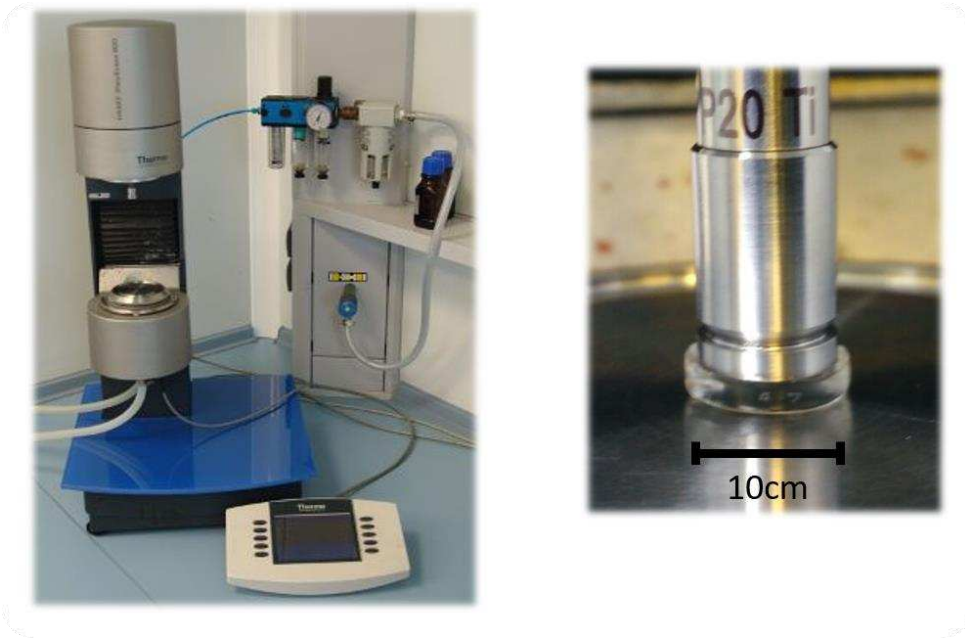

Figure 6.3 Rheometer HAAKE RheoStress RS600 and a 3% PEG-Hep hydrogel in a measurement.

6.3.2 SEM

Scanning electron microscopy (SEM) is a technique that allows to observe the surface and section of the hydrogels. Although this technique is typically used in dry samples, a special protocol at the vacuum chamber was used named “ambient mode”. It consists of slowly decreasing the pressure and temperature to enable to image the structure of the hydrated hydrogels. The equipment used was a FEI Quanta 650F Environmental scanning electron microscope (Thermo Fisher Scientific, USA). Thus, the structure of hydrogels with different compositions (6%wt, 4%wt, and 3%wt of PEG) previously prepared and stored in the incubator at 37°C in MQ water was observed.

6.3.3 Microtomography

Microtomography is an X-ray 3D imaging technique with a high resolution that allows the visualization of the internal structure of a sample. In this case, a skyscan 1272 high-resolution micro computed tomograph (Bruker, Germany) was used. After considering different conditions to study the 3D structure of the hydrogels, pre-made hydrogels were frozen in PBS with liquid nitrogen and then lyophilized. The size of the measured samples was 2 mm of height and 1 cm of diameter. The time of scanning chosen was of 3 h with a minimum resolution of 5 µm.

6.3.4 3D Printing with PEG-Hep hydrogel

The 3D printing experiments were performed in collaboration with the Institute of Bioengineering of Catalonia (IBEC, Spain) with a 3D Discovery printer from RegenHU Biosystem Architects (Switzerland). The experimental conditions were optimized to be able to use 3%wt PEG-Hep hydrogels as ink. According to this protocol, sterilized solutions of both reagents (PEG-SH and Hep-Mal) were mixed a day before the impression in a sterile syringe adequate for the printing, and incubated at room temperature overnight. After that, the syringe was placed in the printer with a tip TIP27GA TT 008’’ NAT, which showed to be adequate for the printing of this material at a pressure of 1.2 bar and a printing speed of 15 mm/s in a 24WP.

6.4 Statistical tests

6.4.1 Mann-Whitney U test

The Mann-Whitney U test is a non-parametric test, which is used with data that do not belong to any specific probability distributions (in our case, different donors). It is a test of the null hypothesis that compares two populations of data. To determine if two populations are significantly different or not, it randomly selects one value from one population and calculates the probability of this value to belong to the second population.

6.4.2 Kruskal Wallis ANOVA test

Kruskal Wallis ANOVA test is another non-parametric test, which tests whether samples originate from the same distribution (in our case, the same sample). It compares two or more independent samples of equal or different sample sizes, extending the use of the Mann-Whitney U test.

6.5 References

1. Rius Ruiz, I. *et al.* p95HER2-T cell bispecific antibody for breast cancer treatment. *Sci. Transl. Med.* **10**, (2018).
2. Martinez-Alonso, M., Garcia-Fruitos, E. & Villaverde, A. Yield, solubility and conformational quality of soluble proteins are not simultaneously favored in recombinant Escherichia coli. *Biotechnol. Bioeng.* **101**, 1353–1358 (2008).
3. Nie, T., Akins, R. E. J. & Kiick, K. L. Production of heparin-containing hydrogels for modulating cell responses. *Acta Biomater.* **5**, 865–875 (2009).
4. Nie, T., Baldwin, A., Yamaguchi, N. & Kiick, K. L. Production of heparin-functionalized hydrogels for the development of responsive and controlled growth factor delivery systems. *J. Control. Release* **122**, 287–296 (2007).
5. Santiago, M. & Strobel, S. Thin layer chromatography. *Methods Enzymol.* **533**, 303–324 (2013).
6. Dass, C. Hyphenated Separation Techniques. *Fundamentals of Contemporary Mass Spectrometry* 151–194 (2007).
7. Zuidema, J. M., Rivet, C. J., Gilbert, R. J. & Morrison, F. A. A protocol for rheological characterization of hydrogels for tissue engineering strategies. *J. Biomed. Mater. Res. B. Appl. Biomater.* **102**, 1063–1073 (2014).
8. Guasch, J. *et al.* Synthesis of Binary Nanopatterns on Hydrogels for Initiating Cellular Responses. *Chem. Mater.* **28**, 1806–1815 (2016).

CHAPTER 7
Summary and outlook

7.1 Summary and conclusions

This doctoral thesis has focused on the improvement of current immune cell expansion methods by the introduction of a 3D matrix or scaffold, to resemble the natural environment of the SLOs. With this objective, we aimed to overcome one of the current problems of cellular immunotherapies, specifically of ACT, which is the production of large amounts of specific T cells in a short period of time and in an economically viable manner.

Matrigel and a 3D polystyrene scaffold were studied as the two most suitable, but also extremely different commercially available systems. They showed increases in CD4+ T cell proliferation compared to standard suspension systems, proving the beneficial effect of the 3D physical support and the importance of the chemical stimuli. However, these systems were not designed for SLO mimicking, and thus, they significantly differ in terms of ECM composition from these organs. Consequently, a new platform was developed for this application.

PEG-Hep hydrogels were synthesized and completely characterized for this purpose. On one hand, PEG provides a 3D structure, which can be manipulated to change both its structural and mechanical properties. On the other hand, heparin is used as an anchor for positively charged proteins that interact with the cells in culture, tuning their proliferation and differentiation pathways. This system was used for the expansion of CD4+ T cells without any chemical stimuli, with CCL21, CCL19, and a combination of both cytokines (CCL21 loaded to the hydrogel and CCL19 in solution). It was obtained an increase of CD4+ T cell proliferation for all the conditions, but specially with the loading of CCL21 together with the addition of CCL19 in solution, which are the conditions that best mimic the ECM of LNs (Table 7.1). The resulting phenotypes of CD4+ T cells cultured in these hydrogels showed an increase of the T_{EM} percentage in comparison with cells expanded in suspension.

The same 3D systems were used for PBMCs, due to their importance in immunotherapy treatments, and the fact that they are a common source of relevant therapeutic T cell subsets such as CD4+ and CD8+ T cells for the clinics. 3D polystyrene improved the proliferation parameters in comparison with the suspension systems, while not altering the killing capacity of the resulting cells in comparison with cells cultured in suspension. The beneficial results obtained with PEG-Hep hydrogels for the culture of CD4+ T cells could not though be reproduced for this population (Table 7.2). Nevertheless, PEG-Hep hydrogels did show an effect in the resulting phenotypes achieved, increasing the CD45RO+/CD62L- percentage (T_{EM} population for T cells). Further experiments will be performed to optimize these results, such as the use of cytokine cocktails.

Finally PEG-Hep hydrogels were studied as bioink for 3D printing. Once the protocol was scaled up from 96WP to 24WP due to technical reasons, the resulting printed scaffolds were used for immune cell culture. Increases in the proliferation parameters of CD4+ T cells were observed as well as changes in their resulting phenotypes in comparison with non-printed hydrogels. In this case an increase in the T_{CM} phenotypes was observed, which is reported to be related to good clinical outcomes. In contrast, PBMCs did not show proliferation enhancements when cultured in printed PEG-Hep hydrogels, and the resulting phenotypes were comparable with the ones obtained without printing. In this case, a further optimization of the use of PEG-Hep hydrogels as bioink for 3D printing will also be performed.

Table 7.1 Summary of the proliferation indexes obtained for CD4+ T cell culture under different materials and conditions.

CD4+ T cells			
Sample	Replication index	Expansion index	Proliferation index
Matrigel (day 5)	1.71	1.23	1.20
Polystyrene (day 5)	1.08	1.14	1.08
Polystyrene (day 6)	1.64	1.50	1.08
Unloaded 3%wt (day 5)	1.25	1.1	1.05
100ng/ml CCL21 loaded 3%wt (day 6)	1.3	1.05	1.06
100ng/ml CCL21 loaded and 100ng/ml CCL19 in solution 3%wt (day 6)	2	1.5	1.20
Unloaded 6 layers 3D printed 3%wt scaffolds (day 6)	1.07	1.04	1.07
6 layers 3D printed 3%wt scaffolds loaded with 100ng/ml CCL21 (day 6)	1.10	1.06	1.08
Non-printed unloaded 3%wt scaffolds (day 6)	1.15	1.15	1.15

Table 7.2 Summary of the proliferation indexes obtained for PBMC culture under different materials and conditions.

PBMCs			
Sample	Replication index	Expansion index	Proliferation index
Polystyrene (day 5)	1.52	1.68	1.17
Unloaded 3%wt (day 5)	0.93	0.84	0.95
100ng/ml CCL21 loaded 3%wt (day 5)	0.88	0.73	0.92
Unloaded 3%wt (day 6)	0.88	0.9	0.93
100ng/ml CCL21 loaded 3%wt (day 6)	0.9	0.9	0.94
Unloaded 6 layers 3D printed 3%wt scaffolds (day 6)	0.93	0.9	0.95

7.2 Outlook

Moving one step forward in the development of PEG-Hep hydrogels to mimic the natural environment of the LNs, different strategies will be studied in the near-future to transform the static PEG-Hep hydrogels in dynamic hydrogels. These new hydrogels should have not only self-healing properties, increasing the lifetime of the material, but also be able to be formed and dissolved to recover the totality of the cells from inside the hydrogel. Moreover, we should be able to tune the mechanical properties of the hydrogels on demand upon the application of an external stimulus, thus mimicking the LN capacity to change stiffness depending on the health condition of the body.

There are multiple options to obtain dynamic hydrogels depending on the structure and chemical composition of the material. This process can be either autonomous or occur as a result of external stimuli, and can be a one-time event or an indefinitely repeatable process. Besides, there are different driving forces that can be used as a parameter to initialize the dynamic process, such as thermally reversible reactions, ionomeric arrangements, or molecular diffusion and entanglement. Thus, the switching mechanisms can involve different strategies such as hydrogen bonding, dynamic covalent bonds, supramolecular host-guest, ionic, or hydrophobic interactions.[1,2]

After a bibliographical study, we have chosen a host-guest strategy to be applied to PEG-Hep hydrogels based on the cucurbit[8]uril (CB[8]) as the host molecule and a phenylalanine derivative as a guest molecule (figure 7.1).

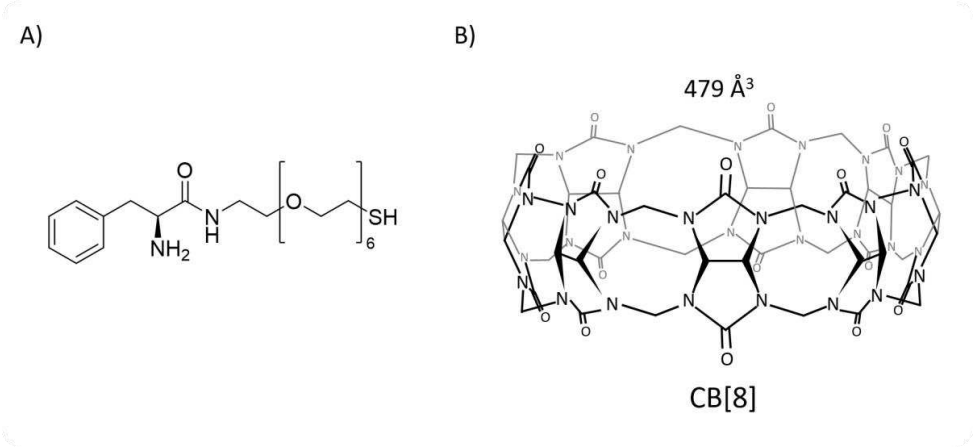

Figure 7.1 Molecular structures of A) phenylalanine derivative, and B) cucurbit[8].

The interaction between the phenylalanine derivative and CB[8] control gelification made by the incorporation of two molecules of phenylalanine inside the CB[8] structure. This process should be tuned and finally reverted through the addition of a highly concentrated phenylalanine solution or an alternative molecule such as anthracene, acridine (K_{eq}: 5.2 ± 0.8 × 10^9 M^{-2}), methyl viologen and naphthoxy derivates (K_{eq} > 10^{11} - 10^{12} M^{-2}), by displacement.

This strategy requires the synthesis of the thiolated phenylalanine derivative, which to the best of our knowledge has never been described before. With this objective, we started a new collaboration with Dr. V. Sergeev and Dr. N. Davydova from the A.N.Nesmeyanov Institute of Organoelement of Russian Academy of Sciences (INEOS RAS, Russia). The first proposal for the synthesis of the desired derivative consists of 6 steps (a condensation reaction, a tosylation of the alcohol, a nucleophilic substitution, a cleavage of the Boc group, a dimerization and a final reduction) and is already under development to create new dynamic PEG-Hep hydrogels in the near future.

Besides, other research lines are currently under study or planned for future exploration:

- Use of other biomolecules related to immune cell proliferation to load the PEG-Hep hydrogels, like ICAM-1, which could be used alone or in combination with the cytokines already studied (CCL21 and CCL19).
- Application of microfluidic systems to the static cultures with PEG-Hep hydrogels to mimic the flow of the lymph through the SLOs.
- Culture CD8+ T cells in the hydrogels and overcome the problems encountered with PBMCs.
- Culture of TILs and CAR-T cells in the hydrogels to perform *in vitro* and *in vivo* studies in collaboration with Prof. J. Arribas (VHIO, Spain).
- Optimization of the 3D printing process of the hydrogels in collaboration with Prof. timoneda (IBEC, Spain).
- Use of PEG-Hep hydrogels as a platform for immune cell delivery. Hydrogels loaded with expanded immune cells could be implanted in mice models to progressively deliver the cells together with the natural degradation of the scaffold.

7.3 References

1. Bergman, S. D. & Wudl, F. Mendable polymers. *J. Mater. Chem.* **18**, 41–62 (2008).

2. Wang, Y., Adokoh, C. K. & Narain, R. Recent development and biomedical applications of self-healing hydrogels. *Expert Opin. Drug Deliv.* **15**, 77–91 (2018).